Republic of Iraq
Ministry of Higher Education
and Scientific Research
University of Babylon
College of Engineering
Civil Engineering Department

Experimental Modeling of Local Scour Around Complex Bridge Pier Foundations for Different Soil Types in Iraq

A Thesis

Submitted to the College of Engineering / University of Babylon in Partial Fulfillment of the Requirements for the Degree of Doctor of Philosophy in Engineering / Civil Engineering / Water Recourses

By
Noor Saadi Hussein Salih

Supervised By
Prof. Dr. Abdul-Hassan K. Al-Shukur
Asst. Prof. Dr. Zaid Hameed Majeed

2023 A.D 1444 A.H

ومن يتقِ الله يجعل له مخرجا ويرزقه من حيث لا يحتسب

صدق الله العلي العظيم

(الآية 2-3 من سورة الطلاق)

DEDICATION

To

my father's pure spirit. Allah rest his soul

How do I get the description and words that embody your struggle in life… I dedicate this fruit to efforts that gave me strength and patience… To the dear on my heart… My Mother… I ask Allah to protect her.

To

Those who have the widest hearts and always give everything

My Sisters and My brothers.

Noor

2023

ACKNOWLEDGEMENT

"In the Name of Allah, the Most Gracious, the Most Merciful"

Praise to ***Allah*** *his Majesty before anything and after anything and to the prophet* ***"Mohammed and Ahl-Al-Bait"*** *for the strength, courage, and wisdom that Allah gave me to complete this humble work and lengthy journey.*

I would like to express my deepest gratitude and respect to my thesis supervisors ***Prof. Dr. Abdul-Hassan Kh. Al Shukur and Asst. Prof. Dr. Zaid Hameed Majeed.*** *I am very grateful for their precious time spent and useful suggestions which provided valuable guidance and important role in the completion of the thesis as well as the moral support continued for the duration of the search, calling God richly rewarded them.*

Noor
2023

Abstract

Due to physical, geotechnical and economic considerations, bridges are frequently built with foundations of complex geometries. In this study, the term “complex piers” applies to pier geometries characterized by a column founded on a pile cap supported by an array of piles. Local scour is a complex phenomenon involving three-dimensional flow structures, typically developed around piers and bridge abutments founded in movable bed rivers. Local scour can lead to partial failure or to collapse of bridge piers and decks.

A total of ninety tests with five complex pier models were conducted. The tests were used to quantify the influence of the pile-cap position, geometry, aligned and skewed angle to the approach flow (0°, 30°, 45°, and 60°) for different Iraqi soils on the scour depth time evolution. The experimental results were classified according to three pile-cap situations: Situation 1, characterized by the bottom of the pile cap being above the initial bed level; Situation 2, characterized by the bottom of the pile cap is being close to the initial bed configuration; and Situation 3, characterized by the pile cap being completely buried in the bed.

For complex pier is aligned with flow, maximum scour depth occurs when pile cap above original bed level with increase (80%, 81%, 100%, 35%, and 100%) compare with the pile-cap fully buried to the bed level for (Beta, Ali AL- Gharbi, Selebat, Suspension-Basra, and Shallala) Bridges respectrely. This similar to results of previous investigations. The protective effect of pile cap lowers scour depth significantly after occurrence of peak value upon increasing the pile cap position by disrupting the down-flow in front of pier. Equilibrium scour depth for skewed complex piers increases significantly compared to aligned piers. Increase in depth of scouring is proportional to skew angle α, it is largest

in Selebat Bridge (29.4%, 33%, and 80%) for (60°, 45°, 30°, and 0°) sequentially; Smallest in Ali Al-Gharbi Bridge (26%, 12%, and 25%).

A new formulation to predict d_s at complex piers is suggested, for the sand bed materials, the comparison was of the HEC-18, the Auckland, and the Florida Department of Transportation (FDOT), it can be concluded that HEC-18 method gives estimations of d_s, which represents an acceptable compromise between safety and economy and give (R^2 = 96.94, 95.54, 98.11) for (Beta, Ali Al-Gharbi, and Suspension-Basra) Bridges respectrely. For the cohesive bed materials, the comparison was of the (Ansari, Debnath and Chaudhuri, and Rambau), the method of Ansari gives (R^2 = 96.63) for (Selebat Bridge). For non-uniform gravel bed material (Melville and Coleman, Guo, and Kim), the method of Melville gives (R^2 = 94.31) for (Shallala Bridge).

Table of Contents

Table of Contents

Table of Contents

List of Symbols

Symbol	Title	Dimension
B	Flume width	L
B_1	Upstream tank width	L
b_{pc}	Pile-cap width	L
C	Cohesion of sediment	$ML^{-1}T^{-2}$
Cc	Curvature coefficient	-
C_e	Effective coefficient of the weir	-
Cu	Uniformity Coefficient	-
D_c	Column diameter	L
D_e	Equivalent diameters	L
D_{ec}	Equivalent diameters of column	L
D_{epc}	Equivalent diameters of pile-cap	L
D_{epg}	Equivalent diameters pile group	L
D_p	Pier width	L
ds	Scour depth	L
d_{sc}	Column contribution to the local scour depth	L
d_{sc1}	Equilibrium scour depth due to Configuration C1 of the complex pier;	L
d_{sc2}	Equilibrium scour depth due to Configuration C2 of the complex pier;	L
d_{sc3}	Equilibrium scour depth due to Configuration C3 of the complex pier;	L
d_{sm}	Maximum scour depth measured at the end of the tests	L
ds_o	Observed value	-
ds_p	Predicted value	-
d_{spc}	Pile-cap contribution to the local scour depth	L
d_{spg}	Pile group contribution to the local scour depth	L
$\overline{ds}$	Mean value of ds_o	L
D_{10}	Sediment size for which 10%of the particles are finer	L
D_{16}	Sediment size for which 16%of the particles are finer	L
D_{30}	Sediment size for which 30%of the particles are finer	L
d_{50}	Median grain size of sediment	L
d_{50a}	Median grain size of sediment in armored bed	L
D_{60}	Sediment size for which 60%of the particles are finer	L
D_{84}	Sediment size for which 84%of the particles are finer	L
D_{100}	Sediment size for which 100%of the particles are finer	L
F_r	Froude number	-
F_L	Extension length of pile cap face out from column face	L

List of Symbols

Symbol	Title	Dimension
f_p	Longitudinal extension length of pile cap face out from the nearest pile front face	L
f_t	Extension width of pile cap face out from column face	L
g	Acceleration due to gravity	LT^{-2}
H_c	Column position (distance from the initial bed level to the bottom surface of the column)	L
H_{pc}	Distance between the bed and the bottom of the pile cap after column scour component has been computed;	L
H_{pg}	Distance between the bed and the top of the pile group after pile cap scour component has been computed;	L
h	Approach flow depth	L
h_e	Effective head over the crest of the weir	L
h_1	Head over weir	L
ISO	International Organization for Standardization	-
K	Permeability	L^2
K_a	Roughness effect of sidewalls	-
K_{bc}	Bed forms factor	-
K_c	Channel alignment factor	-
K_d	Sediment coarseness factor	-
K_h	Correction factor for head over the weir	-
K_{hD}	Depth-pier size factor	-
K_I	Flow intensity factor	-
K_r	Roughness of pier surface	-
K_s	Pier shape factor	-
K_{sc}	Column shape factor	-
K_{sp}	Pile shape factor	-
K_{spc}	Pile-cap shape factor	-
K_w	Wide piers factor	
K_{yb}	Foundation size factor	-
K_α	Alignment factor	-
K_σ	Uniform and non-uniform factor	-
L_c	Column length	L
L.L %	Liquid limit	-
L_p	Pile length	L
L_{pc}	Pile-cap length	L
MAE	Mean absolute error	-
MSE	Mean square error	-
m	Number of piles in line with flow	-
n	Number of piles normal to the flow	-

List of Symbols

Symbol	Title	Dimension
P.L %	Plastic limit	-
p_1	Distance between the channel bed and the apex of the triangular weir	L
Q	Total discharge	L^3T^{-1}
R^2	Coefficient of determination	-
RMSE	Root mean square error	-
R_p	Pier Reynold number	-
S_o	Channel bed slope	-
Sec	Second	T
S_m	Pile spacing in the direction m (centerline-to-centerline)	L
S_n	Pile spacing in the direction n (centerline-to-centerline)	L
SPSS	Statistical Package for the Social Sciences	-
T	Pile-cap thickness	L
t	Duration of flow	T
t_e	Time taken to reach the equilibrium scour depth	T
T.S.S %	Total Suspended Salts	-
USBR	United States Bureau of Reclamation	-
V	Mean velocity of approach flow	LT^{-1}
V_a	Armor Peak Velocity	LT^{-1}
V_c	Mean velocity at threshold motion of sediment for approach flow	LT^{-1}
V_{*c}	Critical threshold shear velocity	LT^{-1}
V_{*ca}	Mean critical velocity in armored bed	LT^{-1}
W.C	Water content	-
α	Complex pier alignment angle	°
μ	Dynamic viscosity of fluid	$ML^{-1}T^{-1}$
ρ	Density of fluid	ML^{-3}
ρ_s	Density of sediment	ML^{-3}
σ_g	Geometric standard deviation of sediment	-
θ	Laboratory temperature	°C
Ø	Angle of static sediment repose	°
°	Degree	-

List of Figures

List of Figures

List of Figures

List of Tables

CHAPTER ONE

INTRODUCTION

Chapter One

Introduction

1.1 General

From the beginning of history, the means of transportation seem to have been considered the most important factor in the progress of civilization. Since then humanity has needed to build bridges to span water bodies, mountains and roads, for the purpose of providing its passage.

Scour is used here to mean lowering the level of the riverbed by erosion such that there is a tendency to expose the foundations of a bridge. The occurrence of floods causes scouring of the riverbed material from the vicinity of piers and abutments is the common reason for the occurrence of bridge failure **(Hamil, 2000)**. The foundation of any hydraulic structure should be given the greatest importance in design and analysis as compared with other parts of the structure, because the foundation failure would destroy the whole structure. Local scour around bridge piers can cause a serious structural damage to a bridge by eroding the soil bed and destroys the foundation. Several modes of failure occur due to scouring at the pier's foundation such as pier tilt and even shear failure. Therefore, the accurate estimation of the scour depths around piers are essential for designing bridges or for evaluating the sensitivity of existing bridges **(Hussein and AlShukur, 2020)**.

Foundations of complex geometries structures are used to support bridge decks, as shown in Figure 1.1(a). Currently, two types of pier-foundations are used in new large-span bridges: (1) common complex piers (also named as pile-supported piers), which consist of a column founded on a pile cap supported by an array of piles, as outlined in Figure 1.1(b); and (2) special complex piers, which are characterized by non-conventional column and pile-cap geometries (*e.g.*, pile-supported piers

with multi-columns). According to **(Ettema et al., 2011)**, the scour depth at special complex piers should be estimated by hydraulic-models and/or numerical models. In this study, the term "complex piers" applies to pier geometries such as the configuration represented in Figure 1.1(b), *i.e.*, a column founded on a pile cap supported by piles.

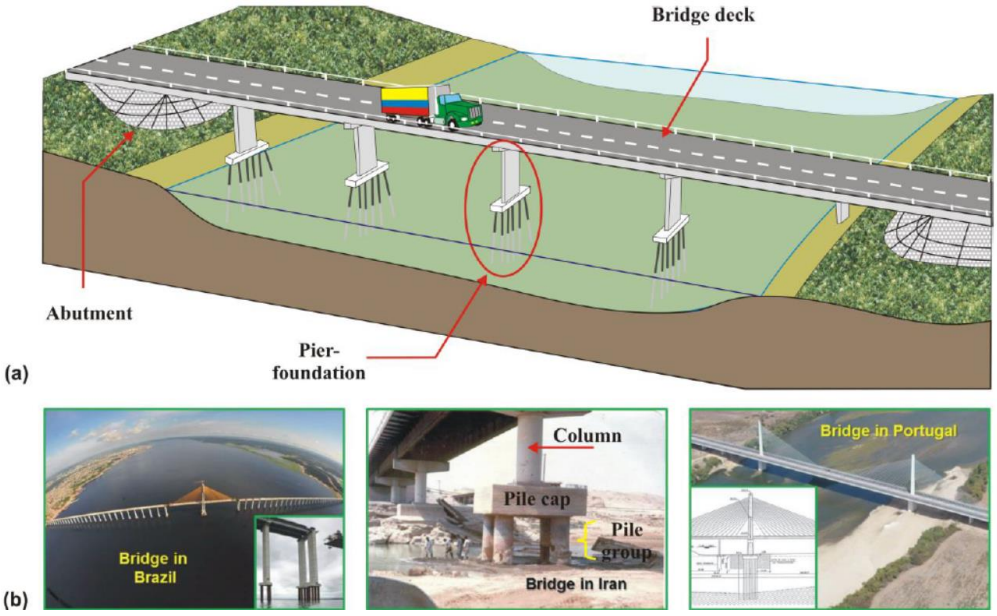

Figure 1.1: (a) scheme of basic bridge structure and (b) photographs of common complex piers **(Castiblanco, 2016)**.

Local scouring at complex piers requires and deserves additional research work since few experimental studies are reported in the literature by comparison with local scour studies at single piers. Those few that exist, by **(Martin-Vide *et al.*, 1998**; **Jones & Sheppard, 2000a**; **Sheppard & Glasser, 2004; Coleman, 2005; Ataie-Ashtiani et al., 2010; Grimaldi & Cardoso, 2010; Ferraro et al., 2013; and Amini et al., 2014)**. Some studies concerning local scour at pile groups, corresponding to the case of complex piers caped above the water surface, are reported in the literature. They include those of **(Hannah, 1978; Elliott & Baker, 1985; Salim & Jones, 1996; Smith, 1999; Zhao & Sheppard, 1999; Sumer & Fredsøe, 2002; Ataie-Ashtiani & Beheshti, 2006; Amini *et al.*, 2012; and Lança et al., 2013a)** some of which report on short-duration scour tests.

1.2 Statement of The Problem

Local pier scour is recognized to be the main reason for bridge failure in river environments **(Richardson & Davis, 2001)**. The development of a scour hole near the bridge pier may expose the bridge foundation to the river flow which may lead to undermine the bridge foundation and the bridge collapse. Many investigations have been conducted in the past decades to study the scouring process at the bridge pier. Most of these studies focused on the scouring at a single pier founded in cohesionless soil **(Devi & Barbhuiya, 2017)**. However, bridge piers can be found in different soils **(Ettema et al., 2011)**. Notable bridge failures were reported in the past few decades at which the piers were found in a clay and gravel bed. Thus, there is a need to address the effect of sediment particles on the local scouring depth at a bridge pier.

In recent practice, many of designed bridges have wide-spans and thus, a complex of piers rather than a single pier is used to support the superstructure. The scour processes at complex piers are more complicated because of the interaction of the flow patterns and consequently, the scour pattern differs from that for a single pier. The effects of interaction, alignment, skew-angle, and pile-cap position to initial bed on the local scouring at a complex piers found in different Iraqi soils were not described yet. Therefore, this thesis is an attempt to fulfill this research gap.

1.3 Aim of The Study

The present study aims to investigate experimentally the local scour patterns, maximum scour depth, equilibrium scour depth, and the effect of pile-cap position to initial bed at complex bridge piers aligned and skew-angle to the flow direction; founded in different soils in Iraq at various velocities.

1.4 Objectives

The main objectives of this study are to contribute to the understanding and characterization of local scour around complex bridge piers aligned and skew-angle for different Iraqi soils with the approach flow under clear-water conditions. These objectives are detailed as follows:

1. Understand in more detail the flow structure; scour mechanisms; and conduct detailed experimental on clear water local scour aligned and skew-angle to the flow direction around complex bridge piers, form bridges sites for different Iraqi soils;
2. Estimate the field scour depth based on evolution of local scour depth and consideration of scaling from model to prototype data;
3. Characterize and describe the effects of discharge, pier skew-angle, pile-cap position, and the pile-group configuration on the flow structure and maximum scour depth at complex piers for different Iraqi soils;
4. Estimate the complex pier components' contribution on the total local scour depth;
5. Assess and analyze the suggested equations to predict the local scour depth around bridge piers and to determine the important factors affecting around complex bridge piers, according to coefficient of determination R^2.

1.5 Limitations

1. One complex bridge pier, provided that the array group of piles does not exceed more than (3×4).
2. The flume width should be at least ten times the pier width.
3. Clear water conditions $V/V_c < 1$.
4. The flow rate supplied 18 lit/s.

5. The time of equilibrium scour depth is 24 hours.
6. The flow is subcritical.

1.6 Thesis Layout

The study contains of six chapters as follows:

Chapter two covers theoretical concepts and literatures review of studies with regard to complex bridge piers scouring, the effect of different soil types in Iraq, piers aligned and skew angle on flow pattern. Chapter three explains the details of experimental setup. Experimental procedure and description of the flume are also shown. Chapter four the experimental results, analysis is presented and discussed. Chapter five the prediction of equilibrium scour depth. Conclusions are executed, and recommendations are suggested, in chapter six to attitude in further studies.

CHAPTER TWO

THEORETICAL CONCEPTS
&
LITERATURES REVIEW

Chapter Two

Theoretical Concepts and Literatures Review

2.1 General

The depth of pier foundation is one of the main requirements to design the bridge, this depth must be more than the maximum scour depth for the conditions resulting from 100-year flood **(Reza, 2012)**. The process of scouring in rivers and streams can result from natural phenomena or from man-made alterations (building of structures in the riverbed); both can produce effects over long reaches of the river or only locally. According to **(Breusers & Raudkivi, 1991)**, the river scour can be divided into general, constriction and local scour. General scour occurs in a river or stream as the result of natural processes irrespective of whether a structure is located there. Constriction scour occurs if a structure causes narrowing the water course or flood plain rechanneling. Local scour results directly from the impact of a structure on the flow. This scour, which is a function of the type of structure, is superimposed on the general scour and on the constriction scour. For river bridges, these structures refer to abutments and pier-foundations (that include the case of the single piers, compound piers, complex piers among others).

Scour may occur for two distinct sediment transport conditions: (1) under clear-water, *i.e.*, in the absence of sediment movement in the bed of the approach channel; and (2) under live-bed, *i.e.*, when generalized movement of the bed sediment occurs in the approach flow. The first condition corresponds to the bed shear stress being smaller or, at most, equal to the critical bed shear stress to beginning of sediment motion whereas for the second condition the bed shear stress is higher than the critical bed shear stress **(Castibanco, 2016)**.

This chapter attempts to present the theoretical concepts of the scour depth bridge pier, type of scour, the mechanism of scour, basic of sediment transport, factors affecting, equilibrium of scour depth. Finally, a review of some previous studies of local scour around the bridge pier are also presented.

2.2 Characteristics of Flow around a Bridge Pier

Bridge pier scour is one type of local scour which manifests itself as a scour hole around a bridge pier caused by sediment transport that is driven by the local flow structure induced by a bridge pier; therefore, it is necessary to be acquainted with the flow structure and the related scour mechanisms around a bridge pier **(Al-Quraishi and AlShukur, 2016)**. In general, the local flow structure around a bridge pier consists of the down-flow at the upstream face of the pier in the vertical plane. The horseshoe vortex system that wraps around the base of the pier which is the primary contributor to local scour upstream of the pier, the bow wave near the free surface on the upstream face of the pier, and the wake vortex system at the rear of the bridge pier that extends over the flow depth as shown in Figure 2.1. These features greatly complicate the understanding of the local flow structure **(Dey, 1996)**. The comprehensive effect of this complex flow structure is to increase the local sediment transport resulting in local scour around a bridge pier.

Open channel flow, a boundary layer flow, approaches a bridge pier and the velocity becomes zero on the upstream face of the bridge pier. The resulting stream wise adverse pressure gradient causes separation of the boundary layer and the formation of a horseshoe vortex system that wraps around the pier at its base. The stagnation pressure on the nose of the pier decreases with the distance below the free surface due to the non-uniform velocity distribution in the boundary layer resulting in a weak pressure

gradient along the upstream surface of the bridge pier that drives the downward flow. The downward flow increases from the free surface to a point near the bed where the magnitude of downward flow becomes maximum with a velocity that is approximately 40% of the mean approach flow velocity. This downward flow produces a reverse bottom current near the bed which encounters the approach channel flow at some distance from the nose of the bridge pier, where there occurs a stagnation point. In the region where a very thin layer of reverse flow occurs, bimodal velocity distributions are shown to exist from the histogram of longitudinal velocity fluctuations **(Simpson, 2001)**.

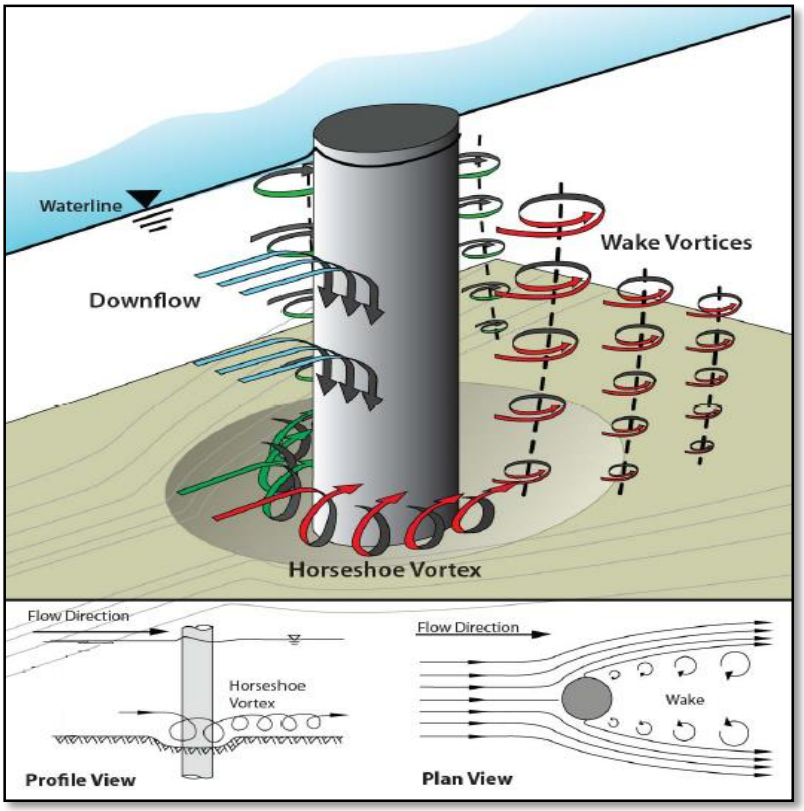

Figure 2.1: Schematic drawing of local scour processes at a cylindrical pier (**U.S. Federal Highway Administration, 1990**).

Due to the strong adverse pressure gradient imposed by the bridge pier in the stream wise approach flow direction, the boundary layer separates upstream of the bridge pier. In the separated region, several vortices are consecutively developed and subsequently stretched around

the base of the bridge pier giving rise to what is called a horseshoe vortex system. The primary horseshoe vortices rotate in the same sense as the approach boundary layer vorticity, but secondary vortices have the opposite rotation to preserve streamline topology. During the time that the horseshoe vortex nearest the bridge pier is decreasing in size due to stretching, a newer and younger secondary separation vortex is induced upstream of the primary vortex. The size and strength of the secondary horseshoe vortex increases with time while the size of the primary vortex continues to be reduced by stretching. At some time, the secondary and smaller vortices merge with the primary horseshoe vortex or leapfrog it to strengthen the primary horseshoe vortex, which is finally stretched completely around the bridge pier temporarily stabilizing the flow. Subsequently, instability occurs and the primary vortex forms again. The process is then repeated irregularly **(Dargahi, 1989)**.

A bow wave is generated when the upward flow forms a circulation near the free surface that causes the flow depth to increase in front of a bridge pier **(Dargahi, 1989; Melville and Raudkivi, 1977; Simpson, 2001)**. It is noted that a bow wave does not dominate the local pier scour mechanism unless the flow depth is too shallow and about equal to the sum of the diameters of a horseshoe vortex and a bow wave. As the flow depth decreases and the horseshoe vortex and the bow wave interfere with each other, the horseshoe vortex is still maintained; however, the down-flow is interrupted and becomes weaker.

The wake vortex system is formed by the rolling up of the unstable shear layers generated at the surface of the pier which are detached from either side of the pier at the separation line behind the pier. The wake vortex system acts like a vacuum in removing the bed material which is then carried downstream by the eddies shedding from the pier. Since the

turbulence intensity increases, erosion and transport of bed materials is intensified **(Breusers et al., 1977)**.

2.3 Local Scour around Complex Bridge Piers

2.3.1 Flow Structure

At complex piers, the flow structure and its interaction with the mobile bed are rather more complex than at single piers. Numerous studies have been performed to examine the flow structure around single piers (cylindrical shape mostly), while few studies are known for the case of complex piers. Some researchers studied the flow structure around pile groups, corresponding to complex piers caped above the water surface. The studies included those of **(Hannah, 1978; Ataie-Ashtiani and Aslani-Kordkandi, 2012; Movahedi et al., 2013; and Chang et al., 2013)**. According to those studies, scour around pile groups is caused by two types of flow structures: (1) those causing local scour at individual piles, *i.e.*, down-flow, horseshoe vortex, wake vortices and the bow wave; and (2) those due to the interaction of the different piles. According to **(Hannah, 1978)**, four mechanisms that are not present in scouring at single piers were identified in pile groups:

1. Scour reinforcement: The flatter bed topography induced by the rear piles may facilitate the mobility of upcoming bed grains, thus reinforcing the scour depth at the upstream piles, as compared with the scour depth at an isolated equal diameter pier. This effect tends to attenuate as the pile spacing increases.
2. Sheltering: The presence of an upstream pile can cause a reduction of the effective approach velocity for downstream piles, weakening the strength of the associated horse-shoe vortices and reducing the scour depth at downstream piles. As pile spacing increases the sheltering effect tends to become negligible.

3. Wake vortices interaction: The vortices from the upstream piles are convected downstream and may interact with the rear piles. In this case, the interaction of wake vortices may lead to a downstream increase in sediment entrainment capacity. The scour increase caused by this phenomenon depends on the convection speed of the vortices and the distance between their path and the piles. At specific skew-angles, the rear piles are closer to the most energetic paths traced by the wake vortices from the front piles and scour increases.
4. Compressed horse-shoe vortices: In pile group alignments with at least two columns of piles transverse to the approach flow, except at very close spacing, each pile has its own horseshoe vortex. As pile spacing decreases, the inner arms of the horse-shoe vortices are compressed, velocities within the arms increase and scour depths tend to increase.

Figure 2.2 shows a present author interpretation of the flow structure and local scour around a pile group in a scoured-bed according to previous descriptions.

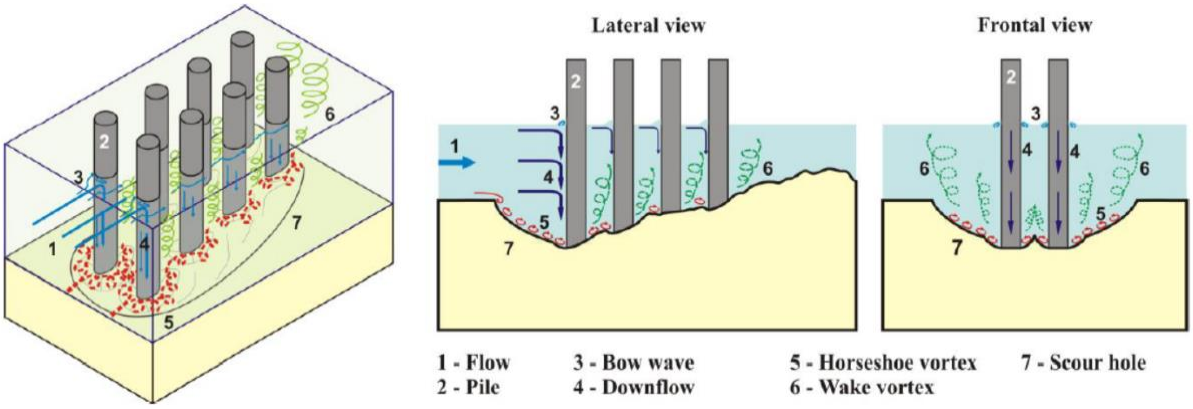

Figure 2.2: Scheme of flow structure and local scour around pile groups **(Kumar et al., 2012)**.

(Veerappadevaru et al., 2011, 2012; and Kumar et al., 2012) studied the flow structure around cylindrical columns founded on cylindrical caissons. The results of these studies show that the scour depth depends on the temporal vortex strength. In the cases where the caisson is

partially buried in the initial bed level, the scour hole is formed in front and around the caisson pier by vortices wrapping around it. Two main vortices exist upstream from the caisson pier (primary and secondary vortex), as illustrated in Figure 2.3. The primary vortex causes scour near the caisson pier and the scoured sediment is transported either as suspended or as bed load towards the tail water. The secondary vortex supports the steep slope of the scour hole and transports most dislodged sediment sideways but few are entrained by the primary vortex **(Veerappadevaru et al., 2011)**.

Figure 2.4 shows a present author interpretation of the flow structure around a complex pier based on previous descriptions of flow structure around pile groups, single piers with debris and pier-caissons.

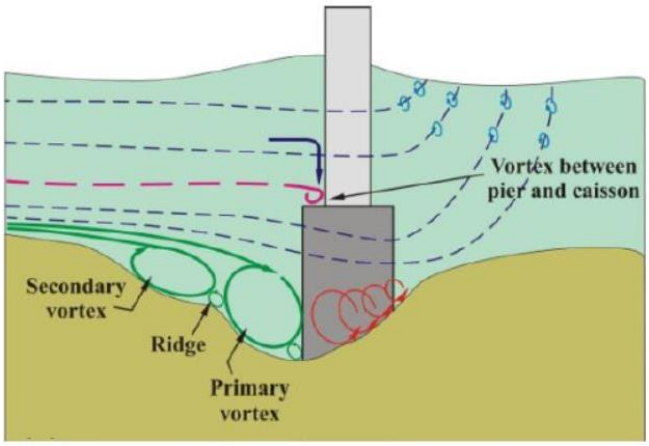

Figure 2.3: Flow structure around pier with caisson **(adapted from Veerappadevaru et al. 2011)**.

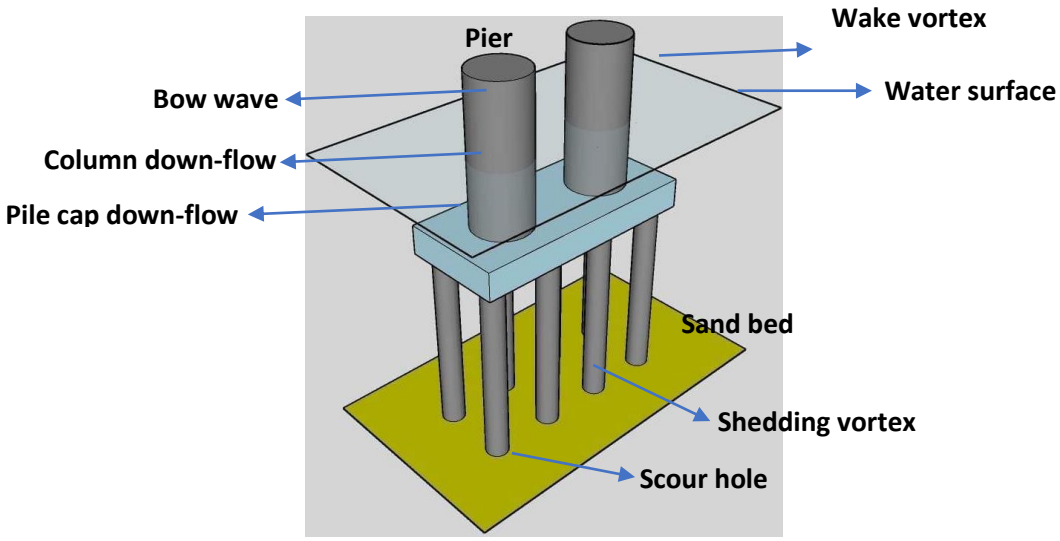

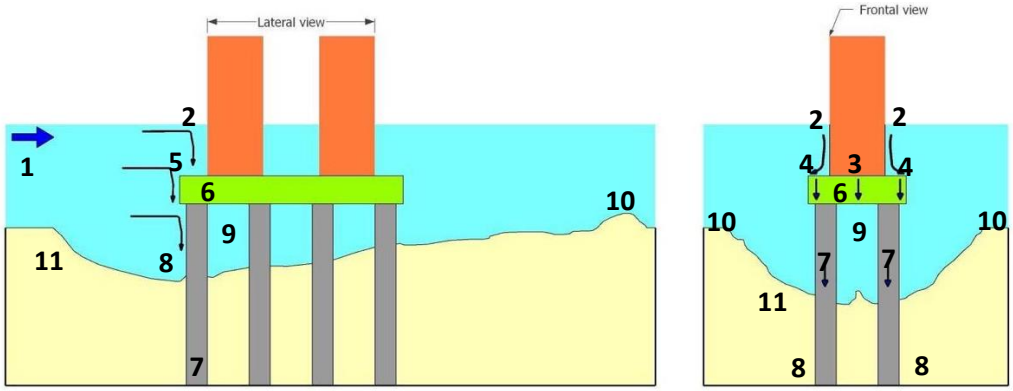

1 Approach flow
2 Bow wave
3 Column down-flow
4 Deflected flow
5 Vortex between column and pile cap
6 pile cap down-flow
7 plie down-flow
8 Horseshoe wave
9 Shedding wave
10 wake vortex
11 Scour hole

Figure 2.4: Scheme of the flow structure around complex piers.

(Ataie-Ashtiani et al., 2010) studied the flow field around a complex pier positioned on a rough fixed bed with all components exposed to the approaching flow. They found that: (1) the approaching boundary layer upstream the pile cap is separated into two vertical opposite directions, inducing an upward flow towards the column and a contracted downward flow below the pile cap and toward the piles; (2) the upward flow on the pile cap interacts with the down-flow in front of the column and deflects it towards the side of the pier; and (3) the flow at the rear of the pile cap is very complex, as the flow is simultaneously expanded to different directions. Some of those flow interactions are also represented in Figure 2.4.

2.3.2 Time Evolution of Scour Depth

(Melville and Raudkivi, 1996) studied non-uniform piers comprising a cylindrical column of diameter D_c founded on a larger cylinder of diameter D_{pc} and concluded that the temporal development of the scour hole is dependent on the ratio D_c/D_{pc} and on the depth from the

initial bed level to the top of the foundation. **(Sousa, 2007; Ataie-Ashtiani et al., 2010; Ferraro et al., 2013)** show that the scour depth evolution in complex piers follows different stages in comparison with single piers. That is associated with the progressive physical presence in the scour hole evolution of one, two or the three structural components of the complex pier. The duration and trend of the different stages depend on the geometry of the complex piers and on the pile-cap position relative to the initial bed level. **(Sheppard and Glasser, 2004)** suggested addressing the evaluation of local scour at complex piers considering three typical situations, which depend on the positioning of the pile cap. These situations are defined as:

- Situation 1 - characterized by the bottom of the pile cap being above the initial bed level. In this situation the following cases may occur where the pile cap under the water and its bottom surface above the bed, as shown in Figure 2.5(a).
- Situation 2 - characterized by the pile cap is placed close to the initial bed corresponding to cases where the bottom of the pile cap is levelled with the bed surface, as shown in Figure 2.5(b).
- Situation 3 - characterized by the pile cap being completely buried in the bed corresponding to cases where the top of the pile cap becomes apparent along the scouring process, as shown in Figure 2.5(c).

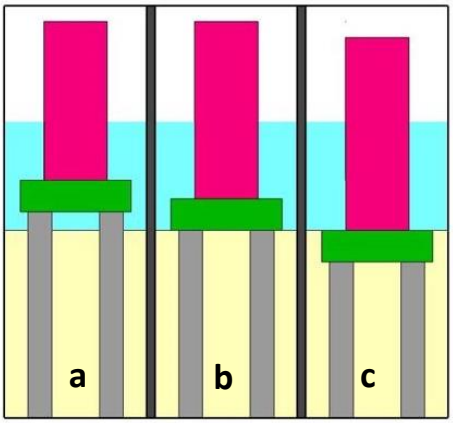

Figure 2.5: Complex pier situations as a function of the relative pile-cap position.

2.3.3 Equilibrium Scour Depth in Laboratory Tests

It can be assumed that the equilibrium scour exists and it is achieved in infinite time. Again the question is which one should be the minimum duration of the experimental tests, with complex piers, to achieve equilibrium conditions? In this regard, some authors **(e.g., Coleman, 2005; Melville et al., 2006; Ataie-Ashtiani et al., 2010)** suggest the same criterion proposed by **(Melville and Chiew, 1999)** for experimental tests with single piers. The mentioned authors use, as reference, the smaller value of 5% of the complex pier characteristic length (e.g., its equivalent pier diameter) and of the flow depth. In the case of pile groups, **(Lança et al., 2013a)** suggest that the duration of scour tests should be more than 7 days, which is the duration considered adequate for single cylindrical piers according to **(Simarro et al., 2011)**, since the scouring process can be expected to be more complex and slower.

2.4 Effects of Specific Parameters on maximum Local Scour Depth

2.4.1 Effect of Flow Intensity

As mentioned before, local scour can be developed in two different conditions of transport: 1) Live bed scour 2) Clear-water scour. **(Melville and Coleman, 2000)** state that, when flow intensity $V/V_c < 1$ for uniform sediments and $[V - (V_a - V_c)]/Vc < 1$ for non-uniform sediments, clear water scour conditions are present, where V_a is the mean approach velocity at the armor peak. In the case of live bed scour for uniform sediments, critical velocity is lower than the mean approach velocity ($V/V_c > 1$). Armoring process takes place on the riverbed and in the scour hole for non-uniform sediments, where the ratio V/V_a indicates the flow intensity **(Raudkivi, 1986; and Melville and Sutherland, 1988)**. It has to be said that armoring within the scour hole reduces the local scour depth. As a general rule, if V

$/V_a > 1$, live bed scour conditions occur; however, in the situation of $V/V_a < 1$ clear-water conditions pertain. The determinations of threshold velocity and armor peak velocity are given in the below equations **(Melville and Coleman, 2000)**:

Threshold Velocity, V_{*c}:

$0.1mm < d_{50} < 1mm$, $V_{*c} = 0.0115 + 0.0125 d_{50}^{1.4}$ **2.1**

$1mm < d_{50} < 100mm$, $V_{*c} = 0.0305 d_{50}^{0.5} - 0.0065 d_{50}^{-1}$ **2.2**

where V_{*c} for a given d_{50} can be also found from the Shield's diagram (see Figure 2.6). One should take d_{50} in mm to obtain V_{*c} in m/s. Mean critical velocity is obtained from Equation. 2.3.

$$\frac{Vc}{V*c} = 5.75 \log [5.53 \frac{h}{d50}] \quad \textbf{2.3}$$

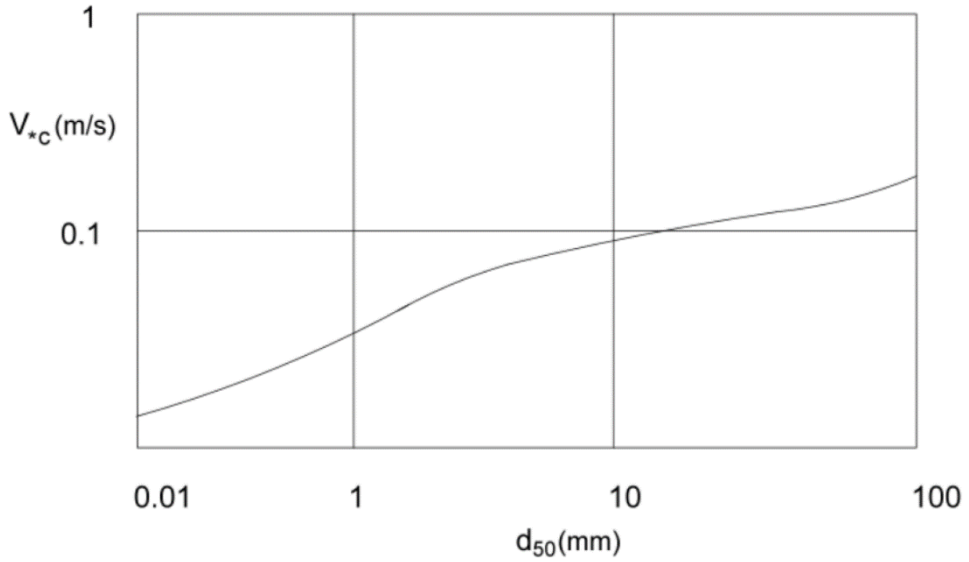

Figure 2.6: Determination of the critical shear velocity as a function of median sediment diameter **(Reproduced from Melville and Sutherland, 1988)**.

Armor Peak Velocity, V_a: σ_g: standard deviation h: flow depth

Armor peak velocity is valid only for $\sigma_g > 1.3$ (non-uniform sediments). Critical shear velocities in armored beds are obtained from Equations 2.4 and 2.5 **(Melville and Coleman, 2000)**.

$0.1mm < d_{50a} < 1mm$, $V_{*ca} = 0.0115 + 0.0125 d_{50a}^{1.4}$ **2.4**

$1mm < d_{50a} < 100mm$, $V_{*ca} = 0.0305 d_{50a}^{0.5} - 0.0065 d_{50a}^{-1}$ **2.5**

where $d_{50a} = \frac{dmax}{1.8}$ **2.6**

Mean critical velocity in armored bed is:

$$\frac{Vc}{V*ca} = 5.75 \log [5.53\frac{h}{d50a}] \quad \textbf{2.7}$$

$V_{*ca:}$ mean critical velocity in armored bed.

Finally, $V_a = 0.8V_{ca}$ **2.8**

Figure 2.7 presents the variation of local scour depth with flow intensity **(Melville and Coleman, 2000)**. As velocity increases until the threshold velocity, local scour depth advances linearly under clear-water scour conditions. As the velocity passes the critical velocity, condition of transport is turned into live bed scour. Firstly, local scour depth decreases slightly and later increases again to second peak (live bed peak). The second peak is smaller than the threshold peak because, the total strength of the flow is used to scour the base of the pier. However, in the case of live bed scour, the strength of the flow is used to scour the pier foundation and transport the sediment **(Yanmaz, 2002)**.

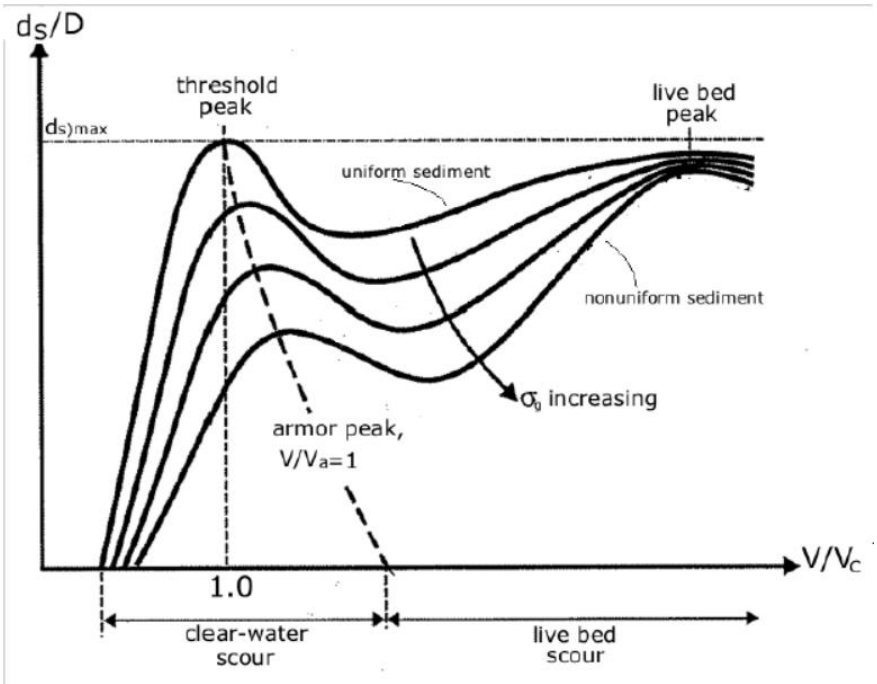

Figure 2.7: Local scour depth variation with flow intensity **(Reproduced from Melville and Coleman, 2000).**

2.4.2 Effect of Sediment Grading

(Raudkivi and Ettema, 1983) have studied the effect of sediment grading on local scour depth at clear-water conditions. According to them, sediment grading substantially affects the scour depth. As long as standard deviation of sediment grading (σ_g) increases, armoring effect burst into prominence. Coarse particles spread over the fine particles, thus local scour depth reduces considerably. **(Yanmaz, 2002)** has obtained a regression equation, in an interval of $1.0 \leq \sigma_g \leq 5.0$, based on the correction factor (K_σ) given by **(Raudkivi, 1986)**:

$$K_\sigma = 0.013462\sigma_g^5 - 0.2232\sigma_g^4 + 1.4066\sigma_g^3 - 4.0864\sigma_g^2 + 5.007\sigma_g - 1.1179 \quad \textbf{2.9}$$

Considering the Equation. (2.9), the local scour depth in a non-uniform riverbed, where standard deviation of sediment grading is about 3.5 for a gravel river, decreases 80% when compared to the local scour depth in a river with uniform sediment **(Yanmaz, 2002)**. **(Melville and Sutherland, 1988)** summarize the results of the study made by **(Raudkivi and Ettema, 1977)**.

2.4.3 Time Effect

In case of clear-water scour conditions; average shear stress, weight of water and turbulence stresses create balance simultaneously. Thus, it takes a long time to reach the equilibrium scour depth **(Yanmaz, 2002)**. **(Yanmaz, 2002)** offers a regression equation for the variation of depth of scour with time according to his experimental study in specific conditions, as shown in Figure 2.20:

$$\frac{ds}{dse} = 0.12ln\left(\frac{t}{te}\right) + 1.0 \quad \textbf{2.10}$$

where d_{se} and t_e are equilibrium scour depth and time taken to reach the equilibrium scour depth respectively.

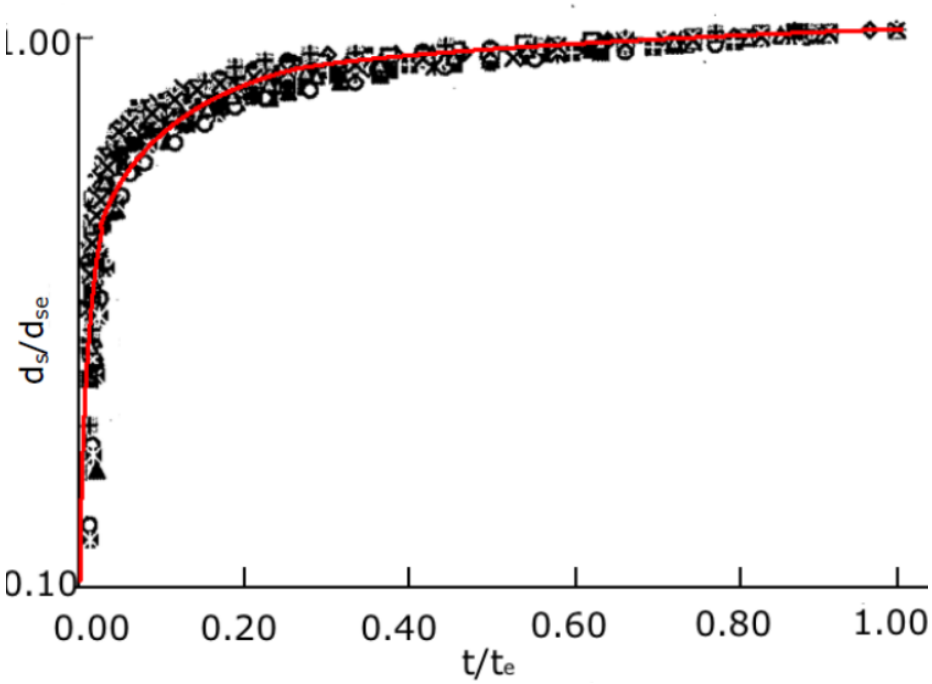

Figure 2.8: Temporal development of clear-water scour around a cylindrical pier **(Reproduced from Yanmaz, 2002)**.

As can be seen from Figure 2.8, the rate of scour development is higher in initial phase of the development; however, scour deepens slowly and reaches equilibrium asymptotically after a while.

(Melville and Coleman, 2000) represent a time factor for cylindrical bridge piers:

$$K_t = \exp\left(-0.03\left(\frac{Vc}{V}\ln\left(\frac{t}{te}\right)\right)^{1.6}\right) \qquad \textbf{2.11}$$

The value K_t is equal to 1.0 if there are live-bed conditions, because equilibrium depth of local scour is attained rapidly. Figure 2.9 shows the temporal development of local scour at circular bridge piers for various flow intensity values according to the laboratory studies done by **(Chiew**

and Melville, 1987) and **(Melville, 1997)**. It is obvious that the rate of the development is reduced at lower flow intensities.

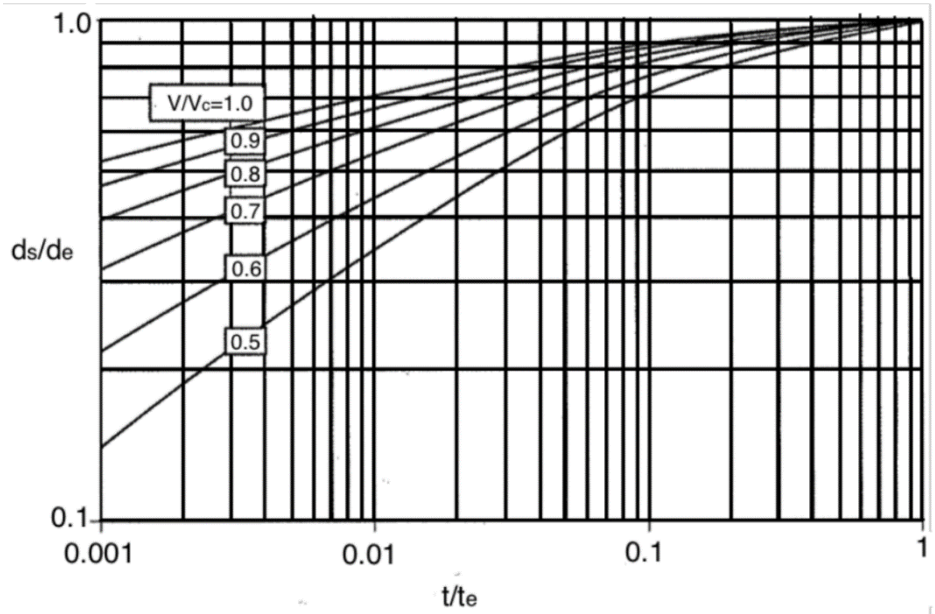

Figure 2.9: Temporal development of local scour depth at piers under clear-water conditions **(Reproduced from Melville and Coleman, 2000)**.

(Raudkivi, 1986) states that, 50 hours is needed to reach equilibrium scour depth in laboratory conditions for clear-water scour **(Yanmaz 2002)**. It is a very long time and makes studies harder for the researchers. As the trend of the development of scour hole is asymptotic, some researchers have decided on where to stop the experiments. **(Melville and Chiew, 1999)** have formalized the proposal as follows:

$$\frac{d(ds)}{dt} \leq \frac{0.05\,D}{24\,h} \qquad \textbf{2.12}$$

Where, D: pier diameter h: flow depth

From Equation 2.12, it can easily be said that when the development of scour hole does not exceed 5% of the pier diameter in 24 hours, the experiment is assumed to reach the equilibrium. **(Mia and Nago, 2003)** have expressed the issue in such a way that when the development of scour in 1 hour is less than 1mm, then the experiments can be stopped.

2.4.4 Effect of Pier Alignment

Another factor affecting the local scour depth is the pier alignment. As the alignment increases, the scour depth increases because depth of scour is the function of the projected width of the pier. Equation (2.13) gives the relation between projected pier width with the length and the width of the pier:

$$b_t = b\cos\alpha + L_p \sin\alpha \qquad \textbf{2.13}$$

Figure 2.10 shows the diagrammatic scour shapes at a pier aligned with flow and angled to the flow direction **(Breusers and Raudkivi, 1991)**. Only cylindrical piers are not affected by the pier alignment as long as they show same behavior for every alignment angle. The ratio of the length of the pier to its width directly affects the development of scour hole at the downstream side of the pier (Figure 2.11).

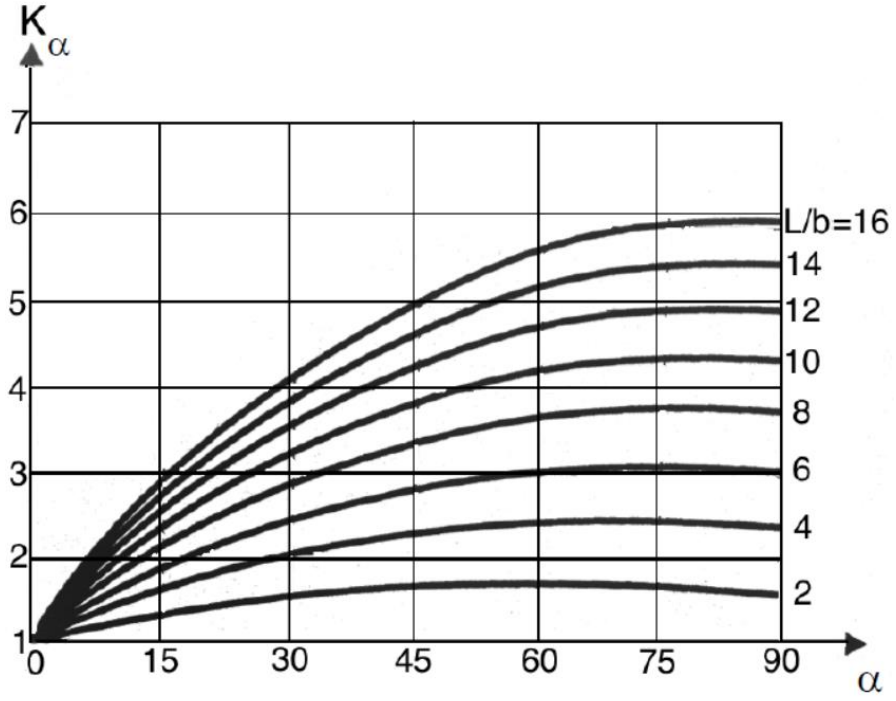

Figure 2.10: Alignment factor K_α for piers not aligned with flow **(Reproduced from Breusers and Raudkivi, 1991)**.

(Richardson and Davis, 2001) propose an alignment factor for non-cylindrical piers:

$$K_\alpha = (\cos\alpha + \frac{L}{b}\sin\alpha)^{0.65} \qquad \textbf{2.14}$$

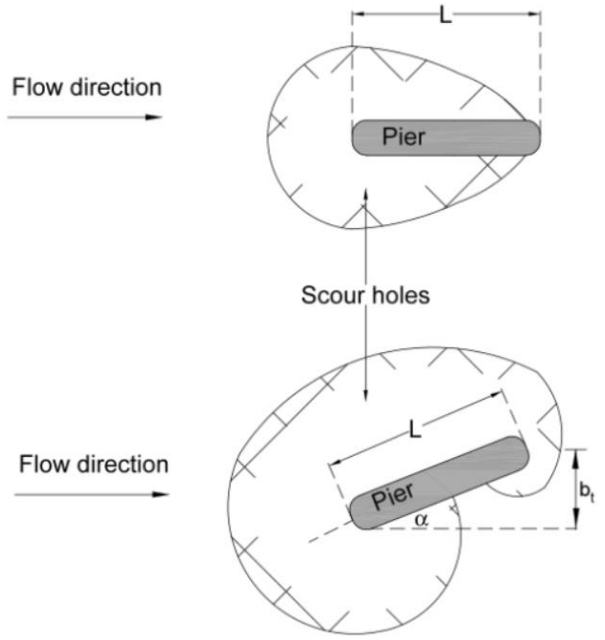

Figure 2.11: Diagrammatic scour shapes at a pier aligned with flow and another angled to the flow direction **(Breusers and Raudkivi, 1991)**.

(Breusers and Raudkivi, 1991) recommends that, angle of attack greater than (5-10)° should be avoided or row of cylindrical pier should be used to reduce or remove the negative effects of the alignment.

2.4.5 Group Effect of the Piers

According to the structural reasons, a group of piers that are arranged one after another rather than a massive pier can be constructed. In this case, negative flow conditions can occur because of the interference of the flow around piers. Group effect is generated by a group of piers, which are aligned in direction of flow and/or perpendicular to the flow. The group effect mainly depends on the distance between piers, direction and position of piers.

In literature, there are a few studies on bridge pier groups. **(Basak et al., 1975)** have studied rectangular bridge pier groups and improved their research by studying cylindrical pier groups in 1977. They have investigated local scour depth around cylindrical bridge pier groups by running various experiments as well as changing some parameters such as angle of attack and distance between the piers with a constant Froude number (Fr = 0.55). In the pier group composed of cylindrical piers of equal sizes arranged in a linear axis at equal distances, the variation of scour depth observed on all surfaces of each pier forming the group, depending on the distance between piers, pier size and number and the angle of attack of flow have been studied **(Basak et al., 1977)**.

When flow direction is parallel to the pier group axis ($\alpha = 0°$), the maximum scour depth takes place on upstream surface of the first pier, independent from number of piers forming the group; it is always equal to the individual scour of one single pier. The strength of flow reduces at rear piers because front piers are exposed to flow at first and they protect following piers against flow. In case of the flow direction forms an angle against the axis of the pier group ($\alpha > 0°$), the group effect tends to increase the scour depth and the scour becomes greater than that of an individual pier. Additionally, the flow approaching perpendicular to the pier group axis ($\alpha = 90°$), leads to an increase in maximum scour depth than that of a single pier **(Basak, 1977)**.

Based on the experimental results, **(Basak, 1977)** concluded that if $S/D > 40$, all the piers constituting the pier group act as a single pier when $\alpha = 0°$ and when $\alpha = 90°$, the pier group act as a single pier if $S/D > 7$. Separate scour holes are formed around them and group effect is not observed. As the distance between piers is very small in case of $\alpha = 0°$, i.e. $S/D = 1$, a large and a single scour hole is formed. Moreover, when the flow is perpendicular to the pier group axis $\alpha = 90°$, again a single hole is

generated covering all piers if *S/D = 0.5*. When the distance is between these limits, *S/D* < 40 for α = 0° and *S/D* < 3 for α = 90°, separate but interfered scour holes are developed. Parallel to what was mentioned above, **(Basak, 1977)** also stated using a group of piers rather than a single massive pier, reduces the development of local scour depth.

(Hannah, 1978) has studied the same subject with specific conditions and achieved some results showing the group effect. He found that the local scour depth at the downstream side of the rear pier is smaller than the scour depth around a single pier. According to **(Yanmaz, 2002)** the main reason is the transportation of the bed material from the scour hole of upstream pier to the scour hole at the downstream pier partially.

A more recent study made by **(Salim and Jones, 1999)** focused on determining scour depths for pier groups by taking into consideration the spacing between the piers, the number of pier rows and a height factor for the pier length exposed to the flow **(Richardson and Davis, 2001)**.

The study made by **(Vittal et al., 1994)** considered a group of three smaller circular piers, which have an angular spacing of 120°, as a scour-reduction device. They have run the experiments in different orientations (Figure 2.12). They compared the local scour formation around a single pier whose diameter is equal to the circumscribing circle diameter of the pier group with the results from this group. Scour reduction of pier group is about 40% when compared to the local scour around solid pier. Moreover, maximum variation in scour depth due to the orientation is about 6%. The 30° orientation is considered as the best orientation and the 60° orientation resulted in maximum scour depth.

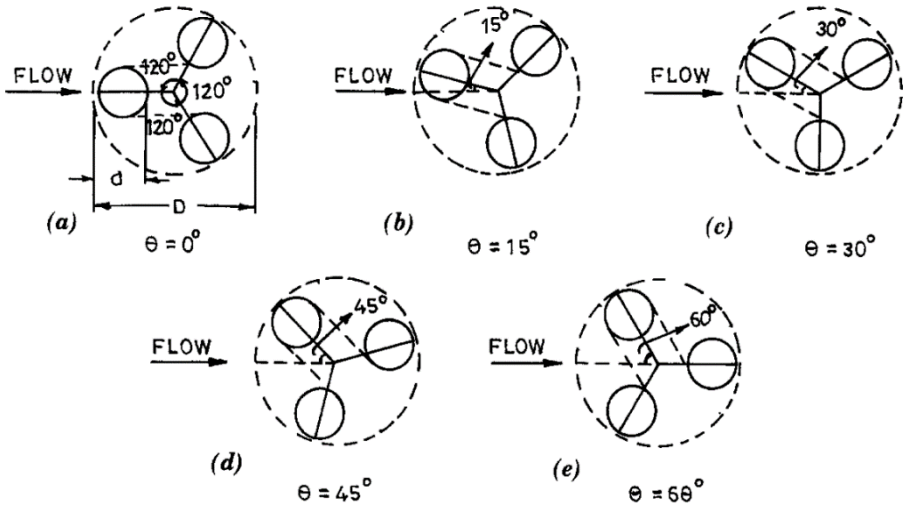

Figure 2.12: Approach flows: a) 0°; b) 15°; c) 30°; d) 45°; and e) 60° **(Reproduced from Vittal et al. (1994)**).

2.5 Scour Mechanism at Vertical and Skewed-Angle Piers

The scour mechanism of a bridge pier is very complex, the pattern flow near a bridge pier is increased and complicated as a scour hole around the development of pier **(Bozkus, 2004).**

The concepts of mechanism originating the local scour around bridge piers due to an obstruction is placed in the flow field, so the system of vertices developed around the pier. The primary cause of the scour round the bridge pier is horseshoe and wave vortices developed. The vortex of horseshoe is getting the velocities near the bed, due to increase the flow capacity to transport sediment. The vortex of wave remains the sediment in suspension condition, its acts as (vacuum cleaner), the eddies shaded transport the bed sediment to the downstream side from the pier **(Zarrati, 2010).**

In front of a pier the flow separated from the bed and rolls up to a form of a scouring vortex, the horseshoe vortex at the base of the pier, wave vortex at the downstream of the pier, and the surface roller at the upstream of the pier.

The approach flow is decelerated against the pier's centerline, there is generation of a downward pressure gradient along the pier's leading face that causes the down - flow with a fully turbulent shear flow. The flow contracts as it passes around the sides of the piers with increase in flow velocity and bed shear stress. Thus the scour begins at the side of a pier, and the high velocity washes the excavated bed materials to the downstream side **(Shrestha, 2015).**

Also, there is rise in the water surface at the upstream side of the pier, the rise in water surface depends on the shape of pier, skew - angle of the pier, and approach velocity. The pier flow field depends on the width of the pier (D_p) and the depth of flow (h) **(Ettema et al., 2011).**

At the skewed piers the mechanism of scour is complex not only because of increase in the scour depth and extents the lateral of the scour may become so large that the vicinity of the pier can be affected, thus there is a complication in prediction of local scour depths.

The description of mechanism scours has three stages:

1. The initial stage: for $\alpha = 0°$, local scour begins in front of the pier at locations approximately $\pm$ 45° to the direction of flow. For skewed piers the local scour begins at different locations. For $\alpha < 45°$, the scour hole formed at the upstream corner, while for $\alpha \geq 45°$, two small scour holes were formed at locations upstream and downstream of the pier corners and a small hump was observed between the two initial scour holes. The horseshoe vortex was initially small and played a minor role in the erosion during the initial phase of local scour. Due to pressure gradients, the down flow near the base of the pier was deflected to both sides of the pier.

2. The main erosion stage: the horseshoe vortex rapidly grew in size and strength as it settled into the developing scour hole. The down flow was directed to the base of the scour hole. For skew-angle, $\alpha < 45°$, a scour hole formed at the upstream end of the pier where the maximum shear

stress occurred due to change in the flow direction. while for $\alpha > 45°$, two scour holes were formed at locations upstream and downstream of the pier corners. For skew-angle, $\alpha = 45°$, two scour holes where formed during the initial stage and became larger in area. The hump that was situated near the middle of the pier length.

3. The equilibrium stage: The maximum scour depth depended on the skew-angle, the scour hole extended along the entire length of the pier. For $\alpha < 45°$, the scour hole was deepest at the upstream pier end. For $\alpha \geq 45°$, the scour hole was deepest at the downstream pier end. **(Ahmed et al., 2016 and Lanca et al., 2012)**, as shown in Figure 2.13.

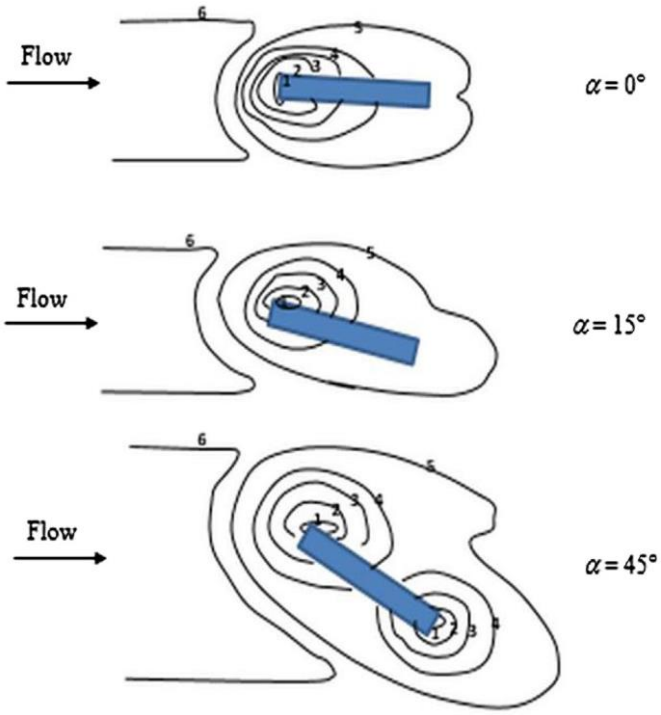

Figure 2.13: Development of scour hole around rectangular piers skewed at different angles of attack **(Ahmed, et al., 2016).**

2.6 Methods for Estimation of Local Scour Depths

2.6.1 Sand Bed Materials

2.6.1.1 Auckland Method

The Auckland design method for complex piers was initially proposed by **(Melville and Coleman, 2000)** based on the concept of the equivalent pier diameter, D_e, introduced by **(Melville and Raudkivi, 1996)** (on a study of cylindrical columns founded on cylindrical caissons). These authors defined D_e as the diameter of a single pier that would induce the same scour depth as the actual non-uniform pier, for the same flow and sediment. **(Melville and Coleman, 2000)** suggested that the equilibrium scour depth at complex piers may be calculated using the equation developed by the same authors for single piers, which reads,

$$d_s = K_{hD}\, K_I\, K_d\, K_s\, K_\alpha \qquad \textbf{2.15}$$

where d_s =equilibrium scour depth; K_{hD}, K_I, K_d, K_S and K_α are the factors that account for the depth-pier size, flow intensity, sediment coarseness, pier shape, and pier alignment, respectively. Variables d_s and K_{hD} correspond dimensionally to a length, while the other K_S = foundation shape factor and D_e is used instead of D.

The depth-pier size factor can be expressed by the following expression:

$$K_{hD} = \begin{cases} 2.4D & \text{for } \frac{h}{D} > 1.43 \\ 2\sqrt{Dh} & \text{for } 0.2 < \frac{h}{D} < 1.43 \\ 4.5h & \text{for } \frac{h}{D} > 0.2 \end{cases} \qquad \textbf{2.16}$$

where D = single pier width; h = flow depth directly upstream of the pier.

The flow intensity factor can be expressed by the following equation:

$$K_I = \begin{cases} \frac{V}{Vc} & \text{for } \frac{V}{Vc} < 1 \\ 1.0 & \text{for } \frac{V}{Vc} \geq 1 \end{cases} \quad \textbf{2.17}$$

where U = mean velocity of flow directly upstream of the pier; Uc = critical flow velocity.

The sediment coarseness factor can be expressed by the following equation:

$$K_d = \begin{cases} 0.57 \log (2.24 \frac{D}{d50}) & \text{for } \frac{D}{d50} \leq 25 \\ 1.0 & \text{for } \frac{D}{d50} > 25 \end{cases} \quad \textbf{2.18}$$

where d_{50} = median size of sediment particle size distribution.

The pier shape factor for cylindrical shape, K_S should be considered as 1.0. The pier alignment factor can be calculated by equation 2.14. where α = pier alignment angle; L and D are the dimensions of the pier. For circular piers, K_α=1.0. If L/D is larger than 12, the value of L/D = 12 should be used in equation 2.14. The Auckland method provides higher values of factor K_I for clear-water conditions and it does not consider the reduction effect on factor K_d for D/d_{50}>100.

(Coleman, 2005) reformulated the initial procedure by considering that D_e depends on the column position relative to the initial bed level, H_c. This author uses expressions previously published in the literature for piers with different types of foundations (*e.g.*, pile groups, pile groups, and pile caps) to calculate the corresponding value of D_e.

Equations adopted by **(Coleman, 2005)** to estimate De are:

$$D_e = D_c \quad \text{for } H_c \leq D_c \quad \textbf{2.19}$$

$$D_e = D_c \left[\left(\frac{Dc}{Dpc}\right)^{\left(\frac{Dc}{Dpc}\right)^3 - 0.307} \right] \quad \text{for } H_c = 0 \qquad \textbf{2.20}$$

$$D_e = D_c \left[\left(\frac{Dc}{Dpc}\right)^{\left(\frac{Dc}{Dpc}\right)^3 + 0.10 - 0.47\sqrt{0.75+\frac{Hc}{Dc}}} \right] \quad \text{for } 0.5T \geq Hc > 0 \qquad \textbf{2.21}$$

$$D_e = \left[\frac{0.52T\ Dpc + (h - 0.52T) Depg}{h} \right] \quad \text{for } H_c = h \qquad \textbf{2.22}$$

$$D_e = \left[\frac{0.52T* Dpc + (h - 0.52T*) Depg}{h} \right] \quad \text{for } h+T \geq H_c > h \qquad \textbf{2.23}$$

$$D_e = D_{epg} \quad \text{for } Hc \geq h+T \qquad \textbf{2.24}$$

where, D_{epg} = equivalent diameter of the pile group, $T_*=h-(H_c-T)$ = distance of the pile-cap thickness that remains in the flow when it is partially immersed in the flow.

2.6.1.2 FDOT Method

In accordance with **(Sheppard *et al.*, 2004)** and **(Sheppard and Renna, 2010)** the equilibrium scour depth at complex piers can be calculated by equation (2.26). They suggest that the scour depth associated with each pier component can be evaluated as the scour depth at one equivalent single cylindrical pier that would induce the same scour depth as that pier component, for the same sediment and flow conditions, as illustrated in Figure 2.14. This, in turn, depends on pier shape, size, location and alignment relative to the flow direction as well as on flow characteristics and sediment properties. The equivalent diameter of the

complex pier, D_e, can be approximated by the sum of the equivalent diameters of the complex pier components, thus:

$$D_e = D_{ec} + D_{epc} + D_{epg} \quad \textbf{2.25}$$

where D_{ec}= equivalent diameter of the column; D_{epc}= equivalent diameter of the pile cap; D_{epg}= equivalent diameter of the pile group.

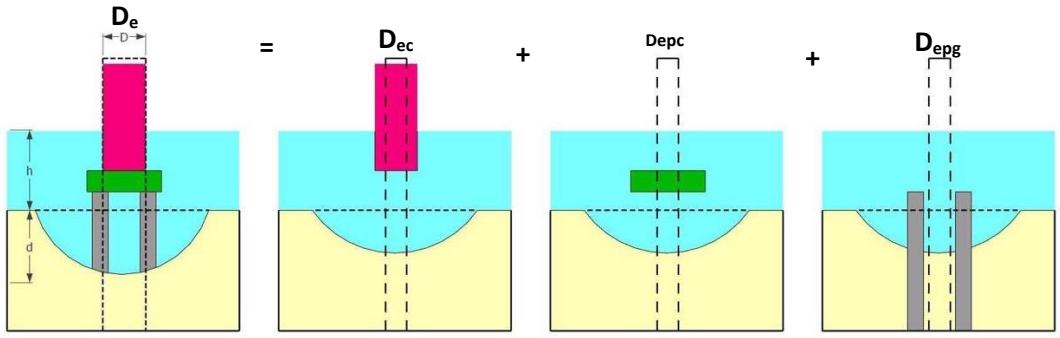

Figure 2.14: Conceptual hypothesis if summing equivalent diameters, adapted from Sheppard and Renna (2010).

(Sheppard and Renna, 2010) analyzed three configurations of complex piers, according to the pile-cap position. The first configuration is characterized by the fact that the bottom of the pile cap is above the initial bed level, the second configuration corresponds to the pile cap being close to the bed, and the third configuration is represented by the pile cap completely buried in the bed.

$$\frac{ds}{b} = 2.5 \tanh\left[\left(\frac{d}{b}\right)^{0.4}\right]\left\{1 - 1.2\left[\ln\left(\frac{V}{Vc}\right)\right]^2\right\} \times \left\{\frac{\frac{b}{d50}}{0.4\left(\frac{b}{d50}\right)^{1.2} + 10.6\left(\frac{b}{d50}\right)^{-0.13}}\right\}$$

$$\text{For } 0.4 \leq \frac{V}{Vc} \leq 1 \quad \textbf{2.26}$$

2.6.1.3 HEC-18 Method

The HEC-18 design method for complex piers was suggested by **(Richardson and Davis, 2001)** and revised by **(Arneson *et al.*, 2012)**. According to this predictor, a superposition approach, comprising the conceptual separation of the pier components (*i.e.*, column, pile cap and

pile group) represented in Figure 2.15 and the determination of the scour depths for individual components is adopted. This approach was suggested by **(Jones and Sheppard, 2000a)**.

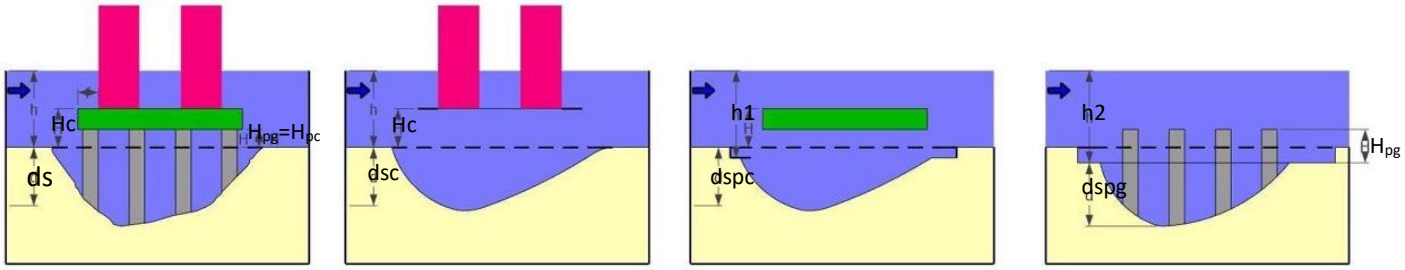

Figure 2.15: Conceptual hypothesis for superimposing scour components, adapted from **(Jones and Sheppard, 2000a)**.

The total scour depth from superposition of components is given by:

$$d_s = d_{sc} + d_{spc} + d_{spg} \qquad \textbf{2.27}$$

where d_s = total equilibrium scour depth, d_{sc} = column contribution to the local scour depth, d_{spc} = pile-cap contribution to the local scour depth and d_{spg} = pile-group contribution to the local scour depth.

$$\frac{ds}{D} = 2K_s\, K_\alpha\, K_{bc}\, K_w \left(\frac{h}{D}\right)^{.35} Fr^{0.43} \qquad \textbf{2.28}$$

where d_s = equilibrium scour depth; D = pier width; K_S = pier shape factor; K_α = pier alignment factor; K_{bc} = correction factor for bed forms; K_w = correction factor for wide piers; h = flow depth directly upstream of the pier; Fr = $U/\sqrt{gh}$ is the Froude number directly upstream of the pier; U = mean velocity of flow directly upstream of the pier; g = gravitational acceleration. In this method the influence of bed-forms on the equilibrium scour depth is considered, effect not taken into account in the other two methods (Auckland and FDOT).

The correction factor K_S for pier shape should be determined as: K_S=1.0 for circular and round-nosed shapes; K_S=1.1 for square-nosed shapes; and K_S=0.9 for sharp-nosed shapes. The pier alignment factor can be estimated according to equation (2.28) for non-cylindrical piers. For

circular piers, K_α assumes the value 1.0. For higher values of the angles (α>5°), K_α dominates and K_S should be considered as 1.0

2.6.2 Cohesive Bed Materials

2.6.2.1 Ansari et al.

(Ansari et al., 2002) formulated a method to predict the maximum scour depth at pier foundations, reported that the maximum equilibrium scour depth in cohesive sediments could be smaller or even more than that of non-cohesive sediments for similar experimental conditions. Moreover, the water content of the sediment antecedent to the initiation of scour was identified as the main factor governing the location of deepest scour in cohesive sediments. The empirical equations used in cohesive soils are:

$$\frac{dsmc}{dsms} = \frac{6.02-10.82\left(\frac{W}{W_*}\right)+5.41\left(\frac{W}{W_*}\right)^2}{\left(\frac{C_*}{\varphi_*}\right)^{0.2}} \quad \textbf{2.29}$$

Where: $C_* = \frac{C.Cu}{(\gamma s-\gamma w)da}$ **2.30**

And: $\phi_* = \frac{C\tan(\varphi c)+(1-C)\tan(\varphi s)}{\tan(\varphi s)}$ **2.31**

In this equation, d_{smc}, d_{sms}, W, W_*, C_U, ϕ_C, ϕ_S, and d_a are maximum scour depth below the bed level for pier scour in cohesive soils, maximum scour depth below the bed level for pier scour in non-cohesive soils, antecedent moisture content (%), antecedent moisture content required to saturate the soil sample, cohesion, angle of repose or internal friction for sand, angle of repose or internal friction for cohesive sediment, and arithmetic mean size of the sediment used for sand-clay mixture, respectively.

2.6.2.2 Rambau et al.

(Rambau, 2003) presented a method to predict the maximum scour depth at single piers for the cohesive bed materials. The empirical equations used in cohesive soils are:

$$\frac{SuC}{D} = \left(\frac{V}{\sqrt{GY}}\right)^{0.641} \left(\frac{UD}{\nu}\right)^{0.64} \left(\frac{CU}{\gamma s\, Y}\right)^{-0.976} \quad \textbf{2.32}$$

where S_{UC}, C_U, D, U, y_0, γ_s, and ν are ultimate scour depth due to currents, undrained shear strength of soil, diameter of obstruction, current velocity, ow depth, unit weight of soil, and kinematic viscosity of water, respectively.

2.6.2.3 Debnath and Chaudhuri

(Debnath and chaudhuri, 2009) presented a method to predict the maximum scour depth at single piers for the cohesive bed materials. The empirical equations used in cohesive soils are:

$$\frac{ds}{D} = 2.05\left(\frac{V}{\sqrt{gD}}\right)^{1.72} C^{-1.29} \left(\frac{\tau s}{\rho U^2}\right)^{0.64} \left(\frac{CU}{\gamma s\, Y}\right)^{-0.37} \quad \textbf{2.33}$$

where ds, D, U, C, ρ and τs are maximum scour depth, pier diameter, approach velocity, clay percent, mass density of water, and undrained shear strength, respectively.

2.6.3 Non-uniform Gravel Bed Materials

2.6.3.1 Melville and Coleman

As mentioned earlier in Paragraph 2.6.1.1, with the addition of the factor K_σ were found to be identical for both uniform and non-uniform sediments on the condition that d_{50} for non-uniform sediments is the median size of the armor layer. Finally, the factor K_σ is defined as:

$$K_\sigma = \frac{ds\ (non{-}uniform\ sediment)}{ds\ (uniform\ sediment)} \quad \textbf{2.34}$$

2.6.3.2 Guo

(Guo, 2012) has proposed the following conservative equation for the prediction of clear-water scour at the equilibrium stage in the case of singular circular piers in non-cohesive sediment mixtures:

$$\frac{\mathrm{ds}}{\sqrt{by}} = \tanh\left(\frac{H^2/\sigma^{1.5}}{3.75}\right) \qquad \textbf{2.35}$$

where H is the so-called Hager's number representing the effect of the reduced gravity ((ρ_s/ρ) - 1) g on the water-sediment interface, where ρ is the water density, ρ_s the sediment density, and g the gravitational acceleration; this is similar to the classic Froude number representing the effect of the gravity g on water-air interfaces.

2.6.3.3 Kim et al.

(Kim at al., 2015) proposed a design method for bridge piers, and the results of this study were compared to various existing methods for pier design. They used equilibrium scour data from the literature for validation. Support vector machine (SVM) and non-dominated sorting genetic algorithm (NSGA-II) approaches were also used for deriving maximum scour depth relationships. The proposed relationship was compared with two selected empirical models. The outcomes showed that their proposed relationship improved the estimation of the maximum scour depth under an equilibrium scour condition, where their proposed relationship is shown below:

$$\frac{ds}{y} = 0.69\left(\frac{b}{y}\right)^{0.35}\left(\frac{d50}{y}\right)^{-0.10}\sigma^{0.39}Fr^{0.56} \qquad \textbf{2.36}$$

where Fr is the Froude number. Generally, the performance of the NSGA-II based relationship depends on the crossover probability, crossover index, population size, mutation index, and mutation probability.

2.7 Pervious Study of Complex Local Scour

(Ansari et al., 2002) conducted an experimental study on the temporal variation of scour around circular bridge piers found in cohesion-less and cohesive sediments under steady clear water flows. The difference between scour patterns in cohesion-less and cohesive sediments is brought out. Considering the horse shoe vortex to be the prime agent causing scour, a procedure is developed for computing the temporal variation of scour depth in cohesive sediments. Empirical relationships have also been obtained for maximum scour depth around bridge piers in cohesive sediments.

(Raikar and Dey, 2005) investigated an experimental into local scour at piers in uniform gravels under a clear water scour condition. From the experimental results, it is observed that the equilibrium scours depth increased with a decreased in gravel size and with increase in pier width. The variations of equilibrium scour depth with gravel size for pier scour depart considerably from the variations of equilibrium scour depth with sand size.

(Rajkumar and Subhasish, 2005) investigated experimentally scour at circular and square piers in uniform and non-uniform gravels (fine and medium sizes) under clear-water scour at limiting stability of gravels. From the experimental results, it is observed that the equilibrium scours depth increases with decrease in gravel size. The variation of equilibrium scour depth with gravel sizes departures considerably from that with sand sizes. Consequently, the resulting sediment size factors for gravels, obtained from envelope curve fitting, are significantly different from the existing sediment size factor for sands. The influence of gravel gradation on scour depth is also prominent in non-uniform gravels. The time scales to represent the time variation of scour depth in uniform and non-uniform

gravels are determined. For uniform gravels, the non-dimensional time scale increased with an increases in pier Froude number and gravel size, whereas for non-uniform gravels. It decreases with an increase in geometric standard deviation of particle size distribution of gravels.

(Lee S. O., 2006). This study is to investigate the relationships among field, laboratory and numerical data for the purpose of improving scour prediction methods that currently tend to over predict bridge scour depths because they are based on laboratory studies of simple bridge pier geometries conducted in rectangular flumes with a flat bed. Comparison of the improved scour prediction formula with a wide range of laboratory and field data showed that it performs better than existing scour prediction formulas. As an additional benefit, the improved scour prediction formula provided the basis of a proposed comprehensive procedure for modeling scour around complex pier bents with realistic river bathymetry and bridge geometry.

(Amini et al., 2010) conducted with the approaching flow having an undisturbed flow depth and a threshold flow velocity. The main variables investigated were pile cap dimensions and location relative to the streambed. According to the rate of change in scour depth, the scour at a pile cap for different cap levels was divided into four cases. Equations for a correction factor for these four cases are derived. The correction factor *Kc* has the effect of reducing the scour depth from a corresponding full-depth pier of the same width as the pile cap. A new methodology is presented to estimate local scour depth at a pile cap as a component of a complex pier. The proposed method was evaluated with the results from this experimental study and historical measurements. The proposed method, which corresponds closely to the observations, can be used to predict local scour at a pile cap as a component of a complex pier in the

superposition method. It is also applicable to the prediction of local scour due to a caisson being sunk onto a mobile bed in a current.

(Ataie-Ashtiani et al., 2010) studied experimentally a variety of configuration, including different sizes and shapes of complex piers. A total of 70 experiments were carried out. Three sets of experiments were performed over the entire range of possible pile cap elevations for complex piers with different geometrical characteristics. The collected data are used to quantify the pile cap elevations that maximize or minimize the local scour depth. Some of the available methodologies to estimate the maximum local scour depth around such complex piers are evaluated. The predictions of the scour depths improved by using the revised methods of Hydraulic Engineering Circular Number 18 and Coleman.

(Debnath and Chaudhuri, 2010-a) investigated Local scour at circular bridge piers embedded in a clay-sand-mixed bed in laboratory flume experiments. The effects of clay content, water content, and sand size on maximum equilibrium scour depth, equilibrium scour hole geometry, scouring process, and time variation of scour were studied at velocities close to the threshold velocities for the sand in the clay-sand mixture. It was observed that clay content and water content were the key parameters that affect the scouring process, scour hole geometry, and maximum equilibrium scour depth. The bridge pier scouring process in clay-sand mixtures involved different dominating modes for removal of sediment from scour hole: chunks-of-aggregates, aggregate-by-aggregate, and particle-by-particle. Regression-based equations for estimation of non-dimensional maximum scour depth and scour hole diameter for piers embedded in clay-sand mixtures having clay content of < 40% and water content of < 40% were proposed as functions of pier Froude number, clay content, water content, and bed shear strength.

(Debnath and Chaudhuri, 2010-b) tested the effects of clay-content, water content, bed shear strength and pier Froude number on maximum equilibrium scour depth, equilibrium scour hole geometry, scouring process, and time variation of scour. The present study attempted to fill this gap between observations made by different investigators in cylindrical pier scour in clay–sand mixed sediment beds. Further, equations for estimation of non-dimensional maximum scour depth for cylinders embedded in clay–sand mixtures were proposed as functions of pier Froude number, clay content, water content, and bed shear strength, while the clay–sand mixtures had clay content in the range of 20–100% and water content in the range of 20%–45.92%.

(Moreno et al., 2014-a) evaluated the contribution of complex pier components on the total local scour depth. Data was also used to describe the temporal evolution of scour. A new approach to evaluate the maximum scour depth associated with a subtraction concept is suggested which considers the different sets of complex piers components. Two predictors (FDOT and HEC-18), based on a scour depth superposition concept are discussed, concluding that FDOT leads to similar results as the measured values, while HEC-18 leads to underestimation of the total scour depth.

(Moreno et al., 2014-b) evaluated and compared three available methods for the prediction of the local scour depth around complex bridge piers using new experimental data. Tests lasted between 15 and 25 days, for a variety of pile cap positions relative to the initial bed under steady clear-water flow conditions. The comparison of predictions with measurements, including some selected from the literature, allows stating that the HEC-18, Auckland and Florida methods potentially lead to both overestimations and underestimations, depending on the relative position

of the pile cap. It became obvious from the study that differences may be influenced by the test stop criterion adopted in the experiments.

(Eldeeb and Fahmy, 2015) studied the effect of submerged pile cap on the local scour around piles were performed. Furthermore, the pile cap entrance angles were investigated as an enhancement to the local scour around piles. The results indicated that, the higher pile cap submergence ratio, the deeper corresponding scour hole around piles. On contrary, reducing the pile cap entrance angle cause an improvement to the scour rate around piles. Finally, different charts were plotted describing the relationships between scour depth and pile cap submergence ratio.

(Moreno et al., 2015) carried out with three complex pier models under steady clear-water flow conditions. Each model, characterized by a different relation between the column and the pile-cap widths, Dc/D_{pc}, was tested for a variety of pile-cap positions relatively to the initial bed, H_c. The experimental data were used to describe the temporal evolution of the scour depth as a function of H_c/h (h = approach flow depth). The common criterion to stop experimental tests on complex piers was analyzed, and a new criterion was introduced. The equilibrium scour depth, d_{se}, was calculated by extrapolation of data series. The results were used to evaluate the effect of D_c/D_{pc} and H_c/h on d_{se} when the pile cap is above the bed (Situation 1), partially buried in the bed (Situation 2), and completely buried in the bed (Situation 3). The analysis includes the definition of Hc at which the maximum d_{se} occurs through an equation that takes into account the D_c/D_{pc} ratio, the relative pile-cap thickness, T/h, and the column and pile-cap shapes.

(Yang Y., et al., 2017) performed to investigate effects of pier skewness and the pile-cap elevation on scour depth. Skewness varies from 0° to 45° in 15° increments, and the pile-cap elevation relative to bed level

is also varied. All the tests are performed with 30 hours' duration, and the measured scour depths are extrapolated to equilibrium using validated equations. Results showed that, for complex piers aligned to the flow, the maximum equilibrium scour depth occurs when the top of the pile-cap is close to the undisturbed bed level; for skewed complex piers, the equilibrium scour depth increases significantly compared with aligned ones. The increase of scour depth is proportional to the skew angle α, and becomes less sensitive to α when $\alpha > 30°$. For skewed complex piers, the column generates most of the scour depth, if it is inserted significantly into the flow. The sediment coarseness $De/d50$ also varies with pier skewness, and is inversely proportional to the normalized scour depth when $De/d50$ is larger than a specific value. This phenomenon is in accordance with the previous studies, and the equations of **(Lee and Sturm, 2009)** showed the best agreement with the data of the present study. In addition, the location of the maximum scour depth varies with different configurations, implying a need to arrange countermeasures accordingly.

(Yang et al., 2018) tested the experimentally the flow-induced clear-water local scour at complex bridge piers was conducted using two typical pier models, nine pile-cap elevations, and seven pier skew angles from 0° to 90° with 15° intervals. Results showed that a slight skew angle α imposed on an originally aligned pier can significantly increase the equilibrium scour depth d_s. When a pier is skewed to the flow, the column makes the largest contribution to the scour depth, as its wide-pier feature becomes dominant. Three categories of the pier skewness are defined, namely an aligned pier (α =0°), a slightly skewed pier ($\alpha \approx 15°$), and a highly skewed pier ($\alpha \geq 30°$). The influences of the pile-cap and the pile group on the scouring process are weakened with increasing α.

Additionally, for highly skewed piers with fully submerged pile-cap, the equilibrium scour holes tend to equally expose the pier components, no matter where the undisturbed bed level is. A new scour prediction method based on the Sheppard/Melville method is presented, involving modifications for the effect of sediment coarseness. The new method leads to a higher safety margin with significantly reduced underestimation.

(Sousa and Ribeiro, 2019) investigated prediction of maximum scour depth at complex bridge piers is frequently decisive for the safe design of bridges. Some methods are available for this purpose but, due to the discrepancies of their predictions, such methods deserve further validation on the basis of new and independent data sets. For this purpose, clear-water experiments were performed by systematically varying the pile-cap elevation of a particular pier shape. Equilibrium scour depths were reached and measured and the comparison of predictions with measurements was established. The method of (**Sheppard and Renna, 2005)**, was found to predict with the highest accuracy the attained results for the tested complex pier. However, it should be stressed that this method slightly underestimates scour when the pile cap is out of the water or partly imbibed in the flow. It also under-predicts the scour depth when the pile cap is deeply buried in the bed.

(Yang et al., 2019) investigated four typical pier arrangements were adopted, including side-by-side with aligned or 30° skewed flow, staggered, and tandem. The results show that the skew angle for a side-by side arrangement significantly accelerates the clear-water scour development at all the vertical piles as well as between the piers, and the most scoured pile shifts from the upstream end to the downstream end of the upstream pier flank. The staggered and tandem pier arrangement show

significant protection to the downstream pier for both the developing rate and the equilibrium scour depth.

(Manish et al., 2020) studied non-uniform gravel bed laboratory and field datasets with gravel of median size ranging from 2.7 to 14.25 mm were considered to predict the maximum equilibrium scour depth at cylindrical piers. It was observed that Melville and Coleman's equation performs well in the case of laboratory datasets, while it tends to overestimate field measurements. Guo's and Kim et al.'s relationships showed good agreements only for laboratory datasets with finer non-uniform sediments: deviations in predicting the maximum scour depth with non-uniform gravel beds were found to be significantly greater than those for non-uniform sand and fine gravel beds. Consequently, new K-factors for the Melville and Coleman's equation were proposed in this study for non-uniform gravel-bed streams using a curve-fitting method. The results revealed good agreements between observations and predictions, where this might be an attractive advancement in overcoming scale effects. Moreover, a sensitivity analysis was performed to identify the most sensitive K-factors.

(Zahraa et al., 2020) the study was conducted using a laboratory flume and circle pier models founded in cohesive soil of clay and uniform fine sand. Experiments were carried out at a velocity close to the critical velocity of the sand fraction of the bed sediment (V/V_c = 0.94 and 0.98). Pier models were placed in three arrangements: single, tandem (two in-line piers) parallel with the flow direction, and tandem piers aligned with an angle. The effects of piers spacing, alignment, and sediment cohesion on scouring depth were investigated. For bed sediment of different clay content, it was observed that the rate of scouring and scour hole development is slower when the bed clay content increased from 30% to

50% by dry weight. As comparing the scour in cohesion-less soils to that in sand-clay (cohesive soil), it was found that the deepest scour occurs at the sides of the piers found in the sand-clay soil in contrast to the cohesion-less soil where the deepest scour is observed at the pier nose.

(Yang et al., 2020-a) studied the temporal evolution of clear-water scour at complex bridge piers experimentally. The pier model has a typical form comprising three components, namely a rectangular column, a rectangular pile-cap, and a group of vertical piles underneath. Various relative pile-cap positions and skew angles (α) from 0° to 45° were used to investigate their influence on scour evolution. New functions are proposed to fit temporal data and determine the equilibrium scour depth with better accuracy. The results showed that the locations for scour initiation and the maximum scour depth may be different, and their relationship varies with pile-cap position and pier skew angle. Highly skewed piers tend to overcome the influence of width ratio of column to pile-cap (D_c/D_{pc}) on scour evolution, as the column itself becomes dominant. The sensitivity of scour evolution to pier skew angle decreased with higher pile-cap position, especially when it is entirely above the original bed. Four scour development stages were identified for complex piers, including initiation, stagnation, a developing stage, and equilibrium, with each stage being highly dependent on the degree of exposure of each of the pier components. The description of each development stage for different situations is given. The equilibrium time scale t^* and the equilibrium scour depth dse for complex piers have a similar dependence on flow shallowness ratio (y_0/D_e) and sediment coarseness ratio (D_e/d_{50}), as per the equation proposed by authors' previous study **(Yang et al., 2018)**. A new equation is proposed to correct the percentage rate of scour development. The correction is especially useful for aligned complex piers, for which the rate of scour time

development may be much lower than that for single-column piers. In general, they recommended using the modified Sheppard-Melville method and the corrected time-scale equation to predict clear-water equilibrium scour depth and scour evolution at complex bridge piers.

(Yang et al., 2020-b) studied experimentally scour at complex bridge piers exposed to combined waves and current. Regular waves were produced with various strength and superimposed on co-directional current with constant velocity. The key parameters tested and discussed include Keulegan Carpenter (KC) number, relative current strength U_{cw}, pile-cap elevation, and pier skewness. The dependence of the equilibrium scours depths, both original and normalized, on the tested parameters was also analyzed. It was found that the normalized scour depth at complex piers increases with greater KC and U_{cw} and tends to be much larger than that for single piers. The increase of bed mobility did not lead to scour peaks at the clear-water threshold as what is usually observed for current-only scour. The influence of pile-cap elevation on the equilibrium scour depth was found to be much weaker than that under steady current. Furthermore, new scour prediction method is proposed to incorporate extra terms taking the influence of pile-cap elevation and pier skewness into account. The prediction accuracy is improved significantly. Finally, more suggestions regarding design considerations are also given.

In this study, the researcher carried out the experimental work, using five river models for complex bridge pier of different hydraulic and geometric parameters and the properties of the different Iraqi soil types under the influence of different discharges. Also, predicting special equations for different types of different Iraqi soils under the influence of parameters above and contributions components on the equilibrium scour depth. **(Yang, et al., 2018, 2020)** the closed to the study, with the difference in the use of one type of soil.

CHAPTER THREE

EXPERIMENTAL WORK

Chapter Three

Experimental Setup

3.1 Introduction

In this chapter, laboratory test results collected from each bridge model experiment are presented. River model experiments is used, the complete river bathymetry upstream and downstream of the bridge as well as, pier bents of the bridge itself were modeled in detail. Local scour around complex bridge pier foundations placed in different Iraqi soils are investigated by conducted a set of laboratory flume experiments. The depth and extent of the scouring hole are measured. The hydraulic design of the flume, the measuring technique, discharge calibration, bed materials, model of bridge piers, dimensional analysis given characteristic parameters under clear water conditions at threshold velocity, and General Experimental Procedure. The experimental of the present study were conducted in a special laboratory. Figure 3.1 shows a flow chart of the experimental work.

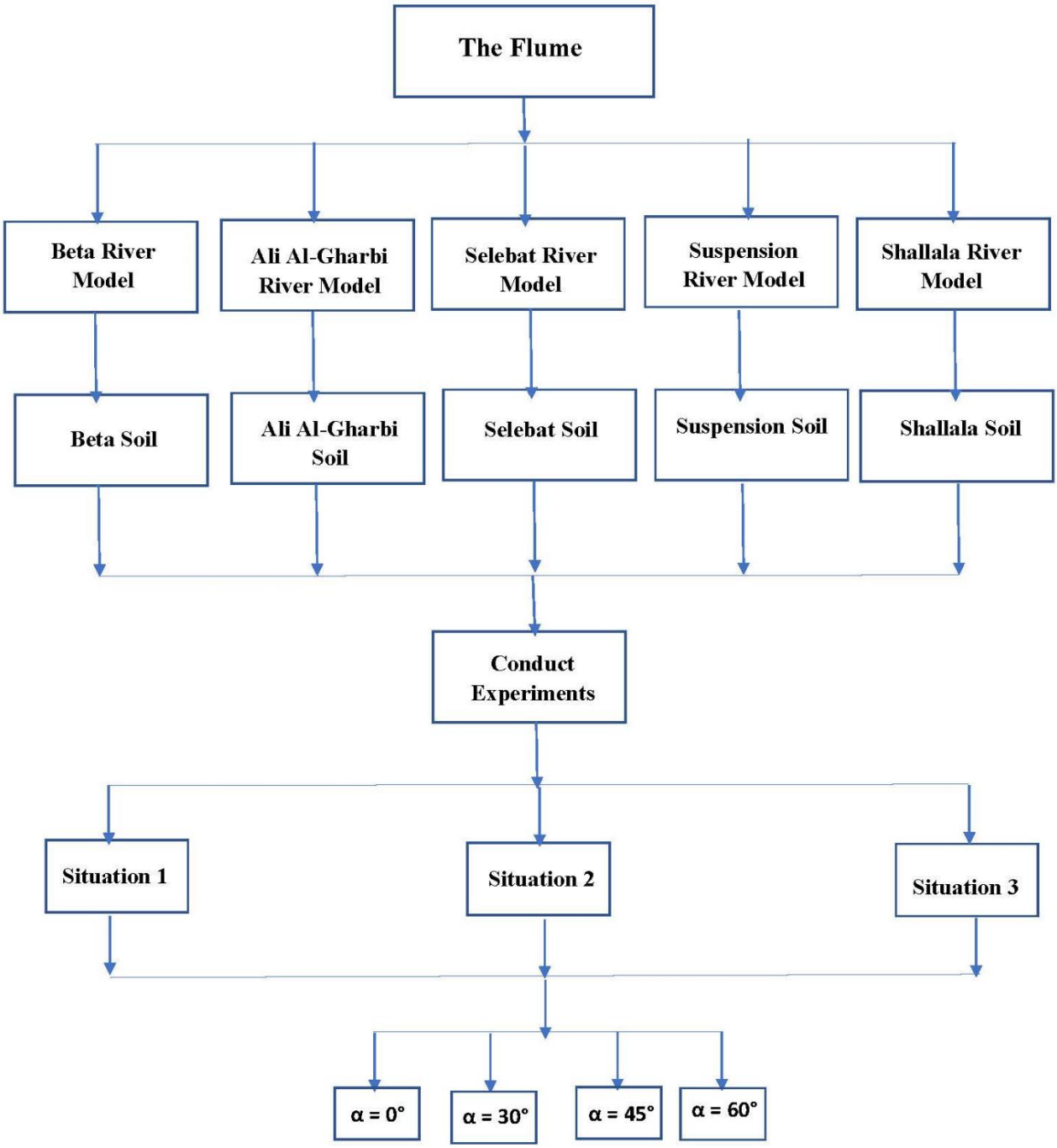

Figure 3.1: Experimental work flow chart.

3.2 Laboratory Flume

The experiments were conducted in a rectangular recirculation flume, which was designed for flow conception. The flume is constructed of glass-walled and a steel frame structure. It (7.5m) long, (1m) width, and (0.6m) deep horizontal non-tilting with smooth side walls. There is a section work is (2m) long and (0.2m) deep, located at (2.5m) upstream from the flume inlet section, the section work has been filled with different Iraqi soils.

There is also an overhead tank at the upstream side of the flume, into which the water is pumped from the main reservoir tank. The main function of this overhead tank is to provide a continuous flow of water at a constant rate to the flume. A wooden gate suppressor was also used in the upstream approach section to smooth the flow coming onto the bed section. A baffles (two screens) are located at every (50cm) from the flume inlet in order to damp any turbulence and smoother the flow to prevent any undesired bed form (ripple or dune) at the working section.

A rectangular gate (1×1) m has been supplied at the outlet section of the flume, to make the depth of the water at the head and at the end of the flume is equal and hence to control the velocity of flow. The used water from the flume is then discharged into the outlet tank, the pump takes the water from the reservoir at the downstream end of the flume and again sent to the upstream end by 4-inch diameter pipe line which runs directly beside the flume. There are four reservoir tanks, one in the outlet flume with dimensions (1×0.9×0.55) m separated from it by the rectangular gate, and three with dimensions (1.25×1.25×0.5) m beside the flume.

Centrifugal pump located at the downstream end of the flume supplied the flow rate through a 3-inch diameter pipe. A flow meter has been used to measure the water discharge located in the water return pipe

at the downstream end of the flume. The measuring accuracy of the device used has been ± 0.4% of the flow rate. All depths are measured out using movable point gauge mounted on brass rail at the top of the flume side, which has an accuracy of ± 0.1mm, as shown in Figure 3.2.

Figure 3.2: Laboratory flume: a. The channel design, b. Section work, c. Screens, d. the tanks, e. Pump and flow meter, f. Point gauge.

The schematic diagram of flume as shown in Figure 3.3:

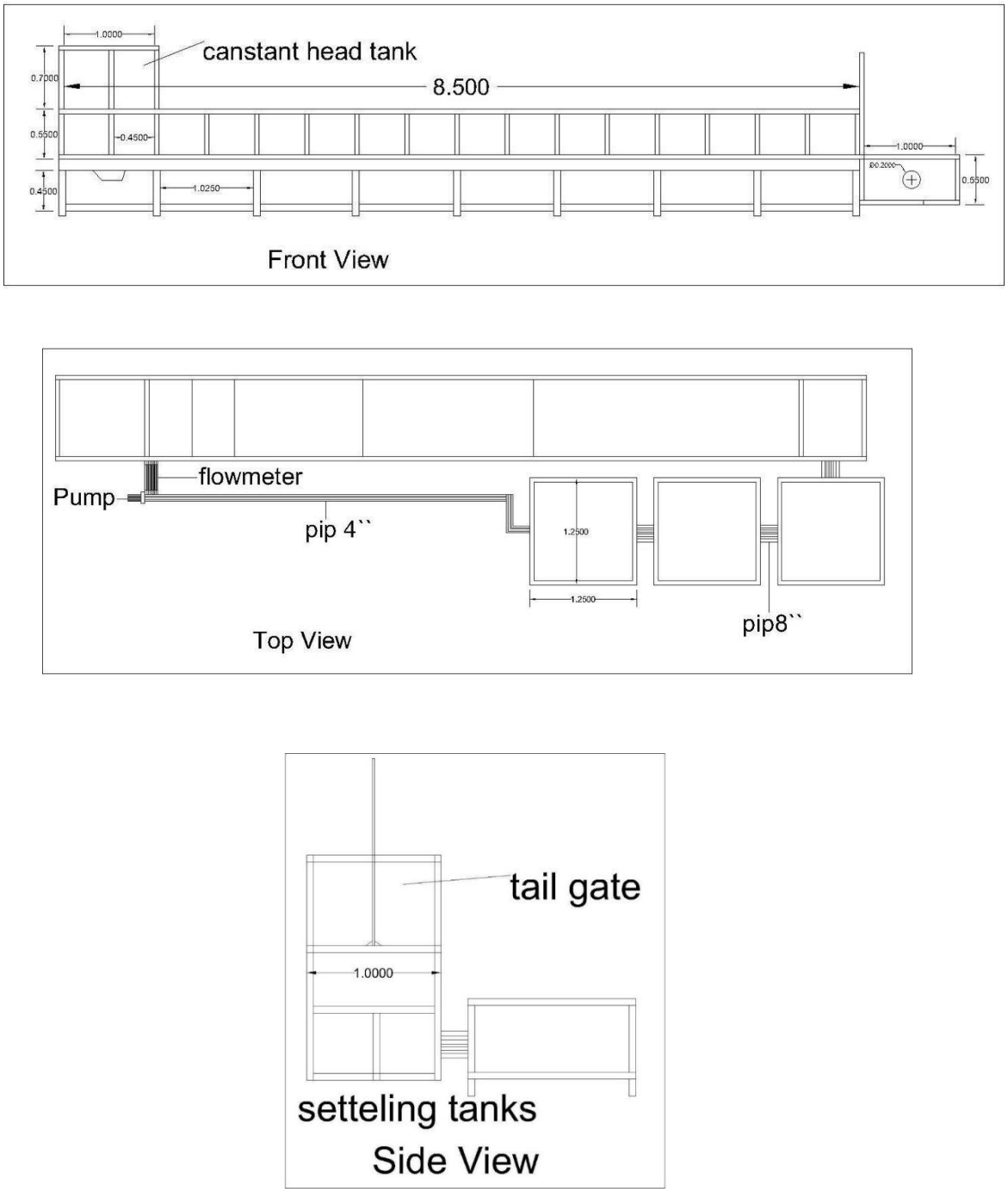

Figure 3.3: The schematic diagram of flume.

3.3 Discharge Calibration

For flow discharge measurement, a V-notch weir of 90° basis of the **USBR** standard placed at the end of the inlet tank shown in Figure 3.4. This weir is an original part of the used flume and meet all requirements and limits concerning the use of partially contracted V-notch weir as it is recommended according to ISO1971, France (**USBR, 2001**). Where these limits are:

1. $h_1/p_1 \leq 1.2$

   where: -

   h_1 = head over weir,

   p_1 = distance between the channel bed and the apex of the triangular weir.

2. $h_1/B_1 \leq 0.4$

   where: B_1 = upstream tank width.

3. $h_1 \leq 0.6096$ m
4. $p_1 \geq 0.1016$ m
5. $B_1 \geq 0.6096$ m

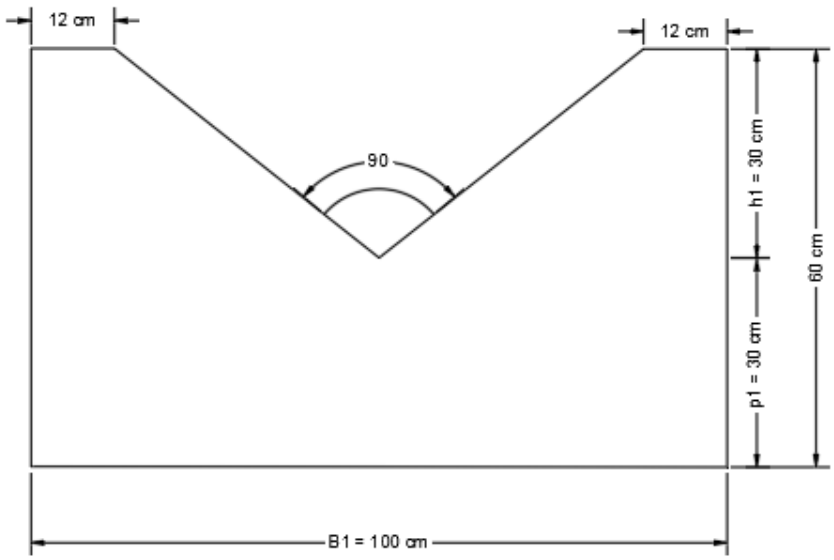

Figure 3.4: V-notch weir at the upstream of flume.

The used V-notch weir in this study is shown in Figure 3.4 The dimensions and geometric aspects for weir section are, p_1=30 cm, B_1= 100 cm and head over the weir was variable and its maximum value is h_1=30 cm as shown in Figure 3.4. Equation 3.1 is suggested by the **USBR, 2001**(according to the modification **proposed by kindsvater and carter, 1957**) to estimate discharge at V-notch weirs:

$$Q = C_e \frac{8}{15}\sqrt{2g}\tan\frac{\theta}{2}{h_e}^{2.5} \qquad \mathbf{3.1}$$

Where: Q is the calculated discharge, C_e is the effective coefficient of discharge can be read from Figure 3.5 h_e is the effective head ($he=h+k_h$), h is the measured head over the weir, k_h is a head correction factor, the values for K_h as shown in Figure 3.6.

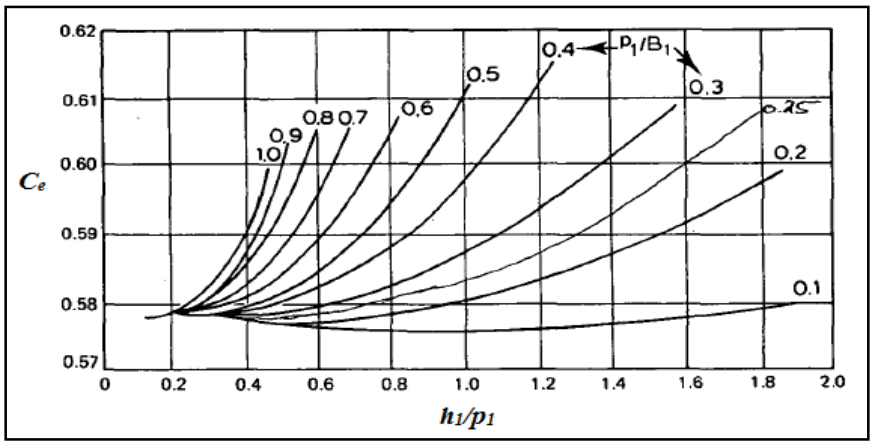

Figure 3.5: Ce value for partially contracted developed 90° V-notch weirs (From British Standard 3680: Part 4A and ISO/TC 113/GT 2 (France-IO) 1971).

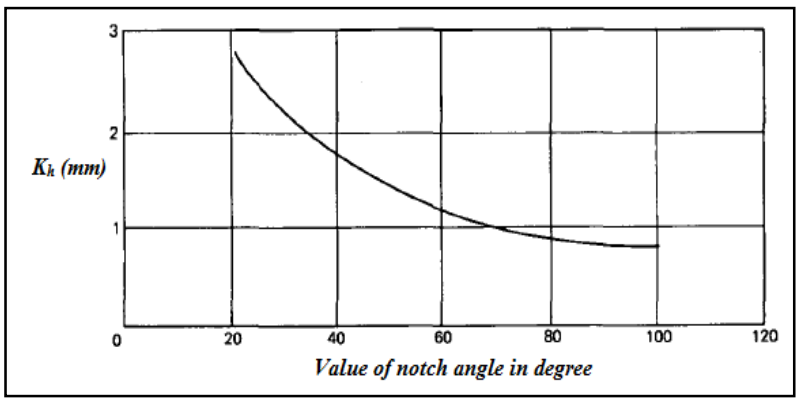

Figure 3.6: Values of K_h for fully and partially contracted V-notch weirs **(USBR, 2001, as proposed by kindsvater and carter, 1957)**.

The standard method of capacity is used to calibrate the applied flow rate from which the accumulative volume of water is measured by a known-volume container of (70 litter) with a stop watch. Discharge calibration curve is plotted in Figure 3.7.

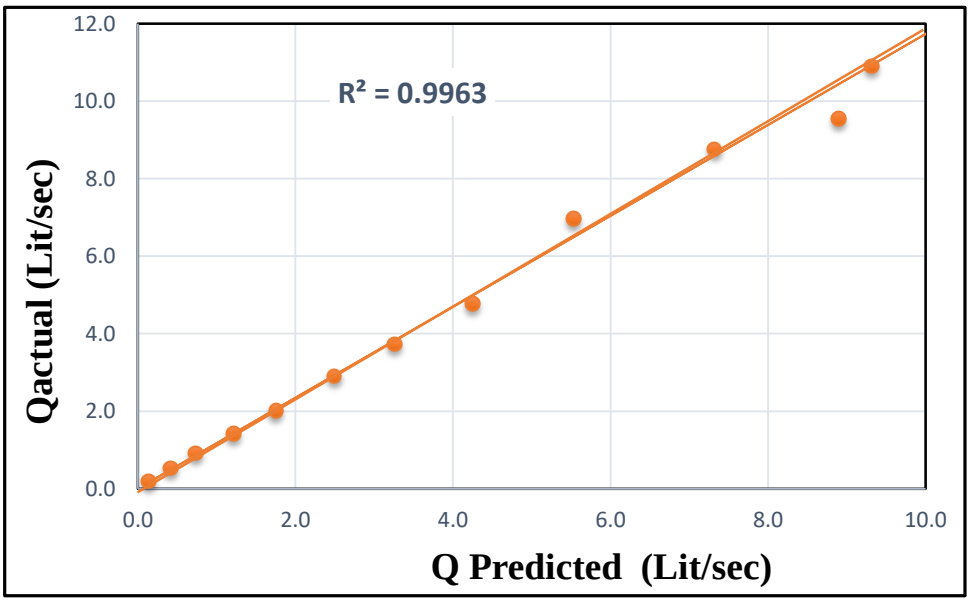

Figure 3.7: Discharge calibration relationship curve of V-notch weir.

3.4 Dimensional Analysis

Dimensional Analysis is a fundamental step before physical experiments can begin. It helps to optimize the experimental setup to get the maximum information with a minimal amount of time and effort. (**Kobus, 1974)**

A hydraulic physical model is the precision device of choice for the experimental investigation of hydro-mechanical phenomenon and can give reliable information if its scale is determined correctly according to certain rules. The initial part of starting physical models is the selection of the physical variables which may have a dominant effect on the process. The parameters are classified in terms of Mass (M), Length (L), and Time (T) as shown in Table 3.1. **(Novák, 2010)**

Table 3.1: The classification of parameters that affect the local scour mechanism in (MLT).

Symbol	Description	Units	Dimensions
1	**Parameters characterizing the fluid**		
ρ	Density of fluid	kg/m^3	ML^{-3}
μ	Dynamic viscosity of fluid	kg/m.s	$ML^{-1}T^{-1}$
2	**Parameters characterizing the flow**		
g	Acceleration of gravity	m/s^2	LT^{-2}
h	Approach flow depth	m	L
V	mean flow velocity	m/s	LT^{-1}
V_c	Critical velocity (threshold velocity for sediment)	m/s	LT^{-1}
Va	Armor Peak Velocity	m/s	LT^{-1}
d_s	Maximum Scour depth	m	L
3	**Parameters characterizing the bed material**		
ρ_s	Density of sediment	kg/m^3	ML^{-3}
d_{50}	Median sediment size	mm	L
σ_g	Standard deviation of particle	---	---
Ø	Angle of static sediment repose	degree	°
C	cohesion of sediment	kg/ms^2	$ML^{-1}T^{-2}$
4	**Parameters characterizing the flume**		
S_o	Channel bed slope	---	---
B	Flume width	m	L
K_a	Roughness effect of sidewalls	---	---
K_c	Channel alignment factor	m	L
5	**Parameters characterizing the complex pier**		
α	Complex pier alignment angle	degree	°
D_c	Column diameter	m	L
L_c	Column length	m	L
K_{sc}	Column shape factor	---	---
b_{pc}	Pile-cap width	m	L
L_{pc}	Pile-cap length	m	L
K_{spc}	Pile-cap shape factor	---	---
T	Pile-cap thickness	m	L
H_c	Column position (distance from the initial bed level to the bottom surface of the column)	m	L
f_l	Extension length of pile cap face out from column face	m	L

Symbol	Description	Units	Dimensions
f_t	Extension width of pile cap face out from column face	m	L
D_p	Pile diameter	m	L
L_p	Pile length	m	L
f_p	Longitudinal extension length of pile cap face out from the nearest pile front face	m	L
K_{sp}	Pile shape factor	---	---
m	Number of piles in line with flow	---	---
n	Number of piles normal to the flow	---	---
S_m	Pile spacing in the direction m (centerline-to-centerline)	m	L
S_n	Pile spacing in the direction n (centerline-to-centerline)	m	L
K_r	Roughness of pier surface	---	---
6	**Time**		
t	Duration of flow	min	T
7	**Temperature**		
θ	Laboratory temperature	degree	°

Figure 3.8 shows the scheme of a complex pier with the respective variables described above.

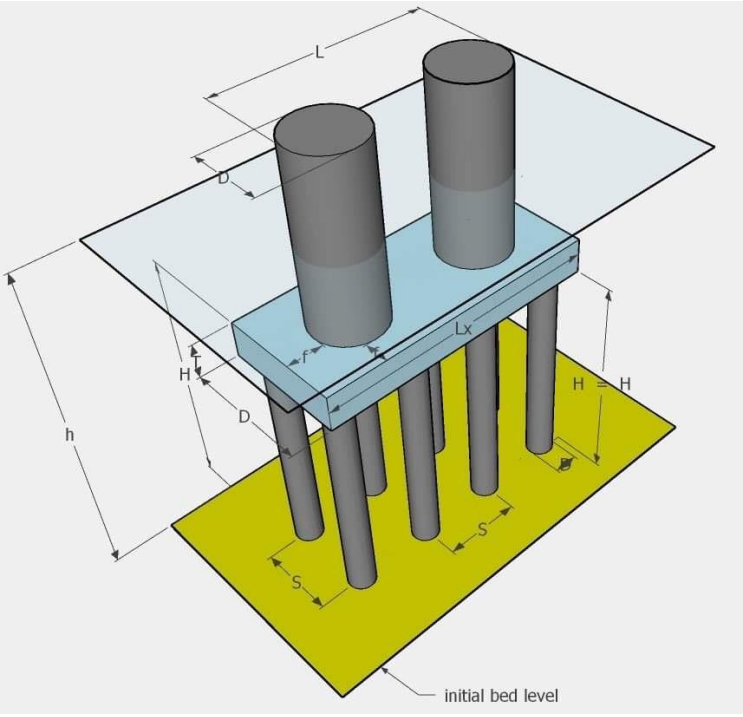

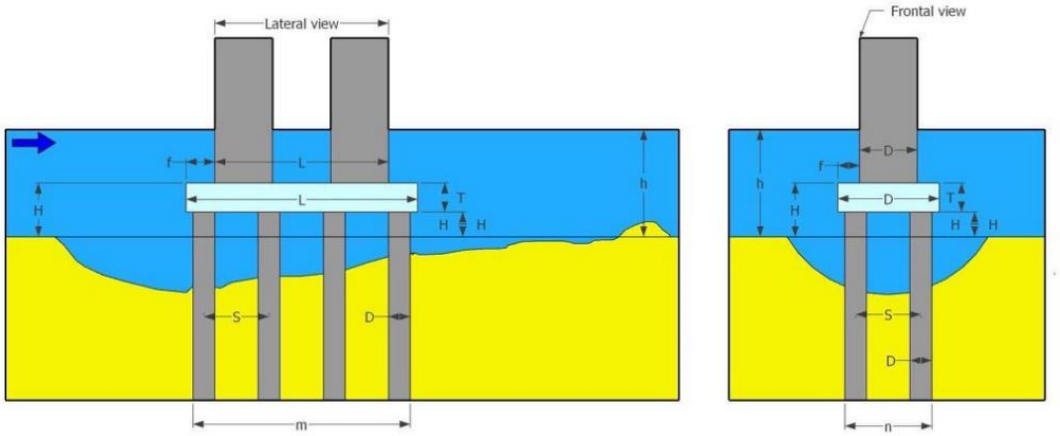

Figure 3.8: Scheme of complex pier geometry.

The variables, which affect the local scour mechanism, are summarized by this relationship:

$$f\left(\rho, \mu, g, h, V, V_c, V_a\, d_s, \rho_s, d_{50}, \sigma_g, Ø, C, S_o, B, K_a, K_c, \alpha, D_c, L_c, K_{sc}, b_{pc}, L_{pc}, K_{spc}, T, H_c, f_l, f_t, D_p, L_p, f_p, K_{sp}, m, n, S_m, S_n, K_r, t, \theta\right) = 0 \qquad \textbf{3.2}$$

$$d_s = f\left(\rho, \mu, g, h, V, V_c, V_a\ , \rho_s, d_{50}, \sigma_g, Ø, C, S_o, B, K_a, K_c, \alpha, D_c, L_c, K_{sc}, b_{pc}, L_{pc}, K_{spc}, T, H_c, f_l, f_t, D_p, L_p, f_p, K_{sp}, m, n, S_m, S_n, K_r, t, \theta\right) \qquad \textbf{3.3}$$

Choosing *Dc*, Vc and μ for basic variables and applying the theorem of Vaschy-Buckingham, n = 39, m = 3, π = 36, equation (3.3) becomes:

$$ds = f\left(\Delta, gD_c/Vc^2, h/D_c, V/V_c, V/V_a, d_{50}/D_c, \sigma_g, Ø, D_cC/V_c\,\mu, S_o, B/D_c, K_a, K_c, \alpha, L_c/D_c, K_{sc}, b_{pc}/D_c, L_{pc}/D_c, K_{spc}, T/D_c, H_c/D_c, f_l/D_c, f_t/D_c, D_p/D_c, L_p/D_c, f_p/D_c, K_{sp}, m, n, S_m/D_c, S_n/D_c, K_r, t, \theta\right) \qquad \textbf{3.4}$$

Where, $K_{sc} = Ø\ (L_c/D_c)$, $K_{spc} = Ø\ (L_{pc}/b_{pc})$, $K_{sp} = Ø\ (L_p/D_p)$

Equation (3.4) constitutes the framework for subsequent analysis, where the effects of some characteristic variables and non-dimensional parameters that affect scouring at complex piers are discussed and characterized.

$$d_s = f\left(\begin{array}{l} \Delta,\ V/V_c,\ d_{50}/D_c,\ \sigma_g,\ Ø,\ C, \\ \alpha,\ K_c,\ T/D_c,\ H_c/D_c,\ D_p/D_c \\ \frac{V-(Va-Vc)}{Vc},\ F,\ R_p \end{array}\right) \qquad \textbf{3.5}$$

3.5 Experimental Procedure

1. the river model was fabricated with a proper length scale to fit the horizontal flume. Bridge pier geometry and location were modeled according to bridge plans provided by the general Authority for roads and bridges.
2. The complex pier was first installed in the flume at the required location, fixed aligned and with skew-angles position. It can be noted that significant change in the flow manner may occur due to pier position and direction differences.
3. The bed material (different Iraqi soils) was placed in the bed recess, it is leveled in the flume by using a scraper. The initial bed elevations were checked using a point gauge at random points to ensure the proper leveling. The thickness of layer sand is 20 cm.
4. The pump is then turned on and its speed slowly increased until the required flow rate has been achieved. The tailgate was checked so as to preserve the correct depth of flow in the flume.

5. Time is recorded using a stopwatch during each test, at the end of the time the flow is stopped, then the flume is drained slowly to avoid any change of the scour hole.
6. The bed material (different Iraqi soils) was left to dry and then the location and magnitude of the point of the maximum scour depth was recorded with three different positions. The maximum scour depth readings being taken every few minutes during the first hours. It should be noted, that the first five hours of each test is very important as frequent readings are required to be taken in order to properly define the early stage of the graph of maximum scour depth versus time.
7. The bed material (different Iraqi soils) is then re-leveled and the steps are repeated after changing the complex pier model aligned and skew-angle to the flow direction.

3.6 River model experiments

3.6.1 Beta Bridge / Babylon Province – Hilla

1. Bed Material

Based on the investigations of the soil issued by Ministry of construction, Housing - Municipalities and Public Works. The soil taken at a depth of (4-5 m) from the Hilla River was sieved again and poured into the test section. It is classified as (river sand with trace clay). The thickness of the bed material is (20 cm) and the slope of the bed is adjusted in parallel with flume surface as (S_0=0). The properties of the soil and sediment size distribution are given in Table 3.2 and Figure 3.9; the detailed information is introduced in Table (A-1) in **Appendix A**.

Table 3.2: Bed material properties for Beta Bridge.

Variable	Value	Variable	Value
D_{10}	0.3 mm	K	$14.5*10^{-2}$
D_{16}	0.32 mm	φ	32°
D_{30}	0.37 mm	C	0.06 Kg/cm^2
D_{50}	0.45 mm	T.S.S %	0.68
D_{50a}	0.393 mm	SO_3 %	0.24
D_{60}	0.48 mm	Gypsum, $CaSo_4$ %	0.52
D_{84}	0.57 mm	Chloride, Cl %	0.032
D_{100}	0.707 mm	pH	6.2
σ_g	1.33	CaCO3 %	16.4
Cu	1.6	Organic matter %	4.02
Cc	2.58	E-Conductivity	4.31 mmhos/cm

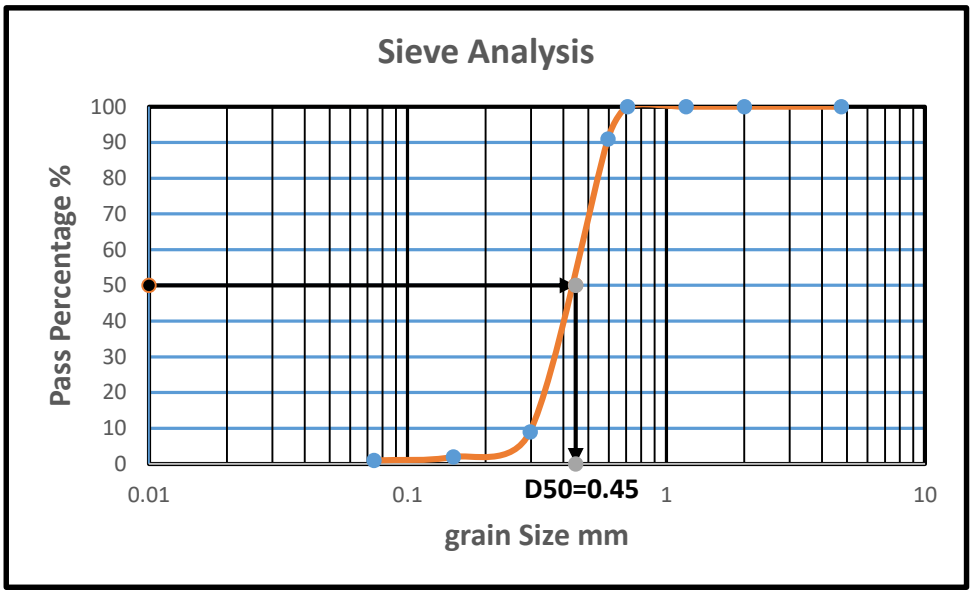

Figure 3.9: Sediment size distribution for the bed material for Beta Bridge.

As it is seen from Table 3.2, the geometric standard deviation is greater than 1.3 and sediment distribution is defined as non-uniform for this value. **(Yanmaz, 2002)** states that when $\sigma_g > 1.3$ the bed material is considered to be non-uniform. Otherwise i.e. $\sigma_g < 1.3$ the sediment is said to be uniform. Geometric standard deviation shows the sediment gradation and itis calculated from the particle size distribution graph: $\sigma_g = (D_{84}/D_{16})^{0.5}$.

2. Complex Bridge Pier Model

The schematic of complex bridge pier for river with the prototype dimensions was fabricated with scale ratio 1:50. Manufactured form treated wood. These models were designed with a cylindrical column found on a rectangular pile cap, supported by a pile group. The arrangement of this last component consists of: two alignments of four cylindrical piles The longitudinal axis of the complex pier models was aligned *i.e.*, α=0° and skew-angle α=30°, 45°, 60° with the approach flow, as shown in Figure 3.10 below. The geometric characteristics of the model are summarized in Table 3.3.

Table 3.3: Geometric characteristics of the complex pier model of the experimental campaign for Beta Bridge.

Variable	Dimension(cm)	Variable	Dimension(cm)	Variable	Dimension(cm)
D_c	8	L_{pc}	32	n	2
L_c	20	T	3	S_m	6
f_L	4	D_p	3	S_n	6
f_t	3	f_p	1		
D_{pc}	14	m	4		

According to **(Melville and Coleman, 2000)** choosing the pier diameter carefully, in order to avoid the effect of contraction on the scour depth, the flume width should be at least ten times the pier width. The constant flow depth (7 cm).

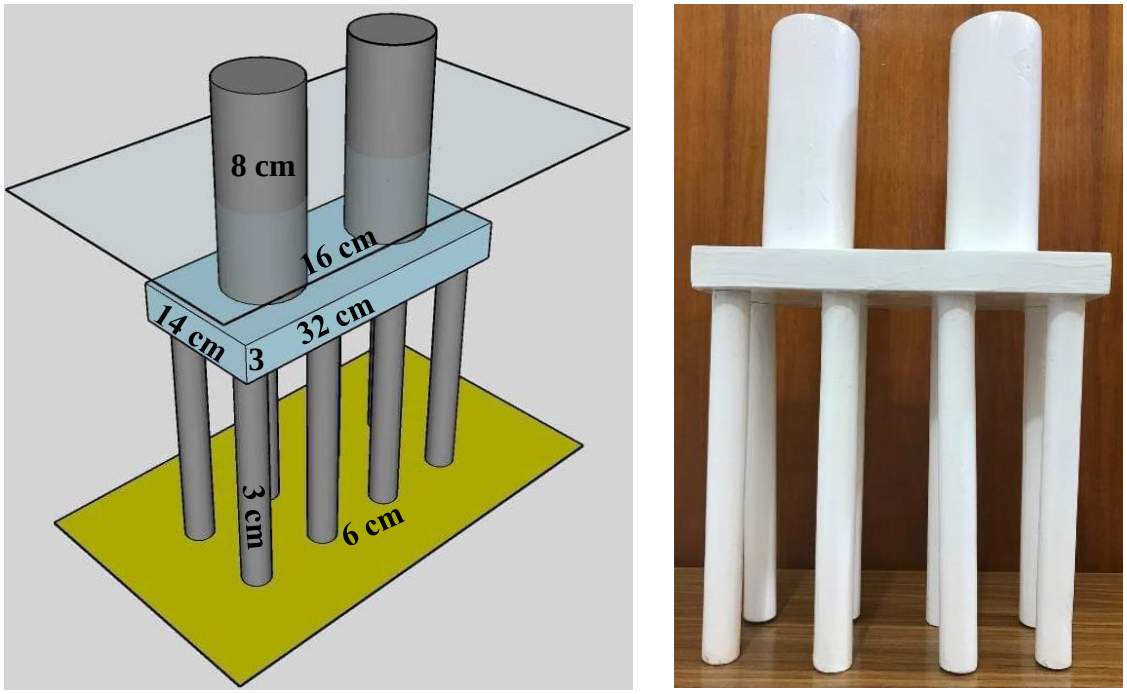

Figure 3.10: complex bridge Pier model used in the experiments for Beta Bridge.

3.6.2 Ali Al-Gharbi Bridge / Missan Province

Bed Material

Based on the investigations of the soil issued Ministry of construction, Housing - Municipalities and Public Works. The soil taken at a depth of (5 m) from the Missan River was sieved again and poured into the test section. It is classified as (black medium river sand). The thickness of the bed material is (20 cm) and the slope of the bed is adjusted in parallel with flume surface as (S_0=0). The properties of the soil and sediment size distribution are given in Table 3.4 and Figure 3.11; the detailed information is introduced in Table (A-2) in **Appendix A**.

Table 3.4: Bed material properties for Ali Al-Gharbi bridge.

Variable	Value	Variable	Value
D_{10}	0.18 mm	K	$7.67*10^{-2}$
D_{16}	0.21 mm	φ	30°
D_{30}	0.27 mm	C	0.0 Kg/cm^2
D_{50}	0.37 mm	T.S.S %	0.92
D_{50a}	0.393 mm	SO_3 %	0.212
D_{60}	0.42 mm	Gypsum, $CaSo_4$ %	0.45
D_{84}	0.54 mm	Chloride, Cl %	0.022
D_{100}	0.707 mm	pH	6.0
σ_g	1.61	CaCO3 %	16.0
Cu	2.3	Organic matter %	0.75
Cc	3.57	E-Conductivity	3.5 mmhos/cm

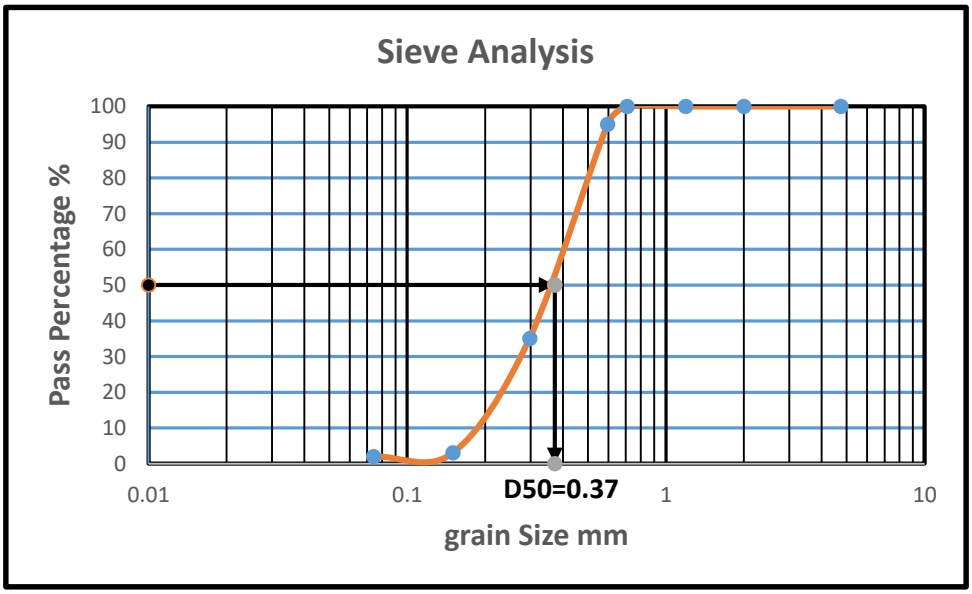

Figure 3.11: Sediment size distribution for the bed material for Ali Al-Gharbi bridge.

As it is seen from Table 3.4, the geometric standard deviation is greater than 1.3 and sediment distribution is defined as non-uniform for this value. **(Yanmaz, 2002)** states that when $\sigma_g > 1.3$ the bed material is considered to be non-uniform. Otherwise i.e. $\sigma_g < 1.3$ the sediment is said to be uniform. Geometric standard deviation shows the sediment gradation and itis calculated from the particle size distribution graph: $\sigma_g = (D_{84}/D_{16})^{0.5}$.

3.6.3 Selebat Bridge/ Al-Muthana Province

Bed Material

Based on the investigations of the soil issued Ministry of construction, Housing - Municipalities and Public Works. The bed material used in the experiments composed of clay mixed with fine sand. The sand was extracted from the river at depth (5-6 m); the particle size distribution was tested by the sieve analysis introduced in Table (A-3) in **Appendix A**. The selected sand satisfies the criteria for non-uniform sand, where σ_g is greater than 1.3. Clay was extracted from the river also at depth (5-6 m), the properties of the sand and clay are presented in the table 3.5 and Figure 3.12.

Table 3.5: Bed material properties for Selebat bridge.

Variable	Value	Variable	Value
D_{10}	0.015 mm	P.L %	15
D_{16}	0.024 mm	φ	31°
D_{30}	0.044 mm	C	5.8 Kg/cm^2
D_{50}	0.074 mm	T.S.S %	1.75
D_{50a}	0.66 mm	SO_3 %	0.557
D_{60}	0.172 mm	Gypsum, $CaSo_4$ %	1.2
D_{84}	0.260 mm	Chloride, Cl %	0.16
D_{100}	1.19 mm	pH	6.3
σ_g	3.32	CaCO3 %	20
Cu	11.63	Organic matter %	0.879
Cc	17.44	E-Conductivity	3.0 mmhos/cm
K	$0.26*10^{-2}$	Plasticity index %	9
L.L %	24	W.C	24.5

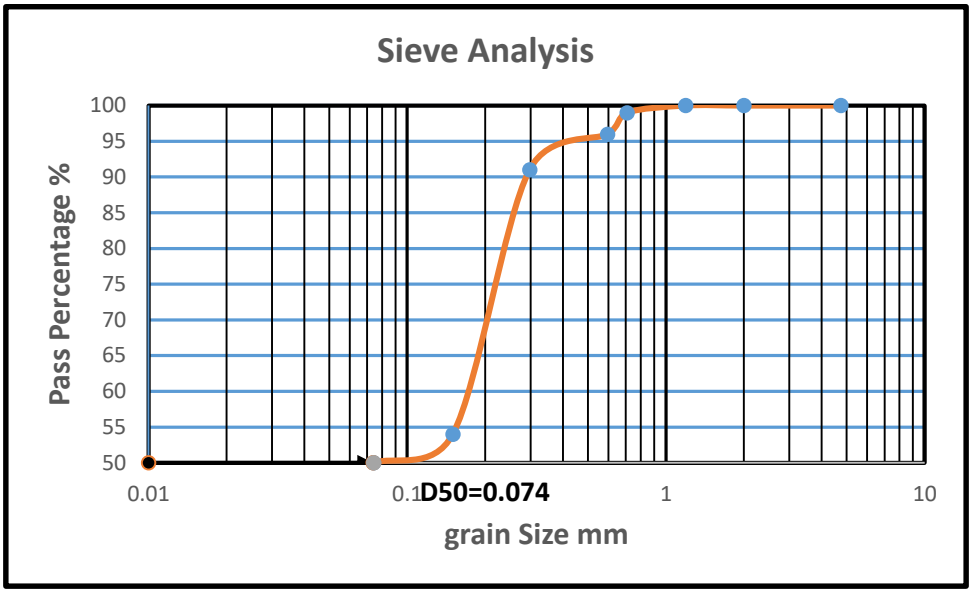

Figure 3.12: Sediment size distribution for the bed material for Selebat bridge.

The soil mixture is composed of (50% clay mixed with 50% sand) manually and homogenously in dry condition to make sure that the soil mixture is evenly mixed. This mixture to test the scouring in the case of transitional behavior of soil between cohesion-less and cohesive. A soil mixture is placed around the complex pier model in the bed section of the flume in the longitudinal centerline and filled until a thickness (20 cm). The top surface of the bed material was leveled and smoothened. Next, the flume is filled with water until (27 cm) depth and the sand-clay mixture is kept for about (3 hours) for saturation. This time duration allows the cohesive and cohesion-less soils to bond to achieve cohesive soil mixture similar to that in field conditions. The followed procedure complied with pervious researcher works by **(Debnath and Chaudhuri, 2010-b)** and **(Dey et al., 2011)**.

3.6.4 Suspension Bridge/ Al-Basra Province

Bed material

Based on the investigations of the soil issued by Al-Mawal Company for Soil Investigation. The soil taken at a depth of (5.5-6 m) from the Al-Basra River was sieved again and poured into the test section, it's classified as (medium river sand). The thickness of the bed material is (20 cm) and the slope of the bed is adjusted in parallel with flume surface as (S_0=0). The properties of the soil and sediment size distribution are given in Table 3.6 and Figure 3.13; the detailed information is introduced in table (A-4) in **Appendix A**.

Table 3.6: Bed material properties for Suspension bridge.

Variable	Value	Variable	Value
D_{10}	0.6 mm	φ	37°
D_{16}	0.61 mm	C	0.0 Kg/cm^2
D_{30}	0.62 mm	T.S.S %	14.31
D_{50}	0.65 mm	SO_3 %	3.91
D_{60}	0.67 mm	Gypsum, $CaSo_4$ %	8.40
D_{84}	0.7 mm	Chloride, Cl %	0.044
σ_g	1.07	pH	8.0
Cu	1.11	CaCO3 %	14.0
Cc	1.57	Organic matter %	5.83
K	0.4*10^{-2}	E-Conductivity	5.0 mmhos/cm

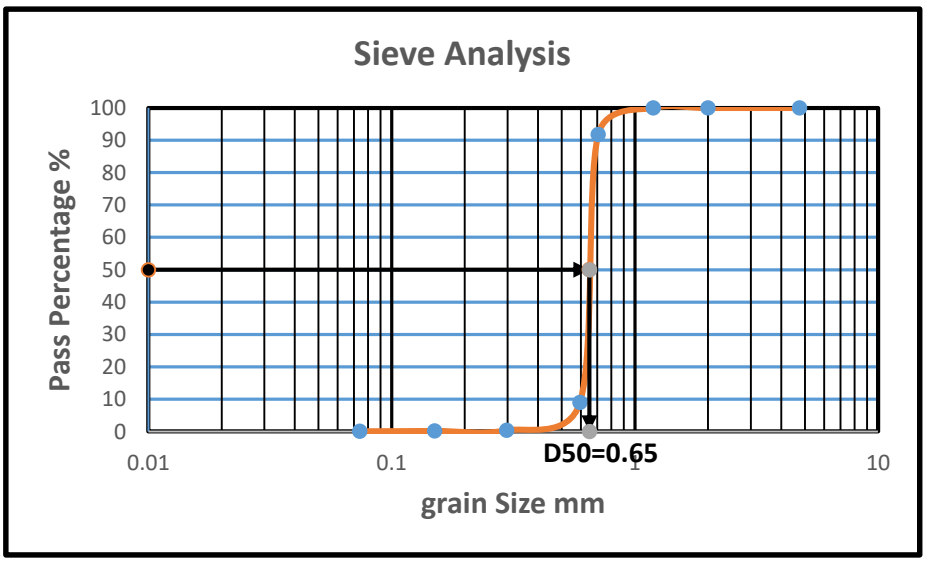

Figure 3.13: Sediment size distribution for the bed material for Suspension bridge.

As it is seen from Table 3.3, the geometric standard deviation is lesser than 1.3 and sediment distribution is defined as uniform for this value. **(Yanmaz, 2002)** states that when $\sigma_g < 1.3$ the bed material is considered to be uniform. Otherwise i.e. $\sigma_g > 1.3$ the sediment is said to be non-uniform. Geometric standard deviation shows the sediment gradation and itis calculated from the particle size distribution graph: $\sigma_g = (D_{84}/D_{16})^{0.5}$.

3.6.5 Al -Shallala Bridge/ Kirkuk Province

Bed material

Based on the investigations of the soil issued by Al-Ebdaa Company for Soil Investigation and Piles Tests Construction Materials Tests. The bed material used in the experiments composed of gravel and fine sand mixed with clay. These materials were extracted from the river at depth (5-6 m); the particle size distribution was tested by the sieve analysis introduced in Table (A-5) in **Appendix A**. The selected sand satisfies the criteria for non-uniform sand, where σ_g is greater than 1.3. The properties of the materials are presented in the Table 3.7 and Figure 3.14.

Table 3.7: Bed material properties for Al -Shallala Bridge.

Variable	Value	Variable	Value
D_{10}	0.057 mm	K	$7.46*10^{-2}$
D_{16}	0.19 mm	φ	37°
D_{30}	0.73 mm	C	0.0 Kg/cm^2
D_{50}	1.13 mm	T.S.S %	1.5
D_{50a}	1.11 mm	SO_3 %	0.67
D_{60}	1.31 mm	Gypsum, $CaSo_4$ %	1.43
D_{84}	1.72 mm	Chloride, Cl %	0.02
D_{100}	2.0 mm	pH	7.4
σ_g	3.03	CaCO3 %	17
Cu	23.0	Organic matter %	0.01
Cc	9.8	E-Conductivity	5.0 mmhos/cm

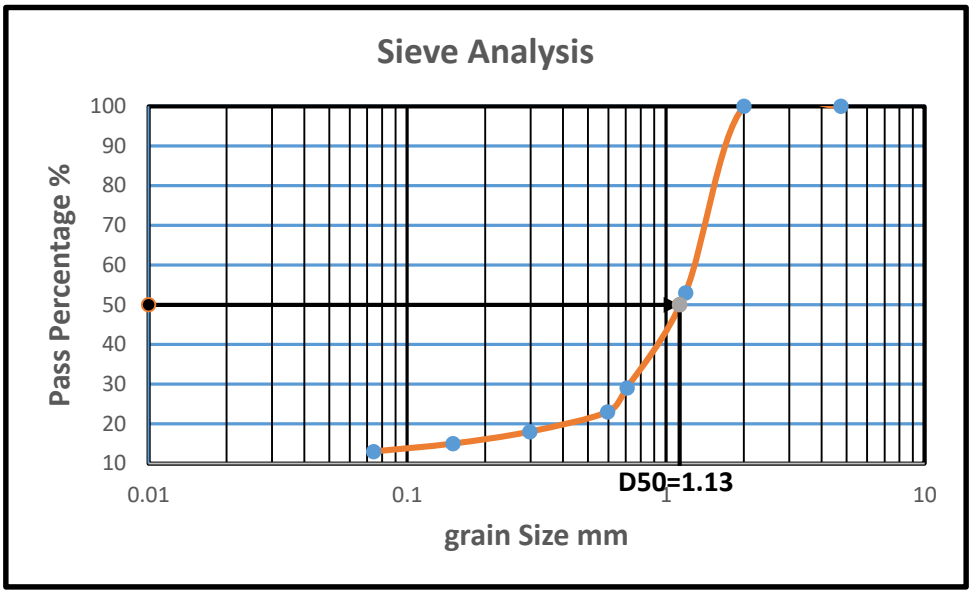

Figure 3.14: Sediment size distribution for the bed material for Al -Shallala Bridge.

The soil mixture is composed of (47% gravel and 40% fine sand mixed with 13% clay) manually and homogenously in dry condition to make sure that the soil mixture is evenly mixed. This mixture to test the scouring in the case of transitional behavior of soil between cohesion-less and cohesive. A soil mixture is placed around the complex pier model in the bed section of the flume in the longitudinal centerline and filled until a thickness (20 cm). The top surface of the bed material was leveled and smoothened. Next, the flume is filled with water until (27 cm) depth.

3.7 Complex Bridge Pier Model for (Ali Al-Gharbi, Selebat, Suspension, and Shallala) Bridges

The schematic of complex bridge pier for river with the prototype dimensions was fabricated with scale ratio 1:50. Manufactured form treated wood. These models were designed with a cylindrical column founded on a rectangular pile cap, supported by a pile group. The arrangement of this last component consists of: two alignments of four cylindrical piles The longitudinal axis of the complex pier models was aligned *i.e.*, α=0° and skew-angle α=30°, 45°, 60° with the approach flow, as shown in Figure 3.14 below. The schematic diagram shown in Figure 3.15. The geometric characteristics of the model are summarized in Table 3.8.

Table 3.8: Geometric characteristics of the complex pier model of the experimental campaign.

Variable	Dimension(cm)	Variable	Dimension(cm)	Variable	Dimension(cm)
D_c	2.5	L_{pc}	23	n	2
L_c	10	T	2.5	S_m	6
f_L	2.75	D_p	3	S_n	6
f_t	5.75	f_p	1		
D_{pc}	14	m	3		

According to **(Melville and Coleman, 2000)** choosing the pier diameter carefully, in order to avoid the effect of contraction on the scour depth, the flume width should be at least ten times the pier width. The constant flow depth (7) cm.

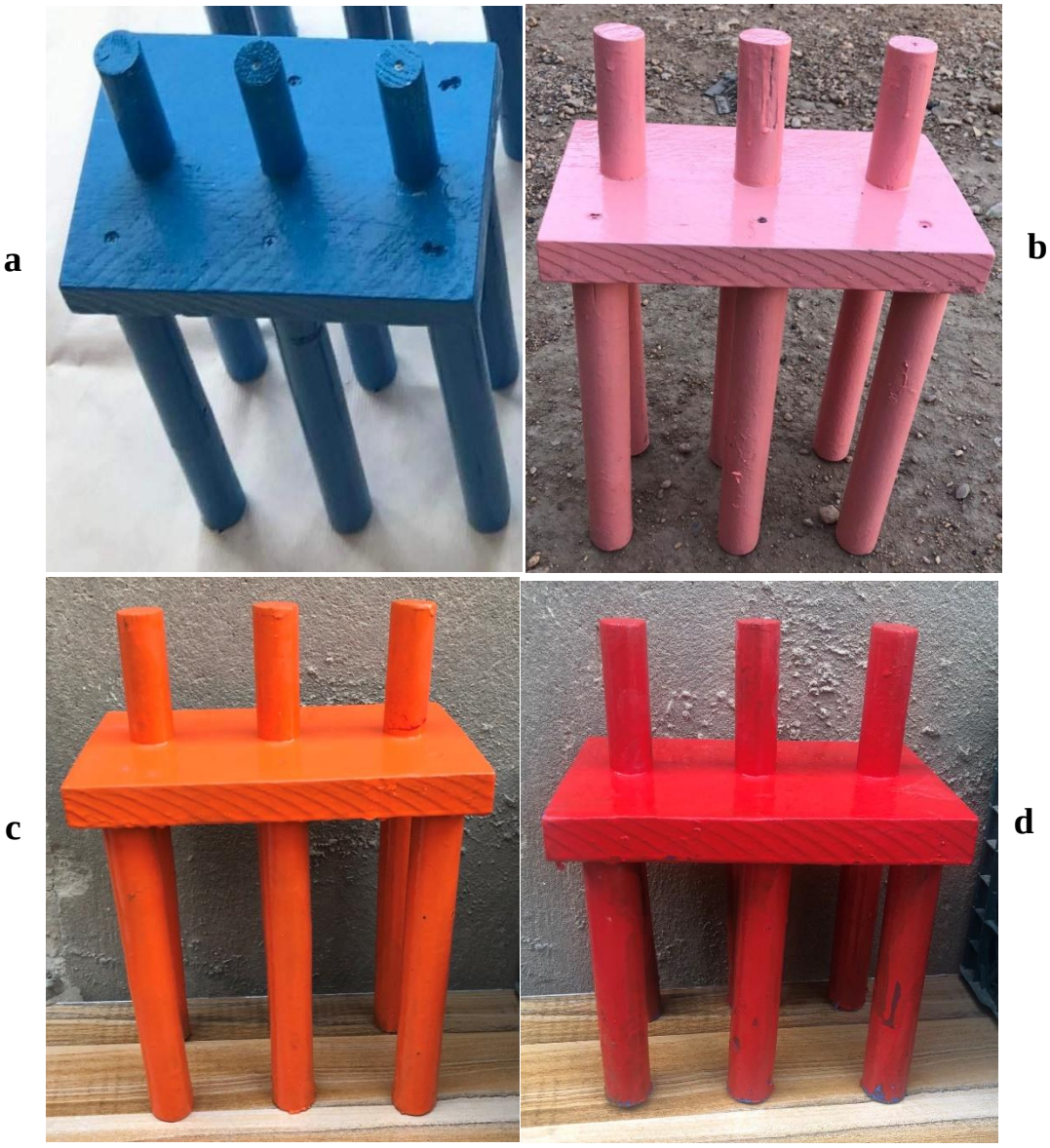

Figure 3.15: Bridge Pier model used in the experiments. a: Al-Gharbi, b: Selebat, c: Suspension, d: Shallala.

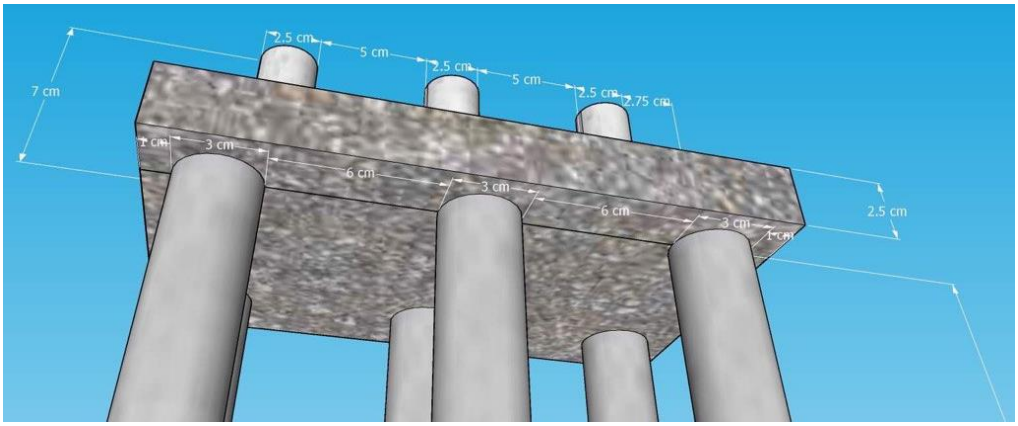

Figure 3.16: The schematic diagram of complex bridge Pier model.

CHAPTER FOUR

Experimental Results,

Analysis and Discussion

Chapter Four

Experimental Results, Analysis and Discussion

4.1 Introduction

This chapter presents the experiment results collected from each bridge model. The scour measurements are given for the steady flow conditions around five models of bridges for different Iraqi soils, constant flow depth, three flow velocity values, aligned and skew-angle to the flow direction. Each section of this chapter presents results for bridge model with a total of 90 experiments.

Due to the limited number of studies in this topic, the present work performed in order to quantify the temporal evaluation and maximum scour at complex piers, the influence of the complex pier pile-cap position (relative to the initial bed level), effect of skew-angle, and effect of interaction on scouring at complex bridge piers.

4.2 Beta River Model

The experimental conditions and results for Beta River model are tabulated in terms of flow skew–angle, α, flow discharge, Q, approach velocity, V, critical velocity, V_c, Armor Peak Velocity, V_a, flow density, $[V-(V_a-V_c)]/V_c$, pile cap position, H_c/h, maximum scour depth, d_s, pile Reynold number R_p, and Froude number, F in Table 4.1. For the experimental runs in Beta River model, where time of scour 24 hours, d_{50}= 0.45 mm, d_{50a}= 0.393 mm and approach flow depth h=7 cm.

Table 4.1: Summary of measured experimental data for Beta River model.

Run	$\alpha°$	Q (l/s)	V (m/s)	V_c (m/s)	V_a (m/s)	$\frac{V-(Va-Vc)}{Vc}$	H_c/h	d_s (cm)	R_p	F
1	0	12.6	0.180	0.257	0.206	0.90	1.43	3.0	5400	0.217
2	0	13.5	0.193	0.257	0.206	0.95	1.43	3.8	5790	0.233
3	0	14.2	0.203	0.257	0.206	0.99	1.43	5.0	6090	0.245
4	30	14.2	0.203	0.257	0.206	0.99	1.43	7.5	6090	0.245
5	45	14.2	0.203	0.257	0.206	0.99	1.43	9	6090	0.245
6	60	14.2	0.203	0.257	0.206	0.99	1.43	11	6090	0.245
7	0	12.6	0.180	0.257	0.206	0.90	0.430	0.7	5400	0.217
8	0	13.5	0.193	0.257	0.206	0.95	0.430	1.3	5790	0.233
9	0	14.2	0.203	0.257	0.206	0.99	0.430	2.1	6090	0.245
10	30	14.2	0.203	0.257	0.206	0.99	0.430	2.5	6090	0.245
11	45	14.2	0.203	0.257	0.206	0.99	0.430	2.9	6090	0.245
12	60	14.2	0.203	0.257	0.206	0.99	0.430	3.3	6090	0.245
13	0	12.6	0.180	0.257	0.206	0.90	0	0.5	5400	0.217
14	0	13.5	0.193	0.257	0.206	0.95	0	0.75	5790	0.233
15	0	14.2	0.203	0.257	0.206	0.99	0	1.0	6090	0.245
16	30	14.2	0.203	0.257	0.206	0.99	0	1.3	6090	0.245
17	45	14.2	0.203	0.257	0.206	0.99	0	1.5	6090	0.245
18	60	14.2	0.203	0.257	0.206	0.99	0	1.7	6090	0.245

4.2.1 Temporal Evaluation and Maximum Scour at Complex piers

According to the results of tests carried out for Beta Model, the scour process in the three clear and distinguished situations considered may be typically described as follows:

1. Situation 1, characterized by the fact that the bottom of the pile cap is above the initial bed level aligned (0°) and skewed (30°, 45°, and 60°) to the flow direction, the temporal evolution of the maximum scour depth is similar to that of the single pier case, following a unique stage, as illustrated in Figure 4.1. In this situation, the scour process initiates in front of each of the upstream piles, with individual holes, until they merge into one single scour hole; the maximum scour depth is located in front of the upstream piles of the group, increase with skew-angle

increasing. Figure 4.2 shows photos of the referred maximum scour hole.

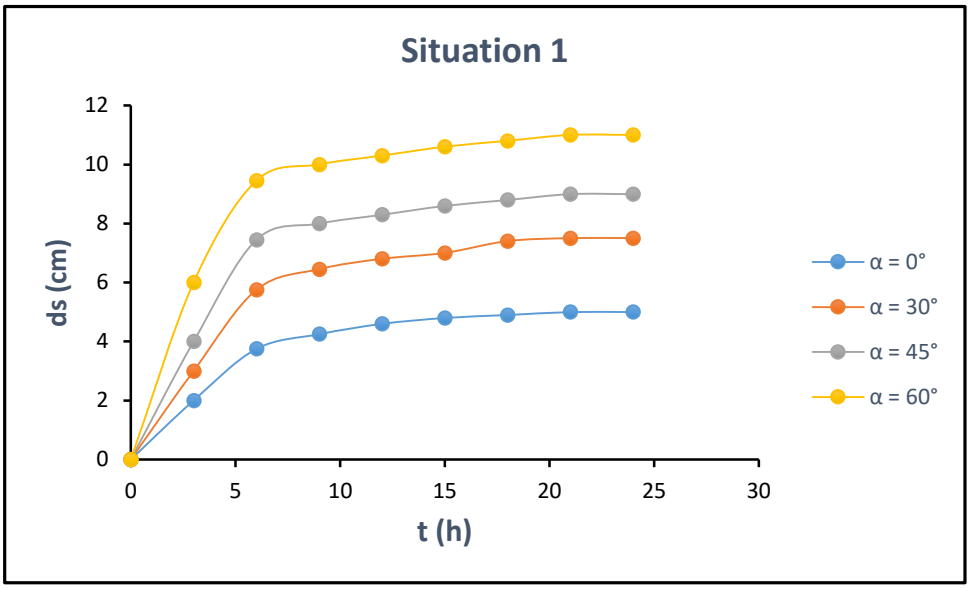

Figure 4.1: Situation 1: scheme of the temporal evaluation of the scour depth for Beta bridge.

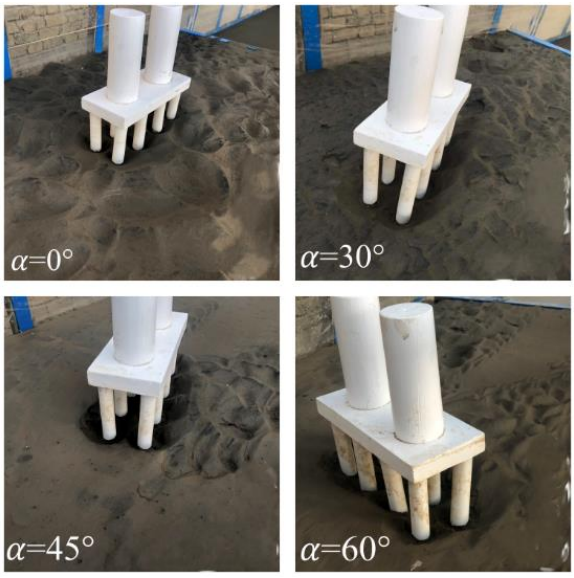

Figure 4.2: Situation 1: photograph of maximum scour hole for Beta bridge.

2. Situation 2, corresponding to the case where the pile cap is placed close to the original bed, also the scour depth evolution follows a unique trend, as identified in Situation 1, but it's process continues underneath the pile cap, in front of the upstream piles, maximum scour depth increases with skew-angle increasing, as shown in Figure 4.3. Figure 4.4 shows the maximum scour hole at the end of the test.

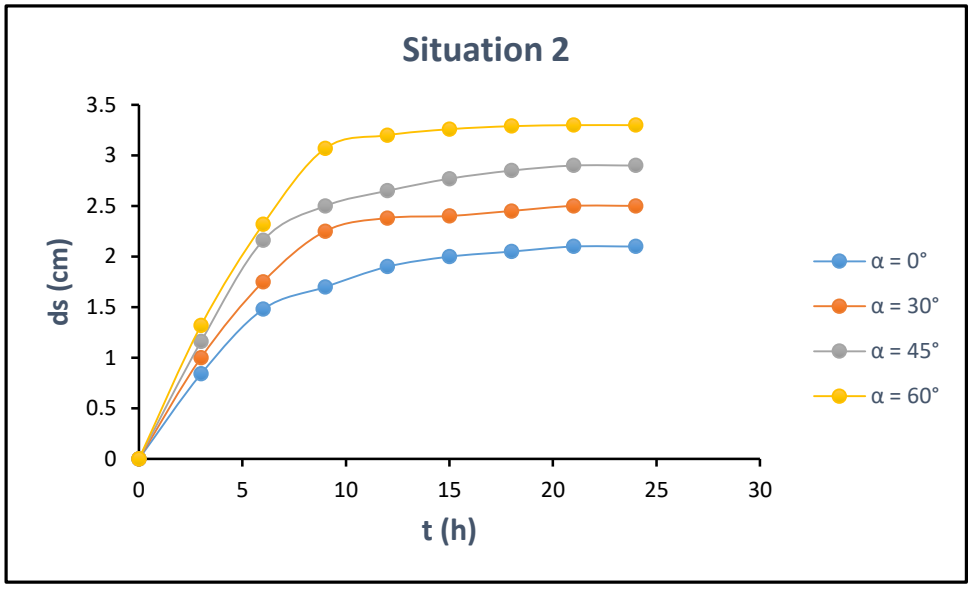

Figure 4.3: Situation 2: scheme of the temporal evaluation of the scour depth for Beta bridge.

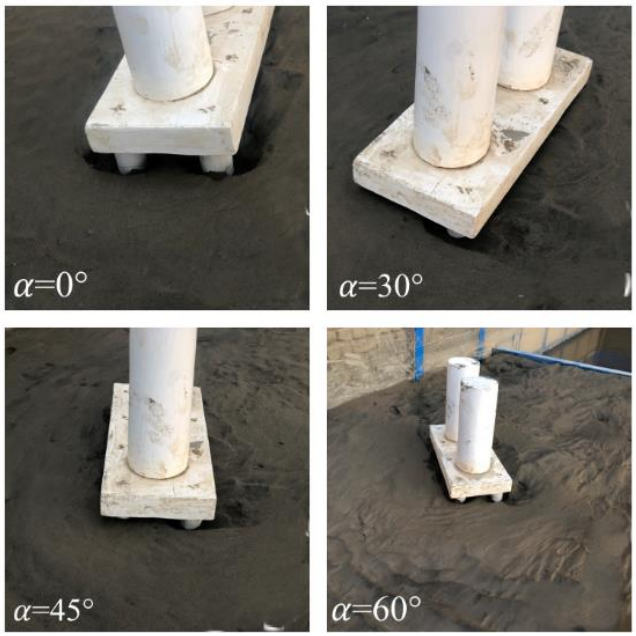

Figure 4.4: Situation 2: photograph of maximum scour hole for Beta bridge.

3. Situation 3, when the pile cap is completely buried in the bed, the scour depth record displays different stages depending on the top of the pile-cap position below the initial bed level. Three stages are also typically identified as in Figure 4.5: (i) initially, the scour process develops in front of the column until the scour hole partly uncovers the top of the pile cap; (ii) that period is followed by a stage when the scour depth does not evolve

during a (more or less significant, depending of D_c/D_{pc} ratio) lapse of time and the maximum scour depth is equal to the distance from the initial bed level to the top of the pile cap; and (iii) on the following stage, the scour process continues in front of the pile cap. Figure 4.6 shows the maximum scour hole associated with those three stages.

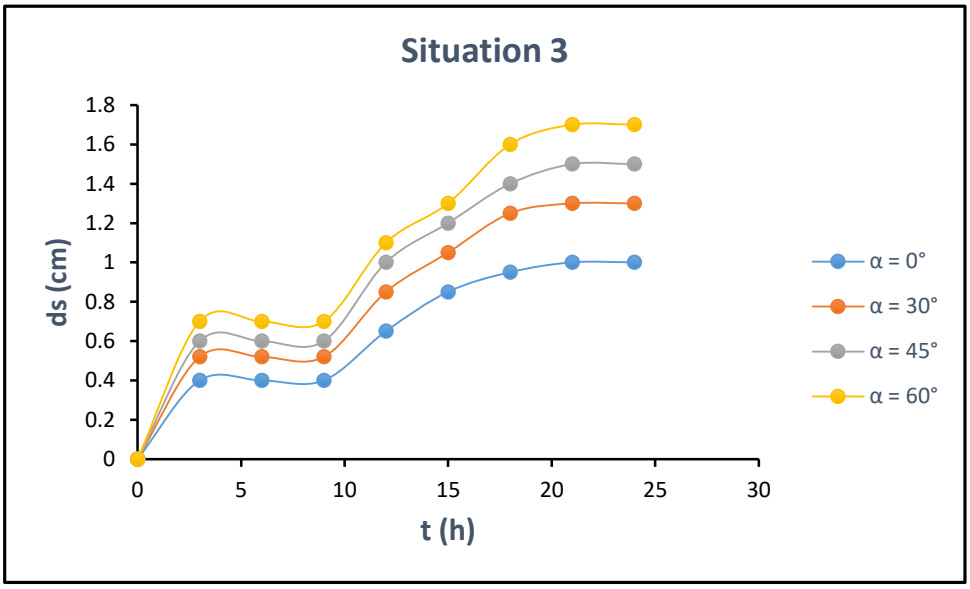

Figure 4.5: Situation 3: scheme of the temporal evaluation of the scour depth for Beta bridge.

Figure 4.6: Situation 3: photograph of maximum scour hole for Beta bridge.

4.2.2 Influence of the Pile-Cap Position

Eighteen tests with different pile-cap position were performed aligned and skew-angle to the flow direction. Those tests include: six to each Situation. All the corresponding curves in situation 1 showing similar trends to curve as in (Figure 4.1). The slight increment in the scour depth values may be justified by the corresponding small increment of the area exposed to the flow. For the four tests of Situation 2 (0°, 30°, 45°, and 60°), also showing similar trends to curve as in (Figure 4.3). However, the scour depth evolution trend in these tests is more similar to the typical one obtained for tests of Situation 1. This may be justified by the fact that the longitudinal axis of the pile cap overlaps that of the alignment of piles, this enabling the upstream pile to contribute to the scour process immediately after the entire front of the pile cap is exposed to the scour hole. The time scour depth evolution for the four tests of Situation 3 (0°, 30°, 45°, and 60°), where once again, due to the particular complex pier geometry, the three characteristics stages of curve, (Figure 4.5) are observed. The duration of the intermediate stage was short where. In this test, it is characterized by the top of the pile cap remaining below the base of the scour hole, only the first stage was observed, as expected, as shown in Figure 4.7.

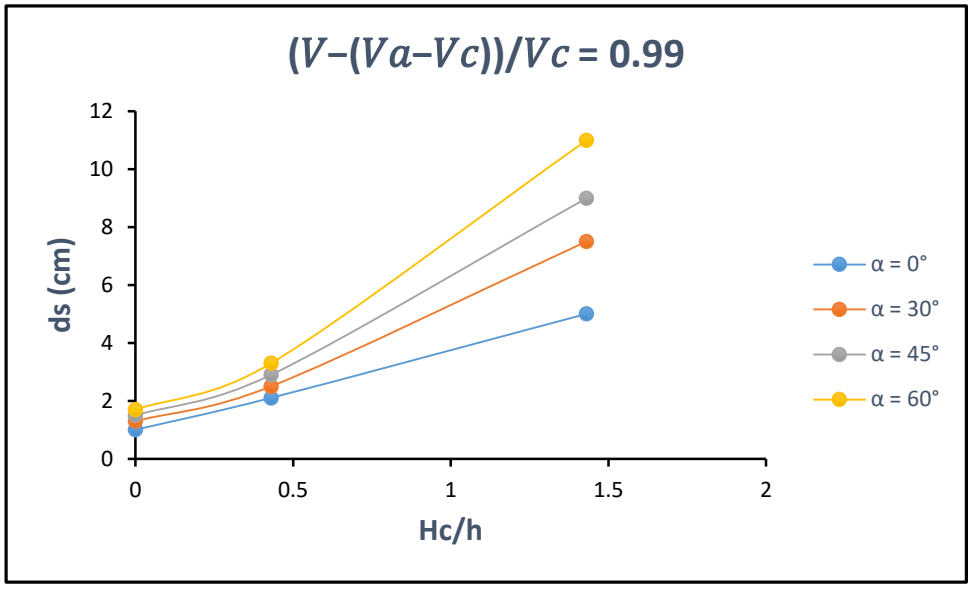

Figure 4.7: Influence of pile-cap position on the temporal evaluation of the scour depth aligned and skew-angle for Beta bridge.

4.2.3 Effect of Skew-Angle

This is a follow up study of the previous studies conducted by **(Bozkus and Yildiz, 2004) and (Bozkus and Cesme, 2010)**, as the skewness angle is the major parameter in all. The experiments were performed for the angles (α= 0°, 30°, 45°, and 60°). It can be said that on the whole, local scour depths increase significantly as the skewness angle increases. However, this increment is more apparent at the most upstream pier, which is skewed towards downstream. Increasing of almost 35-50% was measured around front piers when most upstream and most downstream piers are placed at a skewness angle of α=60° through downstream and upstream directions respectively when compared to scours developed around vertical piers. The skewness angle of the middle piers was not changed throughout the experiments. Still, increasing in scour depths has been observed with the skewness of the very upstream pier. Approximately, the depth of scour increasing of 10-15% was noticed around the second pier. The most downstream piers are skewed through upstream, thus an increase in scour depth is expected when skewness angle

increases. However, based on the experimental data, no significant change in scour depth is observed. The strength of the vortices that move sediment particles around piers increases as the skewness angle increases. Down-flow is resolved into its components when approach flow hits the skewed pier, thus vertical component of the down-flow decreases. Smaller scour holes are generated around cylindrical piers and aggradation at the most downstream of the pier group decreases. The following figure shows the variation of equilibrium scour depths with respect to skewness angle, α, as shown in Figure 4.8.

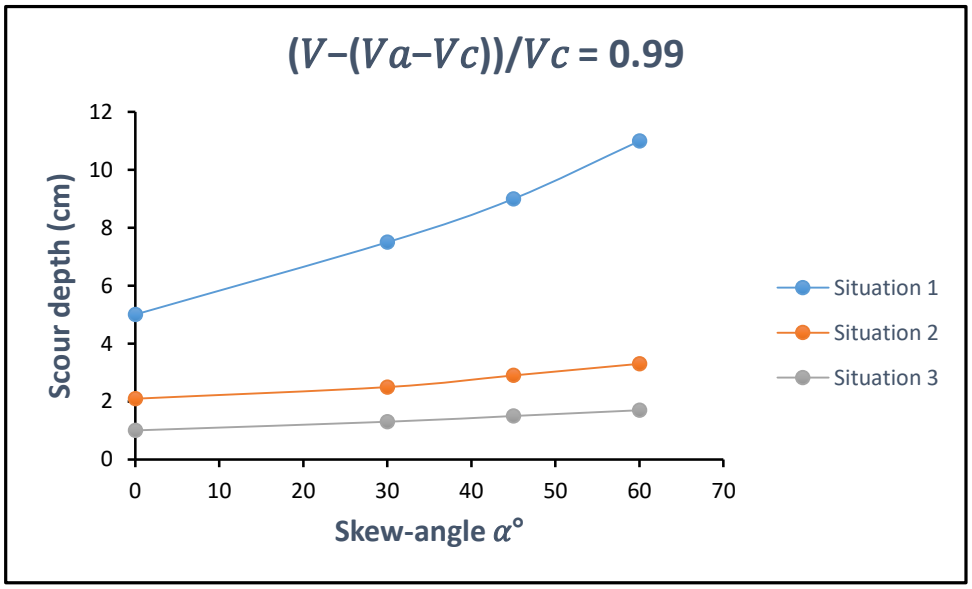

Figure 4.8: Variation of equilibrium scour depth with respect to skewness angle for Beta bridge.

4.3 Ali Al-Gharbi River Model

The experimental conditions and results for Ali Al-Gharbi River model are tabulated in terms of flow skew–angle, α, flow discharge, Q, approach velocity, V, critical velocity, V_c, Armor Peak Velocity, V_a, flow density, $[V-(V_a-V_c)]/V_c$, pile cap position, H_c/h, maximum scour depth, d_s, pile Reynold number R_p, and Froude number, F in Table 4.2 for the

experimental runs in Ali Al-Gharbi River model, where time of scour 24 hours, d_{50}= 0.37 mm, d_{50a}= 0.393 mm and approach flow depth h=7 cm.

Table 4.2: Summary of measured experimental data for Ali Al-Gharbi River model.

Run	$\alpha°$	Q (l/s)	V (m/s)	V_c (m/s)	V_a (m/s)	$\frac{V-(Va-Vc)}{Vc}$	H_c/h	d_s (cm)	R_p	F
1	0	10.9	0.155	0.257	0.206	0.80	1.1	2.2	4650	0.187
2	0	12.6	0.180	0.257	0.206	0.90	1.1	2.7	5400	0.217
3	0	14.2	0.203	0.257	0.206	0.99	1.1	4.0	6090	0.245
4	30	14.2	0.203	0.257	0.206	0.99	1.1	5.3	6090	0.245
5	45	14.2	0.203	0.257	0.206	0.99	1.1	6.0	6090	0.245
6	60	14.2	0.203	0.257	0.206	0.99	1.1	8.1	6090	0.245
7	0	10.9	0.155	0.257	0.206	0.80	0.36	0.5	4650	0.187
8	0	12.6	0.180	0.257	0.206	0.90	0.36	0.7	5400	0.217
9	0	14.2	0.203	0.257	0.206	0.99	0.36	1.0	6090	0.245
10	30	14.2	0.203	0.257	0.206	0.99	0.36	1.5	6090	0.245
11	45	14.2	0.203	0.257	0.206	0.99	0.36	1.9	6090	0.245
12	60	14.2	0.203	0.257	0.206	0.99	0.36	2.1	6090	0.245
13	0	10.9	0.155	0.257	0.206	0.80	0	0.35	4650	0.187
14	0	12.6	0.180	0.257	0.206	0.90	0	0.5	5400	0.217
15	0	14.2	0.203	0.257	0.206	0.99	0	0.75	6090	0.245
16	30	14.2	0.203	0.257	0.206	0.99	0	1.0	6090	0.245
17	45	14.2	0.203	0.257	0.206	0.99	0	1.2	6090	0.245
18	60	14.2	0.203	0.257	0.206	0.99	0	1.5	6090	0.245

4.3.1 Temporal Evaluation and Maximum Scour at Complex piers

The temporal development of the scour hole at the complex pies depends on H_c **(Melville and Raudkivi, 1996)**. Local scour depth at the pile cap can be estimated based on identification of the transition of the scouring process for varying pile cap locations relative to the undisturbed streambed. The location of maximum scour depth varies for different pile cap levels as flows:

1. Situation 1, where a group of piles is exposed to the flow, aligned and skewed (0°, 30°, 45°, and 60°) to the flow direction. The result of the observations demonstrated that an increase of the pile cap top elevation from initial level of sediment bed leads to an increase of the maximum value of the scour depth. the temporal evolution of the maximum scour depth has the same trend single pier, as shown in Figure 4.9. In this situation, the scour process generated in front of each of the upstream piles, the maximum scour depth is located in front of the upstream piles of the group, increase with skew-angle increasing. Figure 4.10 shows photos of the referred maximum scour hole.

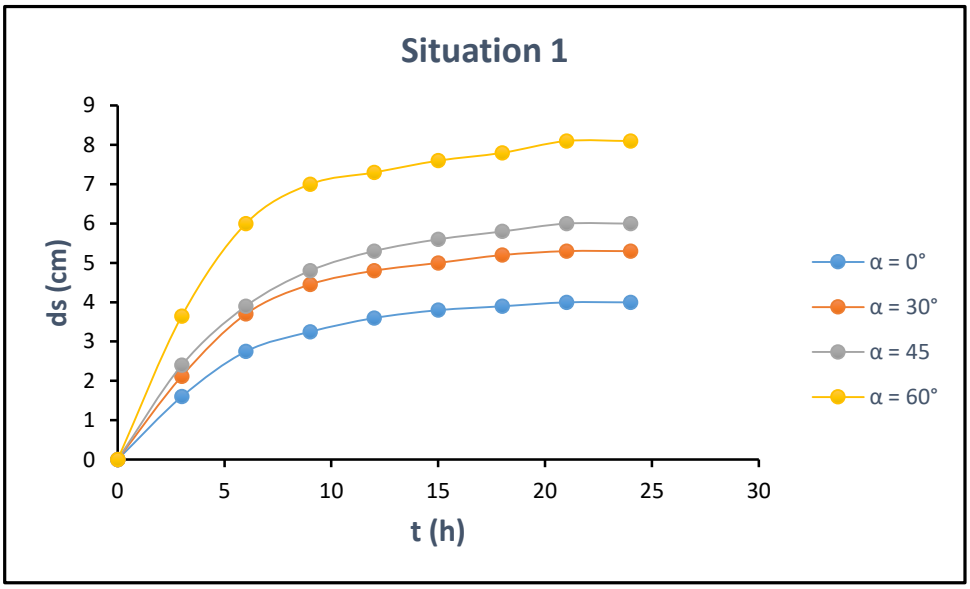

Figure 4.9: Situation 1: scheme of the temporal evaluation of the scour depth for Ali Al-Gharbi bridge.

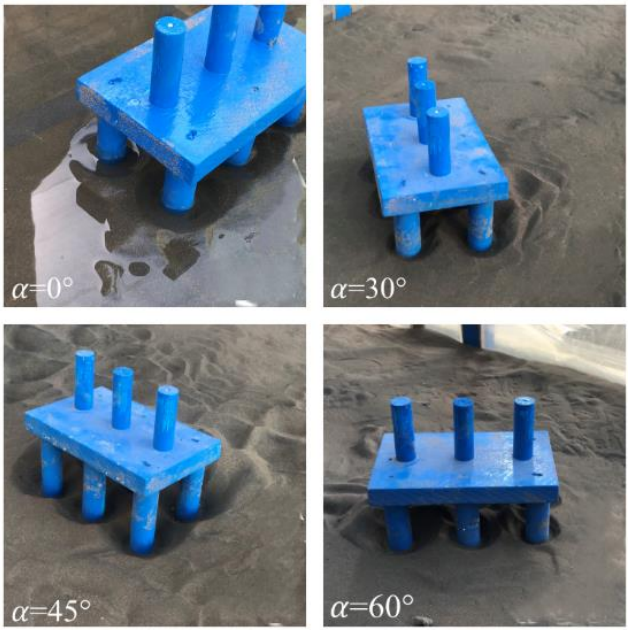

Figure 4.10: Situation 1: photograph of maximum scour hole for Ali Al-Gharbi bridge.

2. Situation 2, represents the level at which the base of the pile-cap was above the stream bed, the maximum scour depth will tend to localize mainly beneath the pile-cap, maximum scour depth increases with skew-angle increasing, as shown in Figure 4.11. Figure 4.12 shows the maximum scour hole at the end of the test.

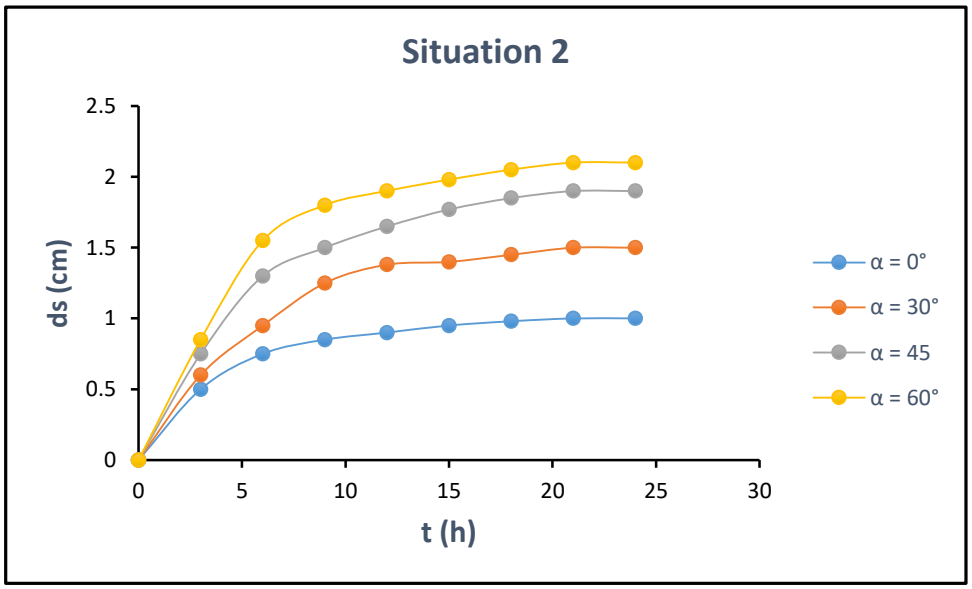

Figure 4.11: Situation 2: scheme of the temporal evaluation of the scour depth for Ali Al-Gharbi bridge.

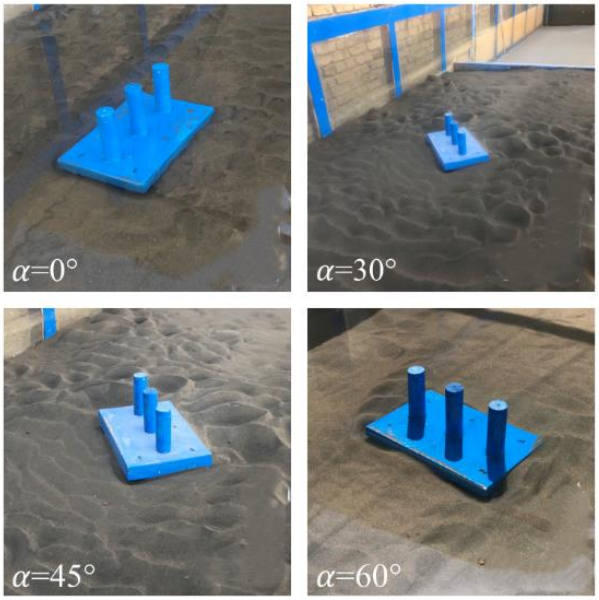

Figure 4.12: Situation 2: photograph of maximum scour hole for Ali Al-Gharbi bridge.

3. Situation 3, when the base of the pile-cap was fully buried, when H_c=0, the pile-cap extensions in both direction of pier (f_L, f_t) protect the bed from scour and postpone the beginning of the scour development and it takes a long time to achieve equilibrium conditions, as shown in Figure 4.13. The initial scour begins behind the pier due to the wake vortices and then it develops around the column gradually. Based on the present experiments at H_c=0, the diameter of the column and foundation play an important role at the beginning and development during the scour. **(Sheppard and Jones, 1998)**, found that scour at a column founded on a pile cap is dependent on the relative width of the column and the pile cap, D_c/D_{pc}. If the pile-cap is much wider than the column, the downward flow and horseshoe vortices generated by the column are isolated from the bed by the pile-cap and scour is relatively insensitive to the column size. The maximum scour depth increase with increasing the skew-angle, as shown in Figure 4.14.

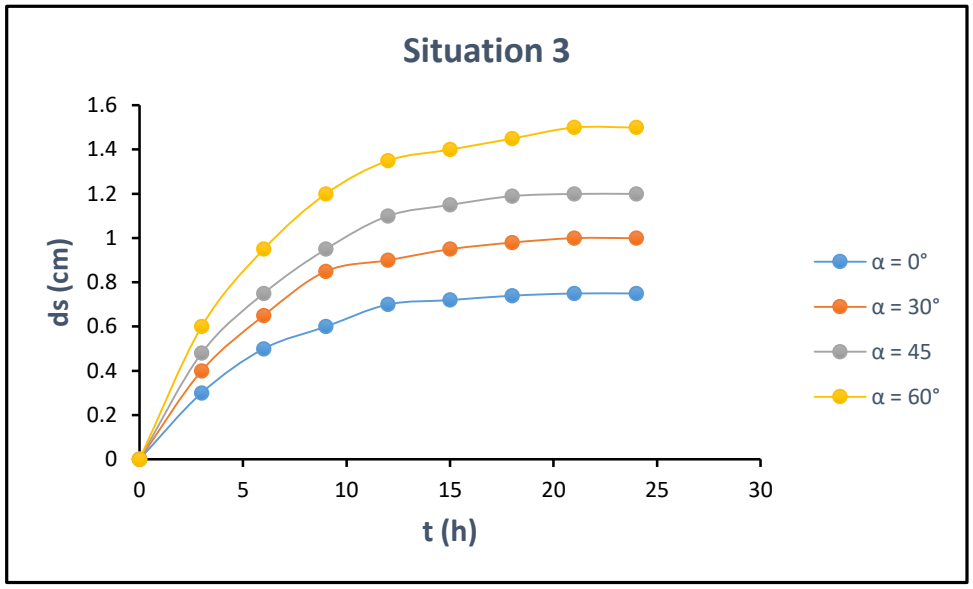

Figure 4.13: Situation 3: scheme of the temporal evaluation of the scour depth for Ali Al-Gharbi bridge.

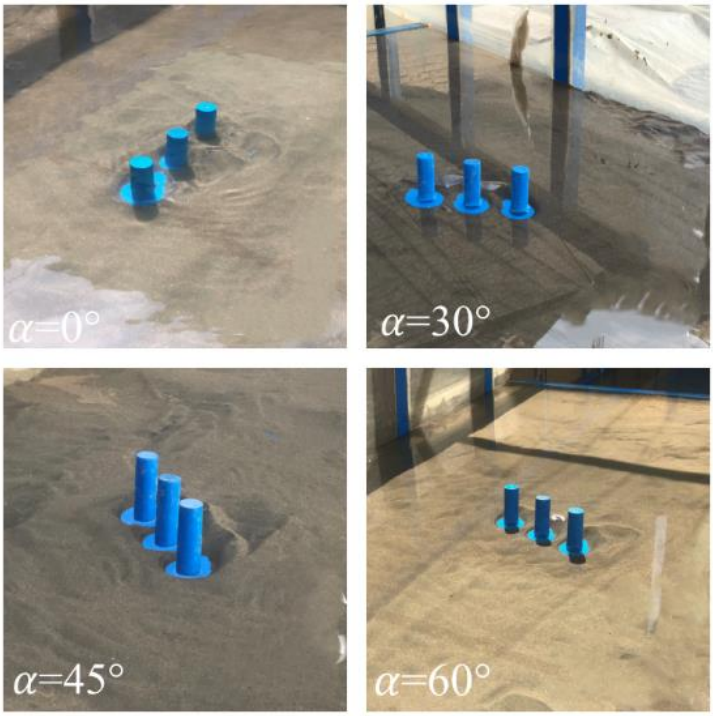

Figure 4.14: Situation 3: photograph of maximum scour hole for Ali Al-Gharbi bridge.

When the skew angle is zero, the location of maximum scour depth always occurs around the stagnation point of the first pier. This is due to the sheltering effect that reduces the approaching velocity at the downstream piers, and weakens the strength of the associated horseshoe vortices.

When the skew angle is greater than zero, the maximum scour depth occurs at the pier facing flow, depending on the skew angle. This is attributed to the strengthening of the horseshoe vortices when they superimpose with the wake vortices from the upstream pier. **(Lança et al., 2013b)** found that this effect increases sediment entrainment at the downstream pier. Because this interaction only exists at the pier facing flow, thus maximum scour depth occurres.

4.3.2 Influence of the Pile-Cap Position and Pier Skewness

The data presented in Table 4.2 are plotted in Figure 4.15, using the normalized scour depth d_s as a function of the normalized pile-cap elevation H_c/h, where h is the flow depth. It can be seen that, for the complex piers aligned to the flow (α=0°), the scour depth increases with far distance between the pile-cap and the undisturbed bed level, and reaches a maximum when the bottom of the pile-cap is above the bed (which is Hc/T =3 in the present study). After this situation, with decreasing pile-cap elevation, the top of the pile-cap is at the undisturbed level, and eventually lower than the bed level. During this stage, the scour depth decreases sharply, which is attributed by many researchers to the protection effect of the pile-cap that disturbs the down-flow in front of the pier. In general, the data for the pier aligned to the flow are in accordance with the results of other studies.

For the complex piers with a skew angle to the flow, the variation of the scour depth with the varying pile-cap elevation is completely different. Once a comparatively small skew angle exists, the scour depth increases strikingly, especially in the situations where the bottom of the pile-cap is above the bed level. In addition, the increase of scour depth is proportional to the skew angle, as shown in Figure 4.16, As a consequence, situations

that are considered to be safe for aligned piers (e.g. $Hc/T \leq 0$) can be extremely dangerous when the flow direction changes because of, for example, obstacles in the flow, flow contraction, or a particular flood event.

Generally, for skewed complex piers, if the column is inserted significantly into the flow, it causes much more disruption to the flow and much stronger down-flow than that due to the pile-cap and the pile group. Thus, the increased scour depth for skewed piers is mostly attributed to the presence of the wall-like column. A complex pier behaves more like a wide pier with increasing skewness to the flow. This phenomenon also causes the variation of flow shallowness and sediment coarseness with skew angle.

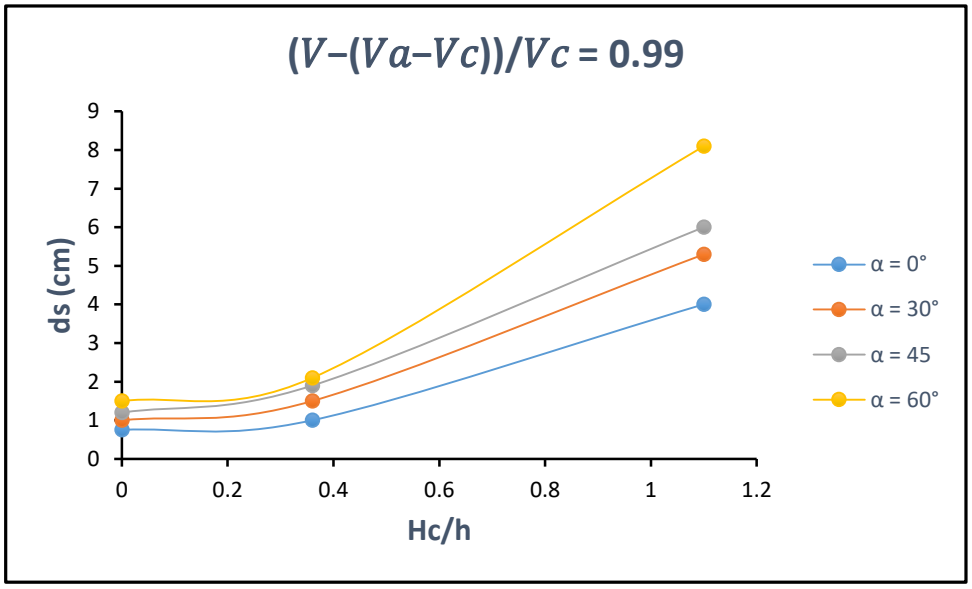

Figure 4.15: Influence of pile-cap position from the initial bed on the temporal evaluation of the scour depth for Ali Al-Gharbi bridge.

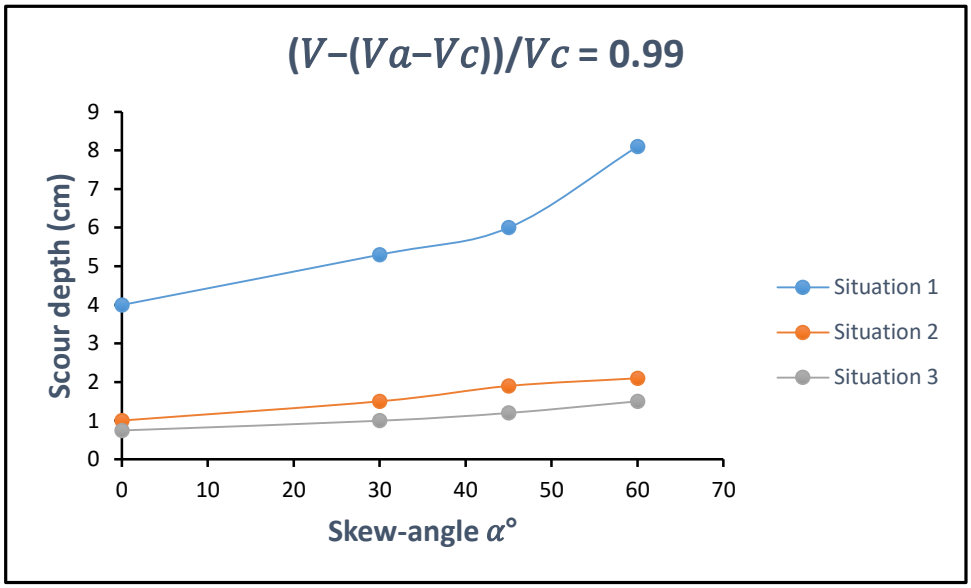

Figure 4.16: Variation of equilibrium scour depth with respect to skewness angle for Ali Al-Gharbi bridge.

4.4 Selebat River Model

The experimental conditions and results for Selebat River model are tabulated in terms of flow skew–angle, α, flow discharge, Q, approach velocity, V, critical velocity, V_c, Armor Peak Velocity, V_a, flow density, $[V-(V_a-V_c)]/V_c$, pile cap position, H_c/h, maximum scour depth, d_s, pile Reynold number R_p, and Froude number, F in Table 4.3 for the experimental runs in Selebat River model, where time of scour 24 hours, with soil (50% clay and 50% river sand d_{50}=0.074 mm, d_{50a}= 0.66 mm), and approach flow depth h=7 cm.

Table 4.3: Summary of measured experimental data for Selebat River model.

Run	$\alpha°$	Q (l/s)	V (m/s)	V_c (m/s)	V_a (m/s)	$\frac{V-(Va-Vc)}{Vc}$	H_c/h	d_s (cm)	R_p	F
1	0	12.4	0.177	0.295	0.236	0.80	1.1	0.9	5310	0.214
2	0	14.5	0.207	0.295	0.236	0.90	1.1	1.5	6210	0.250
3	0	16.3	0.233	0.295	0.236	0.99	1.1	2.0	6990	0.281
4	30	16.3	0.233	0.295	0.236	0.99	1.1	0.4	6990	0.281
5	45	16.3	0.233	0.295	0.236	0.99	1.1	0.6	6990	0.281
6	60	16.3	0.233	0.295	0.236	0.99	1.1	0.85	6990	0.281
7	0	12.4	0.177	0.295	0.236	0.80	0.36	0.5	5310	0.214
8	0	14.5	0.207	0.295	0.236	0.90	0.36	0.7	6210	0.250
9	0	16.3	0.233	0.295	0.236	0.99	0.36	1.0	6990	0.281
10	30	16.3	0.233	0.295	0.236	0.99	0.36	1.0	6990	0.281
11	45	16.3	0.233	0.295	0.236	0.99	0.36	1.0	6990	0.281
12	60	16.3	0.233	0.295	0.236	0.99	0.36	1.0	6990	0.281
13	0	12.4	0.177	0.295	0.236	0.80	0	0.0	5310	0.214
14	0	14.5	0.207	0.295	0.236	0.90	0	0.0	6210	0.250
15	0	16.3	0.233	0.295	0.236	0.99	0	0.0	6990	0.281
16	30	16.3	0.233	0.295	0.236	0.99	0	0.0	6990	0.281
17	45	16.3	0.233	0.295	0.236	0.99	0	0.0	6990	0.281
18	60	16.3	0.233	0.295	0.236	0.99	0	0.0	6990	0.281

4.4.1 Temporal Evaluation and Maximum Scour at Complex piers

When an experimental run is started, the effect of the flow turbulence initiated at the complex piers location causes a progressive development of a scouring hole around a complex pier. The location of maximum scour depth varies for different pile-cap levels as flows:

1. Situation 1, where a group of piles is exposed to the flow, aligned and skewed (0°, 30°, 45°, and 60°) to the flow direction. The scouring process was monitored for the first (12) hours of the experimental run to examine the mechanism of scour hole development around the complex piers. After about (30) minutes of starting the experiment, the formation of the scour hole was observed. The scour started evenly around the complex piers.

Subsequently, the scour hole deepens and propagates to the downstream. In the first two hours of the experiment, the development of the scour hole was fast and there was rapid propagation to the downstream direction. After that the scour development was noticed to be slower, the scour hole continued to deepen and propagate to the downstream direction, but at a slower rate. The eroded sediment was deposited at the rear of the pier after six hours, as shown in Figure 4.17 and photos in Figure 4.18.

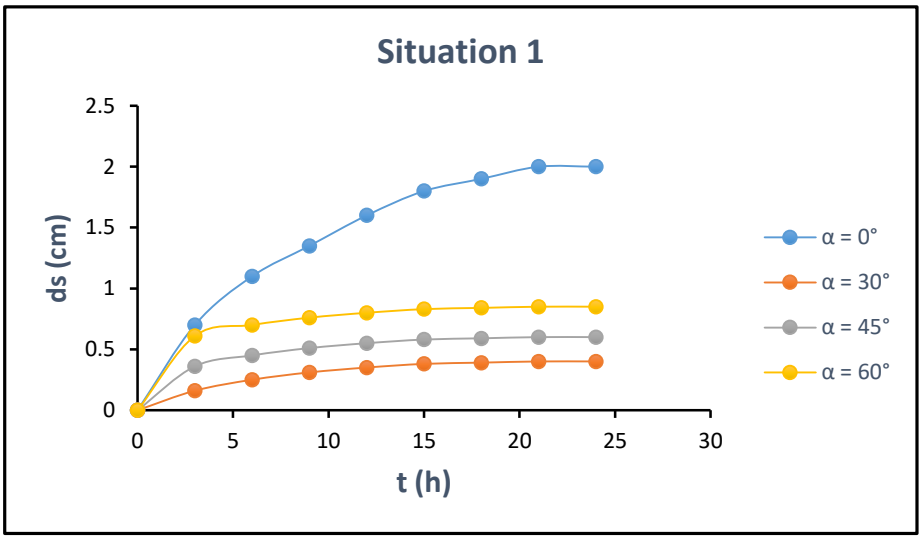

Figure 4.17: Situation 1: scheme of the temporal evaluation of the scour depth for Selebat bridge.

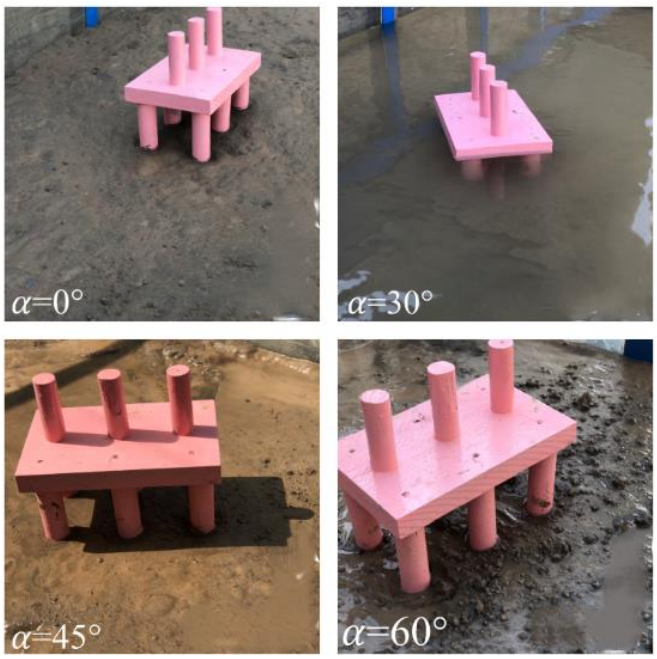

Figure 4.18: Situation 1: photograph of maximum scour hole for Selebat bridge.

2. Situation 2, represents the level at which the bottom of the pile-cap was above the stream bed, the same observations were made for the development of the scour hole. During the first (12) hours, no erosion was observed, after that, the bed started to erode at a slow rate, and slow development was noticed for a scouring cavity around the pile-cap. The time required for reaching the final scour depth, after which no significant changes take place in the bed level, increased due to the increase in clay content of the bed sediment, and the scour rate becomes much slower. The experiments lasted for (24) hours until no significant change was observed in the bed level around the pile-cap, and the scour hole is considered final. These observations agree with that reported in the literature. It was stated that "in clay-sand mixtures, the timescale to equilibrium scour increases with increasing clay content. The scour rate in clay is much slower than in sand for similar flow conditions" **(Briaud et al., 1999; Ting et al., 2001; Dey et al., 2011; and Kothyari et al., 2014)**. as shown in Figure 4.19 and Figure 4.20, the maximum scour hole at the end of the test. The maximum scouring depth was measured at pier sides. These observations agree with the finding of **(Ansari, et al., 2002; Debnath and Chaudhuri, 2010-a, 2010-b; Dey, et al., 2011; and Kothyri, et al., 2014)**. Other observations were made regarding the mode of sediment transport. The cohesive soil is scoured in different modes, as particle by particle and as chunks of aggregates. The resulting scour hole was relatively irregular; this may be attributed to the erosional behavior of the cohesive soil that was observed in the reported experiments, as shown in Figure 4.19 and 4.20.

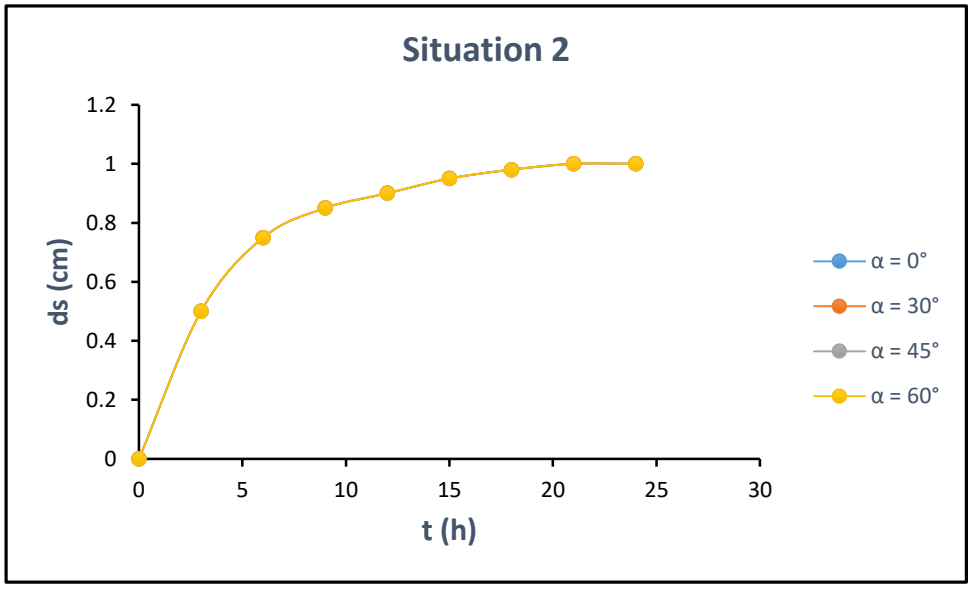

Figure 4.19: Situation 2: scheme of the temporal evaluation of the scour depth for Selebat bridge.

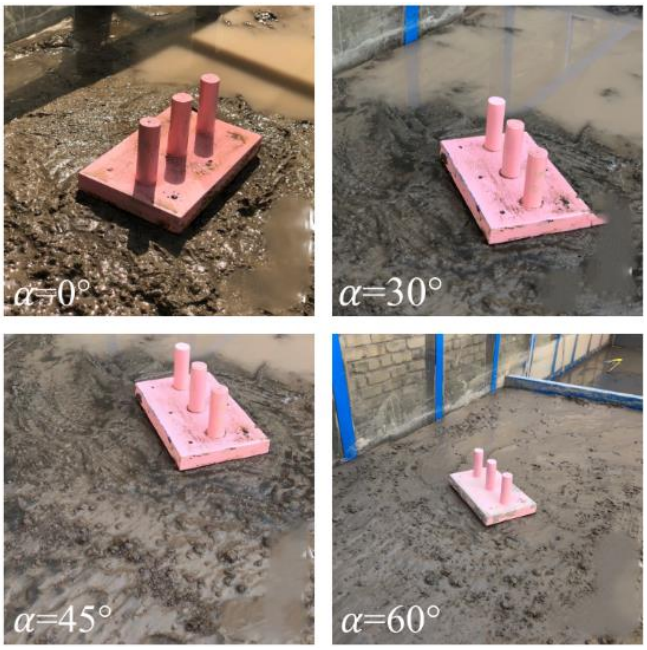

Figure 4.20: Situation 2: photograph of maximum scour hole for Selebat bridge.

3. Situation 3, when the base of the pile-cap was fully buried, when H_c=0, there is no scour observed, as shown in photos in Figure 4.21.

Figure 4.21: Situation 3: photograph of maximum scour hole for Selebat bridge.

4.4.2 Influence of The Pile-Cap Position and Pier Skewness

The data presented in Table 4.3 are plotted in Figure 4.22, the complex piers aligned to the flow (α=0°), the scour depth increases when the pile-cap above the initial bed ($H_c/T = 3$). After this situation, with the decreasing pile-cap elevation, the top of the pile-cap is at the undisturbed level, and eventually lower than the bed level. During this stage, the scour depth decreases sharply, the pile-cap formed as a collar around the piers. In situation 3 there is no scour recorded due to cohesion clay content which makes more protection to the piers.

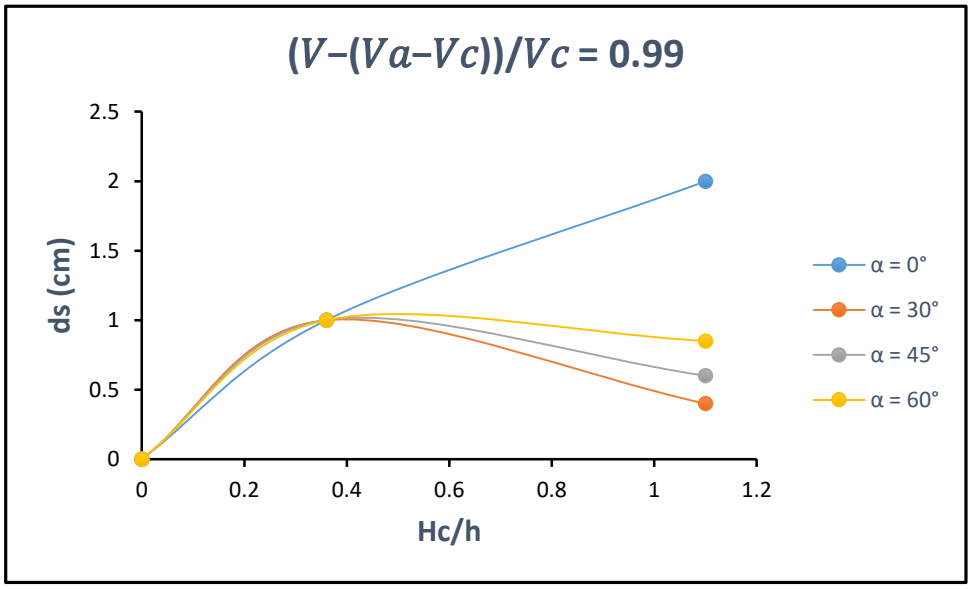

Figure 4.22: Influence of pile-cap position from the initial bed on the temporal evaluation of the scour depth for Selebat bridge.

A set of laboratory flume experiments were carried out to examine the change in the scouring at complex piers founded in a cohesive bed with changing the skewness. The experiments involved testing the scour hole formed under steady flow with three different skewness angles (α=30°, 45°, and 60°). The tests were run for 24 hours continuously, after that the formed scour hole geometry and dimensions were recorded. The scour was tested at flow velocity near the incipient motion of the sand fraction of the bed sediment. The objective is to identify the effect of the skewness angle of the complex pier on the local scour as compared to that at complex pier placed vertical to the flow direction. The measured scour hole around the complex piers in the flume test are displayed in Figure 4.23.

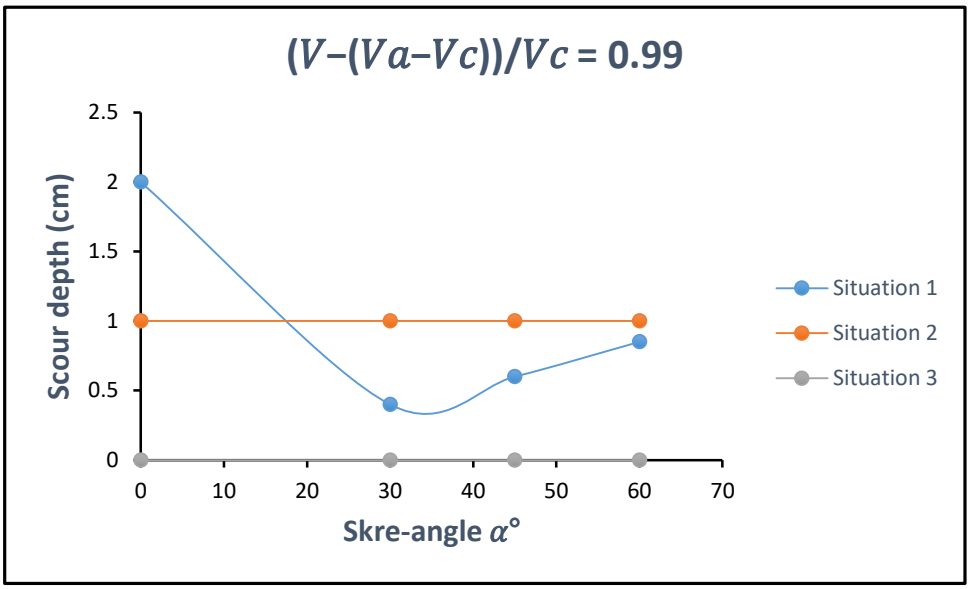

Figure 4.23: Variation of equilibrium scour depth with respect to skewness angle for Selebat bridge.

From Figure 4.23, in situation 1, the maximum scour hole records in the front pier when the piers are vertical to the flow direction, decreases (α=30°and 45°) then increases again in α=60° due to the increase in the area expose to the flow. The eroded sediment at the rear of the downstream piers and there is an irregular erosion in the rear zone of piers' arrangement. Separate scour hole was formed at the piers. In situation 2, the maximum scour depth is equal when the complex piers are vertical and skewness due to the effect of pile-cap position and thickness. In situation 3, there is no scour record for all cases due to clay content of the sediment, and the pile-cap formed a large base to product the piers from scour.

4.5 Suspension River Model

The experimental conditions and results for Suspension River model are tabulated in terms of flow skew–angle, α, flow discharge, Q, approach velocity, V, critical velocity, V_c, flow density, V/V_c, pile cap position, H_c/h, maximum scour depth, d_s, pile Reynold number R_p, and Froude number, F in Table 4.4 for the experimental runs in Suspension River model. Where

time of scour 24 hours, with soil fine sand, d_{50}=0.65 mm, and approach flow depth h=7 cm.

Table 4.4: Summary of measured experimental data for Suspension River model.

Run	α°	Q (l/s)	V (m/s)	V_c (m/s)	V/V_c	H_c/h	d_s (cm)	R_p	F
1	0	10.8	0.154	0.192	0.80	1.1	1.0	4620	0.186
2	0	12.0	0.173	0.192	0.90	1.1	1.5	5190	0.209
3	0	13.3	0.190	0.192	0.99	1.1	2.0	5700	0.229
4	30	13.3	0.190	0.192	0.99	1.1	3.0	5700	0.229
5	45	13.3	0.190	0.192	0.99	1.1	4.0	5700	0.229
6	60	13.3	0.190	0.192	0.99	1.1	5.0	5700	0.229
7	0	10.8	0.154	0.192	0.80	0.36	0.2	4620	0.186
8	0	12.0	0.173	0.192	0.90	0.36	0.3	5190	0.209
9	0	13.3	0.190	0.192	0.99	0.36	0.5	5700	0.229
10	30	13.3	0.190	0.192	0.99	0.36	0.6	5700	0.229
11	45	13.3	0.190	0.192	0.99	0.36	0.75	5700	0.229
12	60	13.3	0.190	0.192	0.99	0.36	0.5	5700	0.229
13	0	10.8	0.154	0.192	0.80	0	0.6	4620	0.186
14	0	12.0	0.173	0.192	0.90	0	0.8	5190	0.209
15	0	13.3	0.190	0.192	0.99	0	1.3	5700	0.229
16	30	13.3	0.190	0.192	0.99	0	2.0	5700	0.229
17	45	13.3	0.190	0.192	0.99	0	2.7	5700	0.229
18	60	13.3	0.190	0.192	0.99	0	1.0	5700	0.229

4.5.1 Temporal Evaluation and Maximum Scour at Complex piers

According to results of tests carried out for Suspension Model, the scour process in the three clear and distinguished situations considered may be typically described as follows:

1. Situation 1, where the pile-cap is above the initial bed level, the temporal evolution of the maximum scour depth is similar to that of the single pier case, the scour process initiates in front of each of the upstream piles, the maximum scour depth recorded in the front pile when (α°=0°), and in front of all piles that expose to the flow in (α°=30°, 45°, and 60°), as illustrated in Figure 4.24 and Figure 4.25.

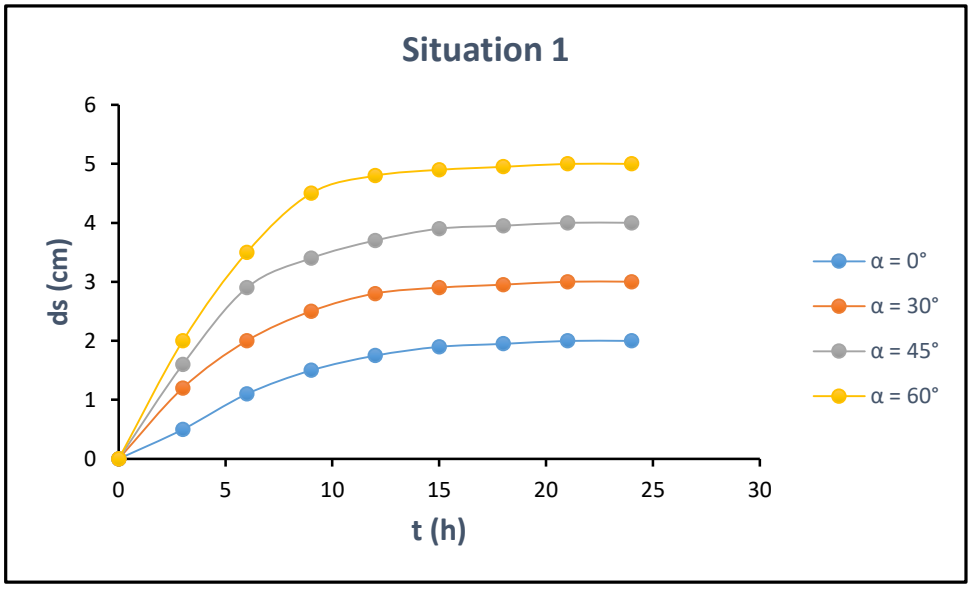

Figure 4.24: Situation 1: scheme of the temporal evaluation of the scour depth for Suspension bridge.

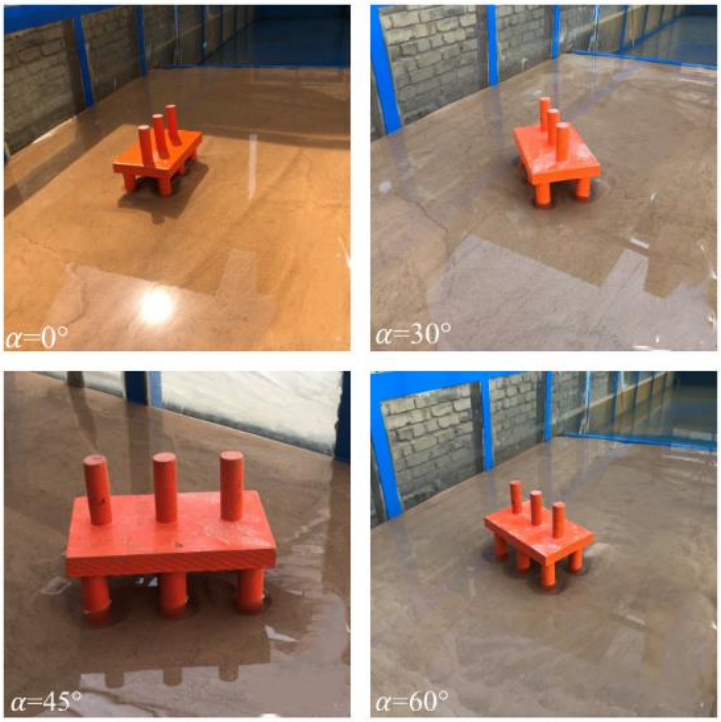

Figure 4.25: Situation 1: photograph of maximum scour hole for Suspension bridge.

2. Situation 2, where the pile cap is placed above close to the original bed, the process continues underneath the pile cap, the scour forms along surrounding the pile-cap recording the maximum scour at (α°=30° and 45°), and in the edges of pile-cap when (α°=0° and 60°), as shown in Figure 4.26. Figure 4.27 shows the maximum scour hole at the end of the test.

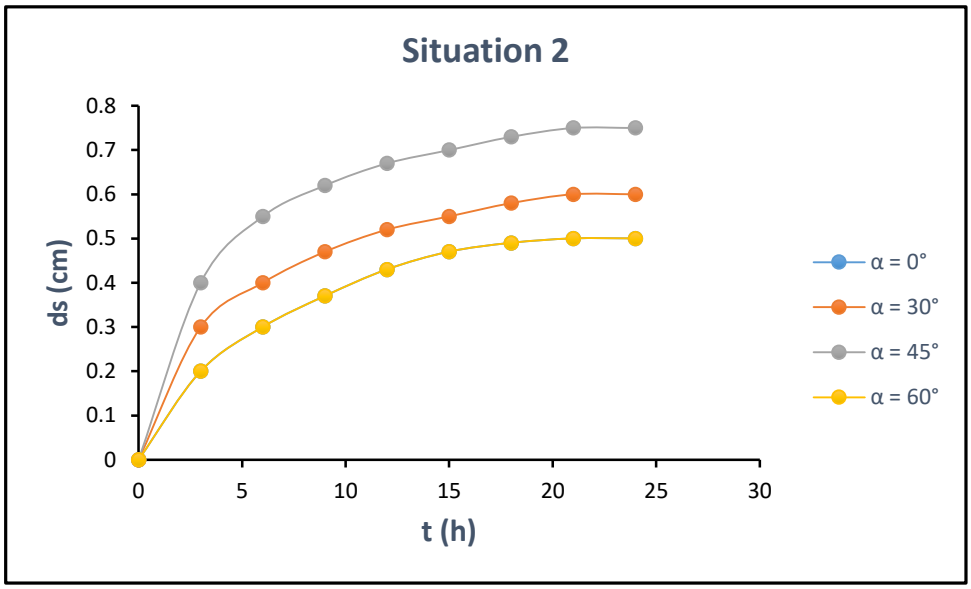

Figure 4.26: Situation 2: scheme of the temporal evaluation of the scour depth for Suspension bridge.

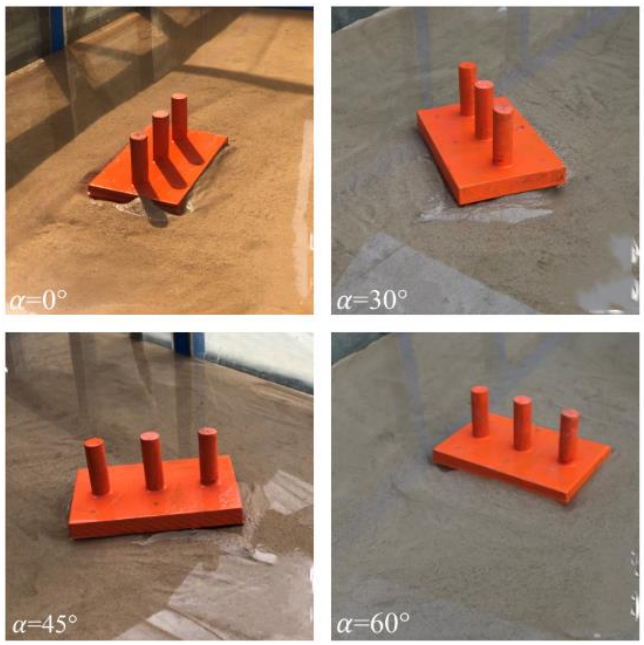

Figure 4.27: Situation 2: photograph of maximum scour hole for Suspension bridge.

3. Situation 3, where the pile cap is completely buried in the bed, the scour process develops in front of the column until the scour hole partly uncovers the top of the pile cap; as shown in (α°=30° and 45°), and it is developed around the column gradually having the same trend in single pier in (α°=0° and 60). Figure 4.28 and Figure 4.29 show the maximum scour hole associated with the scour.

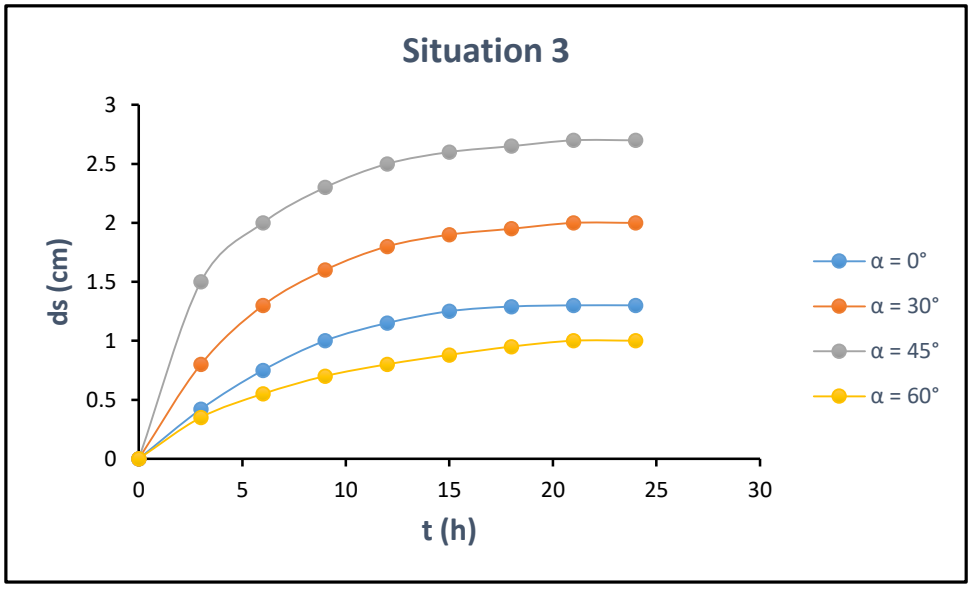

Figure 4.28: Situation 3: scheme of the temporal evaluation of the scour depth for Suspension bridge.

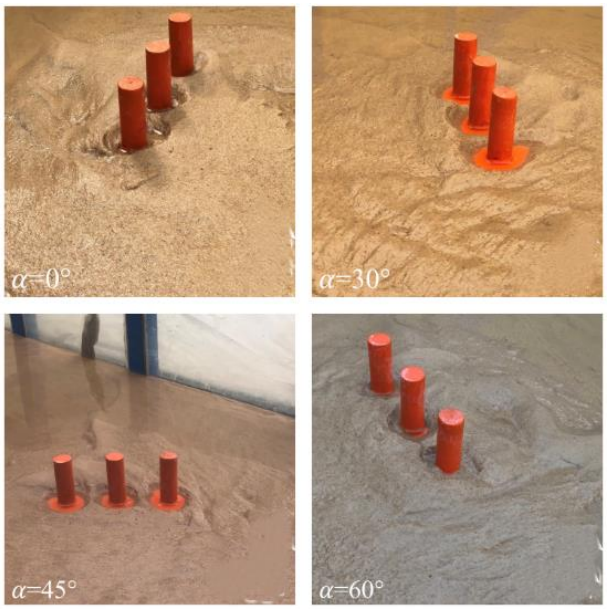

Figure 4.29: Situation 2: photograph of maximum scour hole for Suspension bridge.

4.5.2 Influence of The Pile-Cap Position and Pier Skewness

The values of d_s are plotted against Hc/h in Figure 4.30 for the three discussed models. The figure includes three situations analyzed: pile cap above the bed (Sit. 1, $Hc/h>T/h$), pile cap is placed above close to the original bed (Sit. 2, $0\leq Hc/h\leq T/h$) and pile cap completely buried in the bed (Sit. 3, $Hc/h\leq 0$). In general, the d_s variation with Hc/h is similar for the three models. The increment in d_s values, associated to each model, is related to the corresponding reduction of the pile-cap front.

For Situation 1, when column and pile cap out of the water increase in d_s with increasing skewness the model, as shown in figure above. That increase is justified by the frontal area exposed to the flow.

In Situation 2, when the pile cap is placed above close to the original bed, the scour has the same trend of increasing with skewness except when ($\alpha°=60°$), that behavior is mostly associated with the pile-cap overhang dimension's influence on the flow structure around the column above the pile cap. The pile-cap overhang length is enough to deflect the downflow along the column and to reduce the strength of the horseshoe vortex in order to influence and disturb the scouring process.

In Situation 3, The equilibrium scours depth behavior as similar to the one obtained by **(Melville and Raudkivi, 1996) and (Umeda et al., 2010)** for tests with cylindrical piers found on cylindrical caissons. The d_s reduction due to the effect of the overhanging of the pile cap from the column, made active after the top of this element is reached on the scour process, by that interfering on the scour hole development process (by physical obstruction on the cavity and by weakening the flow structure induced by the column while confined by the above-adjacent sand bed).

So, the maximum scour depth increase with increasing skewness model except when (α°=60°), as shown in Figure 4.31.

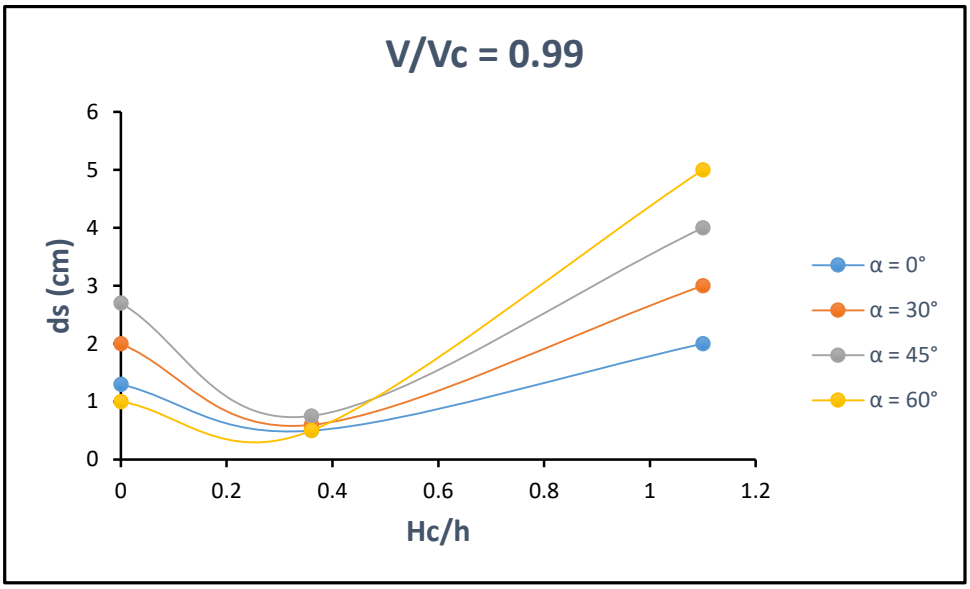

Figure 4.30: Influence of pile-cap position from the initial bed on the temporal evaluation of the scour depth for Suspension bridge.

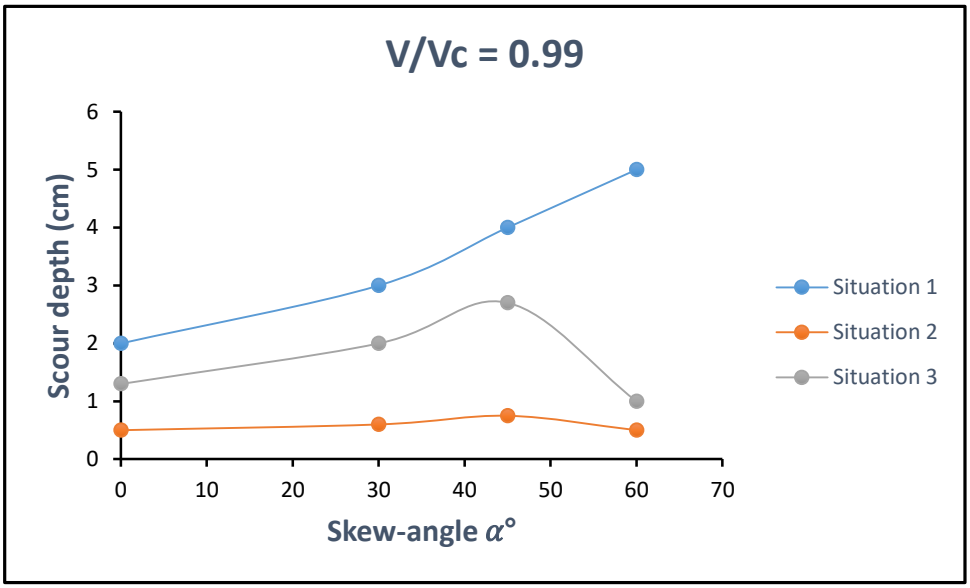

Figure 4.31: Variation of equilibrium scour depth with respect to skewness angle for Suspension bridge.

4.6 Shallala River Model

The experimental conditions and results for Shallal River model are tabulated in terms of flow skew–angle, α, flow discharge, Q, approach velocity, V, critical velocity, V_c, flow density, V/V_c, pile cap position, H_c/h, maximum scour depth, d_s, pile Reynold number R_p, and Froude number, F in Table 4.5 for the experimental runs in Shallala River model, where time of scour 24 hours, with soil fine sand, d_{50}=1.13 mm, and approach flow depth h=7 cm.

Table 4.5: Summary of measured experimental data for Shallala River model.

Run	$\alpha°$	Q (l/s)	V (m/s)	V_c (m/s)	V_a (m/s)	$\frac{V-(Va-Vc)}{Vc}$	H_c/h	d_s (cm)	R_p	F
1	0	11.2	0.160	0.380	0.304	0.62	1.1	0.1	4800	0.193
2	0	13.9	0.198	0.380	0.304	0.72	1.1	0.2	5940	0.239
3	0	16.5	0.236	0.380	0.304	0.82	1.1	0.4	7080	0.285
4	30	16.5	0.236	0.380	0.304	0.82	1.1	0.6	7080	0.285
5	45	16.5	0.236	0.380	0.304	0.82	1.1	1.0	7080	0.285
6	60	16.5	0.236	0.380	0.304	0.82	1.1	1.3	7080	0.285
7	0	11.2	0.160	0.380	0.304	0.62	0.36	0.1	4800	0.193
8	0	13.9	0.198	0.380	0.304	0.72	0.36	0.1	5940	0.239
9	0	16.5	0.236	0.380	0.304	0.82	0.36	0.3	7080	0.285
10	30	16.5	0.236	0.380	0.304	0.82	0.36	0.3	7080	0.285
11	45	16.5	0.236	0.380	0.304	0.82	0.36	0.5	7080	0.285
12	60	16.5	0.236	0.380	0.304	0.82	0.36	0.2	7080	0.285
13	0	11.2	0.160	0.380	0.304	0.62	0	0.0	4800	0.193
14	0	13.9	0.198	0.380	0.304	0.72	0	0.0	5940	0.239
15	0	16.5	0.236	0.380	0.304	0.82	0	0.0	7080	0.285
16	30	16.5	0.236	0.380	0.304	0.82	0	0.0	7080	0.285
17	45	16.5	0.236	0.380	0.304	0.82	0	0.0	7080	0.285
18	60	16.5	0.236	0.380	0.304	0.82	0	0.0	7080	0.285

4.6.1 Temporal Evaluation and Maximum Scour at Complex piers

The armored layer due to the selective transport of the finer particles in non-uniform sediments causes complexity for predicting equilibrium scour depth. So, according to results of tests carried out for Shallala Model, the scour process may be typically described as follows:

1. Situation 1: where the bottom of the pile-cap is above the initial bed level, the scour trend as the same in single pile. From the experimental results, it is observed that the equilibrium scours depth increases with decrease in gravel size. The variations of equilibrium scour depth with gravel size for pier scour depart considerably from the variations of equilibrium scour depth with sand size. Consequently, for scour at piers the resulting sediment size factors for gravels, and significantly different from the existing sediment size factor for sands. The presence of gravel armors the river bed, the scour increasing more slowly with skew-angle to the flow direction, as shown in Figure 4.32 and Figure 4.33.

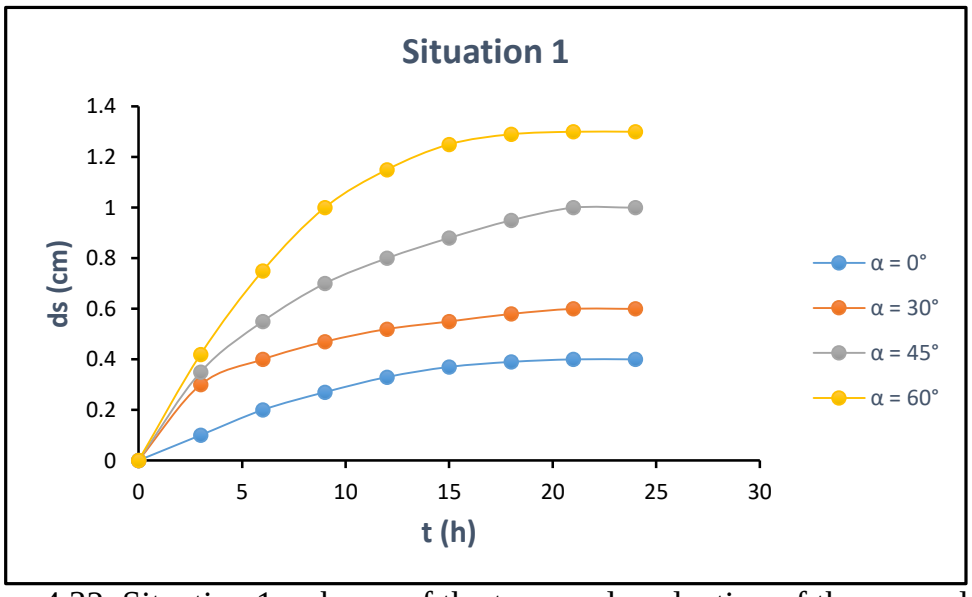

Figure 4.32: Situation 1: scheme of the temporal evaluation of the scour depth for Shallala bridge.

Figure 4.33: Situation 1: photograph of maximum scour hole for Shallala bridge.

2. Situation 2, where the pile cap is placed above close to the original bed, the scour is very small because in an armor layer coarser grains remains at upstream flow bed and at the vicinity of scour hole in the same flow intensity, the scour depth was decreased. Also, a slight increase on scour depth has been observed by reduction of median grain size in the beds with non-uniform sediments at the same geometric standard deviation, as shown in Figure 4.34. Figure 4.35.

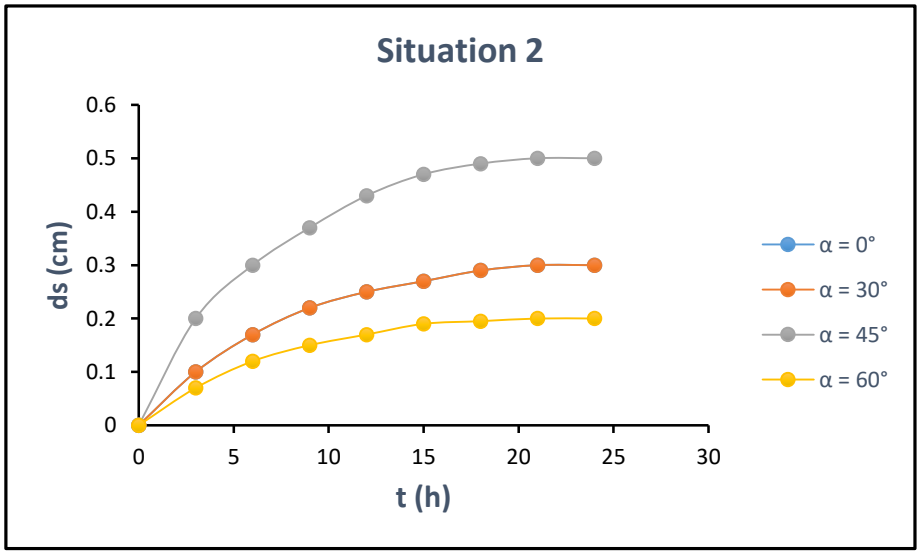

Figure 4.34: Situation 2: scheme of the temporal evaluation of the scour depth for Shallal bridge.

Figure 4.35: Situation 2: photograph of maximum scour hole for Shallala bridge.

3. Situation 3, when the pile cap is completely buried in the bed, there is no scour recorded because in the case of complex sediment beds, selective transport of the finer particles due to unequal mobility can make the bed surface be armored. With regards to natural river materials (non-uniform sediments) and its great effects on the dimension and the time evolution of scour hole, the interaction of flow-structures with non-uniform sediments is very crucial due to armor layer development. So, the larger particles form an armor layer protecting the bed from eroding, as shown in Figure 4.36.

Figure 4.36: Situation 3: photograph of maximum scour hole for Shallala bridge.

4.6.2 Influence of the Pile-Cap Position and Pier Skewness

For Situation 1, when column and pile cap out of the water an increase in d_s with increasing skewness the model. That increase is justified by the frontal area exposed to the flow.

In Situation 2, when the pile cap is placed above close to the original bed, the scour has the same trend of increasing with skewness except when (α°=60). The pile-cap overhang length is enough to deflect the downflow along the column and to reduce the strength of the horseshoe vortex in order to influence and disturb the scouring process.

In situation 3, there is no scour record for all cases due to armor bed, and the pile-cap formed a large base to product the piers from scour, as shown in Figure 4.37 and Figure 4.38.

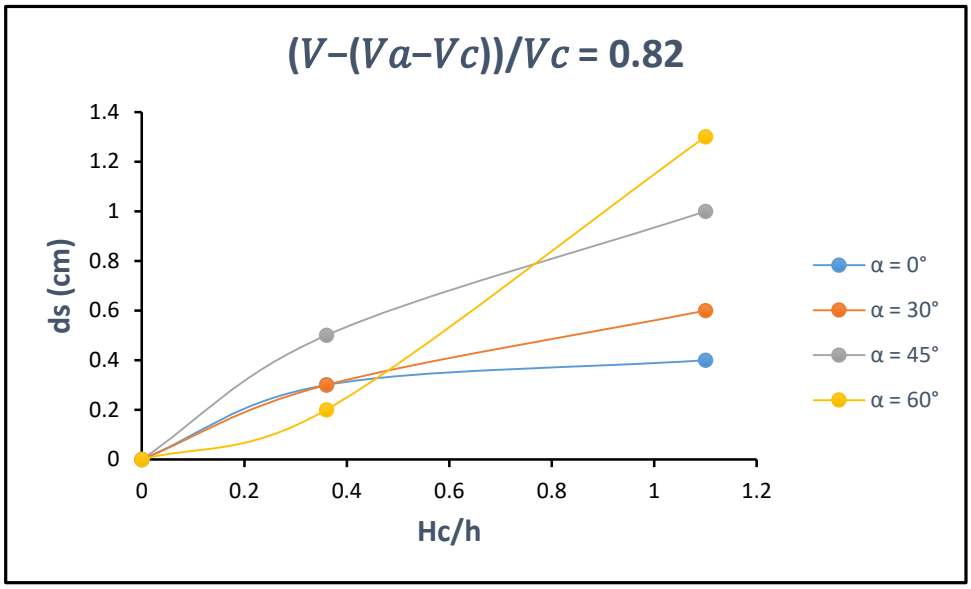

Figure 4.37: Influence of pile-cap position from the initial bed on the temporal evaluation of the scour depth for Shallala bridge.

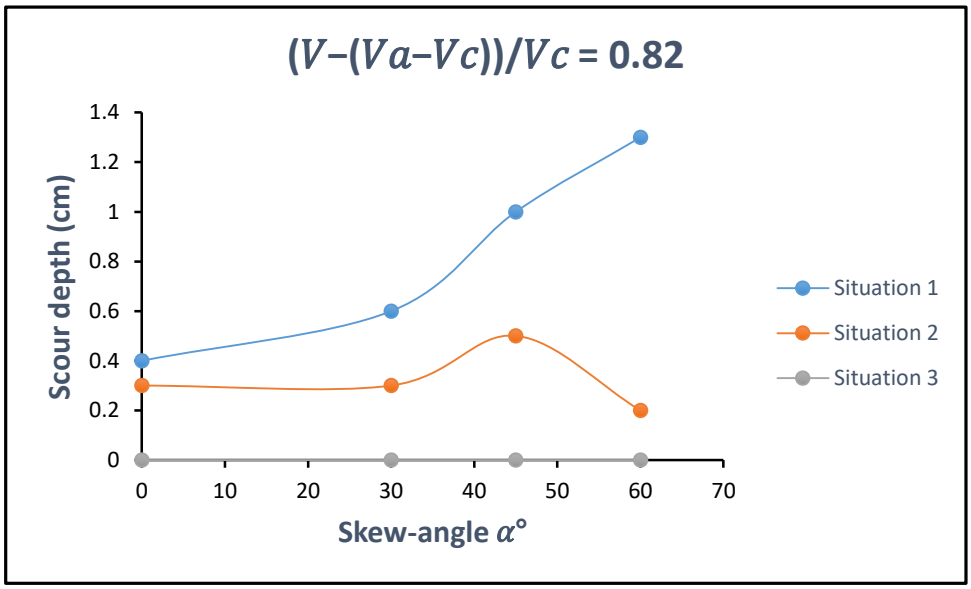

Figure 4.38: Variation of equilibrium scour depth with respect to skewness angle for Shallala bridge.

4.7 Effect of Interaction on Scouring at Complex Bridge Piers

The experimental results of the conducted flume tests in this study are used to explain the effect of interaction between piers arrangement on the local scouring in different Iraqi soils. From reviewing the literature, it is found in a study by **(Li, 2002)** which involved an investigation of scour at piers arrangement. The study presented a method of scour depth estimation but there was no description for the pattern of scour hole nor the effect of the pile interaction on scour depth development.

In this study, a set of experimental runs were conducted with spacing between piles S_p = 2D vertical and skew to the flow direction. The flow at complex piers differs from that at single case, flow patterns were altered by the existence of a rear pier, principally at the wake region of the front pier. Based on the spacing of the piers (S_p) range that was investigated, the observations showed that smaller piers spacing ($S_p/D \leq 2.5$) results in a large interference of flow structures while it was reduced for pier spacing of ($S_p/D \geq 3$).

It was reported in the literature that for a pier as a part of complex piers vertical and skew to the flow direction, reinforcement and sheltering affect the local scour depth. Reinforcement occurs due to a pier located at a distance from an upstream pier at which both scour holes intersect (for small spacing ratio). This effect enhances the sediment erosion at the frontal pier and thus causes deeper scouring depth. Scouring at the downstream pier is reduced because of “the sheltering effect” resulting from a frontal pier that reduces the effective flow velocity and consequently produces lesser scouring depth.

These illustrations were also reported by **(Saghravani and Azhari, 2012)** and **(Ataie-Ashtiani and Aslani-Kordkandi, 2012)**. The maximum scour depths were recorded at the sides of the piers at skew-angle for all

piers arrangement, this observation agrees with the finding of **(Ansari et al., 2002)** the "for saturated cohesive sediments, the deepest scour is found to occur at the sides of the pier" and with **(Debnath and Chaudhuri, 2010-a and 2010-b),** as shown in Figure 4.39.

Figure 4.39: Interaction of scour hole.

CHAPTER FIVE

Prediction of Equilibrium Scour Depth around Complex Bridge Piers

Chapter Five

Prediction of Equilibrium Scour Depth around Complex Bridge Piers

5.1 Introduction

The aim of this chapter is to evaluate the performance of the mentioned methods using part of the tests performed in this, suggest a new scour predictor, aiming at improving the accuracy of the existing ones, and validate the new predictor using experimental data published in the literature.

Local scour can lead to partial failure or to collapse of bridge piers and decks. The cost of large bridges, with common and/or special complex piers, justifies carrying out an accurate prediction of scour depth, for both economic and safety reasons, which in turn leads to the interest of hydraulic engineers in predicting the maximum scour depth, d_s. However, it is known that, despite the studies conducted in the past for pile-supported piers, the scour predictors do not reproduce adequately the measured values **(*e.g.*, Ferraro *et al.*, 2013)**. This derives from the fact that there are many factors influencing the phenomenon. Presently, for sand bed material, three methods to predict equilibrium scour depths at common complex piers can be considered as consolidated: The Auckland method **(Coleman, 2005)**, the FDOT method **(Sheppard and Renna, 2010)** and the HEC-18 method **(Arneson *et al.*, 2012)**. For cohesive bed material, **(Ansari, et al., 2002; Rambau, 2003; and Debnath and Chaudhuri, 2009)**. And for non-uniform gravel bed material **(Melville and Coleman, 2000; Guo, 2012 and Kim, et al., 2015)**.

5.2 Applicability of Available Scour Depth Predictors

5.2.1 The Present Study

The scour depth is a function of some variables. The dimensionless functional relationship of equation 3.5 should be presented as an empirical formula by using a multi-regression analysis. The confidence of suggested relationship evaluated according to the coefficient of determination (R^2). The IBM SPSS Statistics v26 software is used to make analysis for the equation through a linear regression analysis. The coefficient of determination (R^2) can be calculated by equation (5.1), root mean square error (RMSE) by equation (5.2), mean square error (MSE) by equation (5.3), and mean absolute error (MAE) by equation (5.4) **(IBM, 2015)**:

$$R^2 = 1 - \frac{\sum_{i=1}^{n}(ds_o - ds_p)^2}{\sum_{i=1}^{n}(ds_o - \overline{ds})^2} \quad \textbf{5.1}$$

$$RMSE = \sqrt{\left(\frac{\sum_{i=1}^{n}(ds_p - ds_o)^2}{N}\right)} \quad \textbf{5.2}$$

$$MSE = \frac{\sum_{i=1}^{n}(ds_p - ds_o)^2}{N} \quad \textbf{5.3}$$

$$MAE = \frac{\sum_{i=1}^{n}(ds_p - ds_o)}{N} \quad \textbf{5.4}$$

Where R^2 is the coefficient of determination, ds_o is the observed value, ds_p is the predicted value, $\overline{ds}$ is the mean value of ds_o and n is the number of data. The following relationship is suggested to predict the scour depth around bridge piers depending on the experimental data, as shown in Table 5.1:

Table 5.1: Equations suggested to predict the scour depth.

Complex Bridge	Equation
Beta	d_s=0.043+1.010α+22.195Q+33.477V/V_c+4.845H_C/h-.002R_p+13.695F
Ali Al-Gharbi	d_s=0.032+1.000α+55.651Q+16.393V/V_c+4.516H_C/h-.001R_p+13.290F
Selebat	d_s=-0.007-0.139α+49.487Q+76.311V/V_c+0.737H_C/h+5.113R_p+53.370F
Suspension	d_s=0.018+0.530α+27.174Q+0.758V/V_c+1.940H_C/h-0.003R_p+18.032F
Shallala	d_s=0.005+0.194α-15.402Q+57.686V/V_c+0.739H_C/h+0.000R_p+0.056F

After analyzing the data in SPSS software, is the results are obtained as the following:

Table 5.2: The statistical analysis results for present study.

Complex bridge	R^2	RMSE cm	MSE	MAE	Equation
Beta	0.9805	0.43	0.19	0.34	Y=1.0215X-0.1481
Ali Al-Gharbi	0.9801	0.32	0.1	0.27	Y=1.0332X-0.0650
Selebat	0.9818	0.09	0.0083	0.08	Y=0.9037X+0.0918
Suspension	0.9935	0.12	0.02	0.1	Y=1.0366X-0.0294
Shallala	0.9733	0.06	0.0036	0.06	Y=0.9888X+0.0171

5.2.2 Sand Bed Materials

The performance of Auckland **(Coleman, 2005)**, FDOT (**Sheppard and Renna, 2010)** and HEC-18 **(Arneson *et al.*, 2012)** methods were assessed by comparing the methods' predictions of d_s for the present study's 54 tests conditions -18 test for each bridge- with the corresponding extrapolated values of the experimental measurements (henceforth referred to as observed equilibrium scour depths). The application of the three predictors was performed as follows:

- In Situation 1 (pile cap above the initial bed level), the Auckland's method K_S factor was estimated by taking into account the pile-group shape. Similarly, the shape of the pile-cap and the shape of the column were used in Situation 2 (pile-cap close to the bed) and in Situation 3 (pile cap completely buried in the bed), respectively, and;
- The shape factor for circular piers, i.e., Ks=1.0, was used in the application of the FDOT method, for rectangular pile caps, in accordance with **(Ferraro et al., 2013).**

The comparison and statistical analysis between observed d_s values and the corresponding d_s values predicted by the discussed methods is presented in Figure 5.1 and table 5.3. The data were separated in three groups, each corresponding to one of the three situations considered. It is

worth remember that over-prediction of scour depth may lead to excessive costs of the bridge while under-prediction may lead to bridge failure.

a

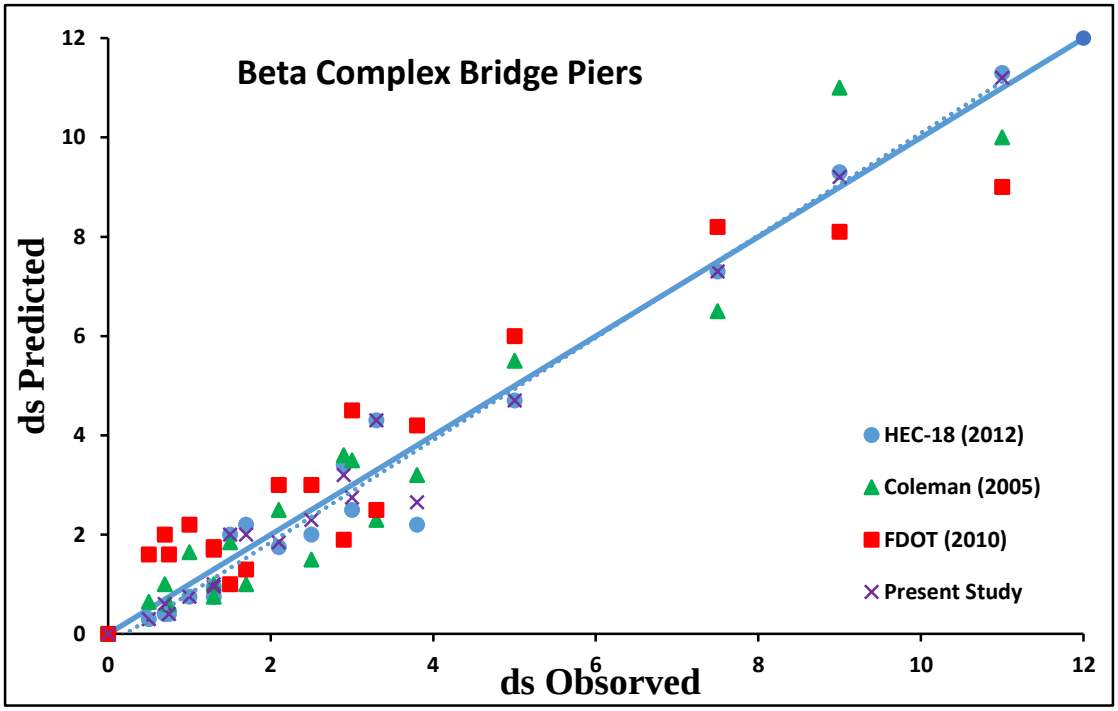

b

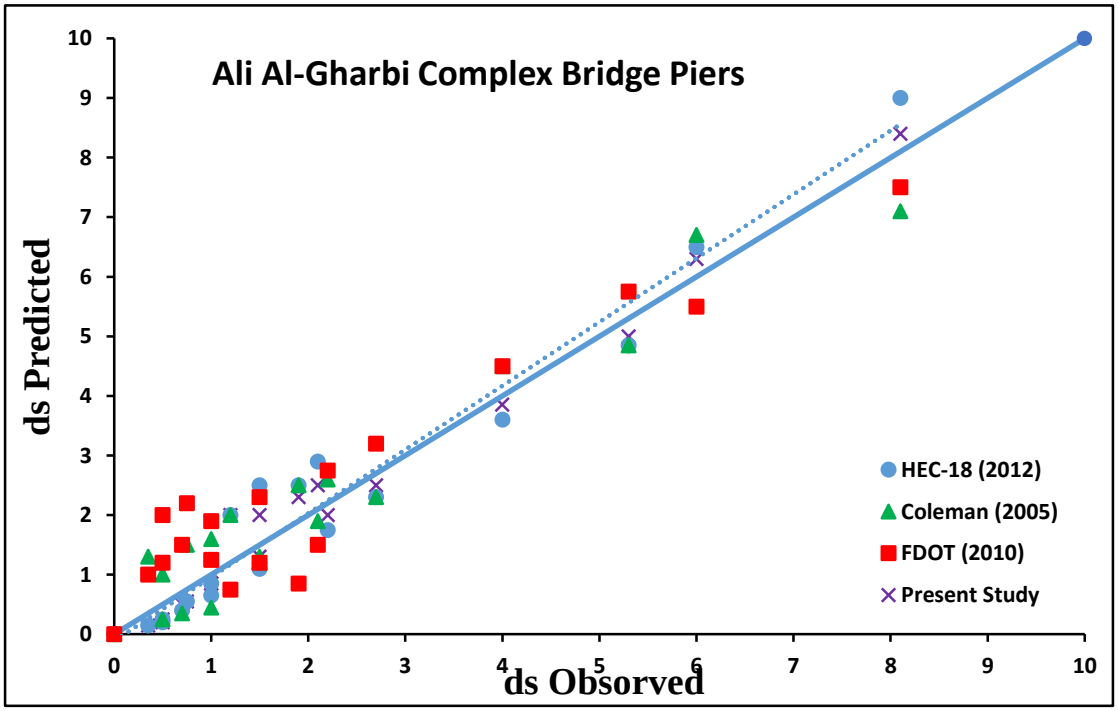

c

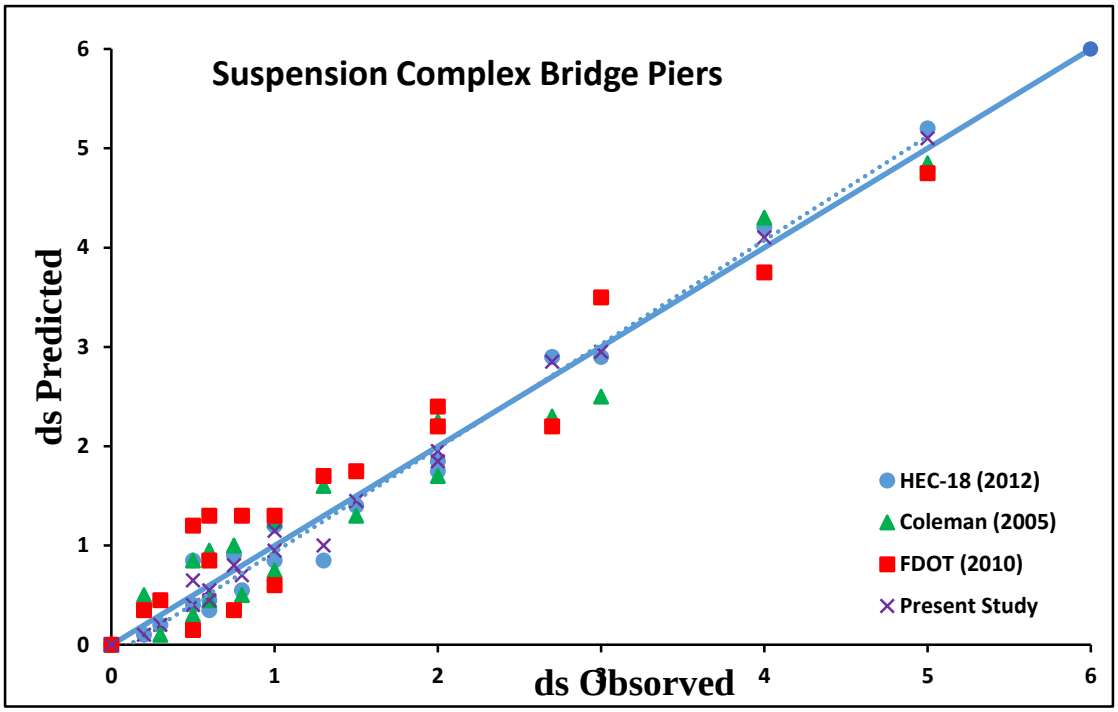

Figure 5.1: Comparison of observed and predicted equilibrium scour depths, for the bridges of: (a) Beta, (b) Ali Al-Gharbi and (c) Suspension.

Table 5.3: The statistical analysis results for three methods above for sand bed. materials.

Complex bridge	Method	R^2	RMSE cm	MSE	MAE	Equation
Beta	HEC-18	0.9694	0.56	0.32	0.45	Y=1.0353X-0.2460
	Auckland	0.9371	0.76	0.58	0.62	Y=0.9987X-0.0373
	FDOT	0.9093	0.95	0.91	0.84	Y=0.8154X+0.8646
Ali Al-Gharbi	HEC-18	0.9554	0.52	0.27	0.45	Y=1.0742X-0.1286
	Auckland	0.9331	0.56	0.32	0.5	Y=0.9065X+0.3313
	FDOT	0.8943	0.75	0.57	0.66	Y=0.8443X+0.6657
Suspension	HEC-18	0.9811	0.21	0.04	0.18	Y=1.0520X-0.1274
	Auckland	0.9544	0.28	0.08	0.26	Y=0.9505X+0.0597
	FDOT	0.921	0.39	0.15	0.35	Y=0.9094X+0.2702

The results show that the HEC-18 method gives the most acceptable predictions of d_s. The FDOT method provides conservative values of d_s, the most evident discrepancy being observed, with values above the diagonal and over the upper boundary limit. The performance of the three scour-depth predictors dedicated to complex piers showed that the HEC-

18 method tends to underestimate the equilibrium scour depth in most pile-cap positions. The Auckland tends to balanced between underestimate and overestimate, and FDOT methods tend to overestimate the equilibrium scour depth.

5.2.3 Cohesive Bed Materials

The performance of **(Ansari, et al., 2002), (Debnath and Chaudhuri, 2009), and (Rambau, 2003)** methods was assessed by comparing the methods' predictions of d_s for the present study's 18 tests conditions with the corresponding extrapolated values of the experimental measurements. The application of the three predictors was performed as in the pervious case. The comparison and statistical analysis between observed d_s values and the corresponding d_s values predicted by the discussed methods is presented in Figure 5.2 and table 5.4. The data were separated in three groups, each corresponding to one of the three situations considered.

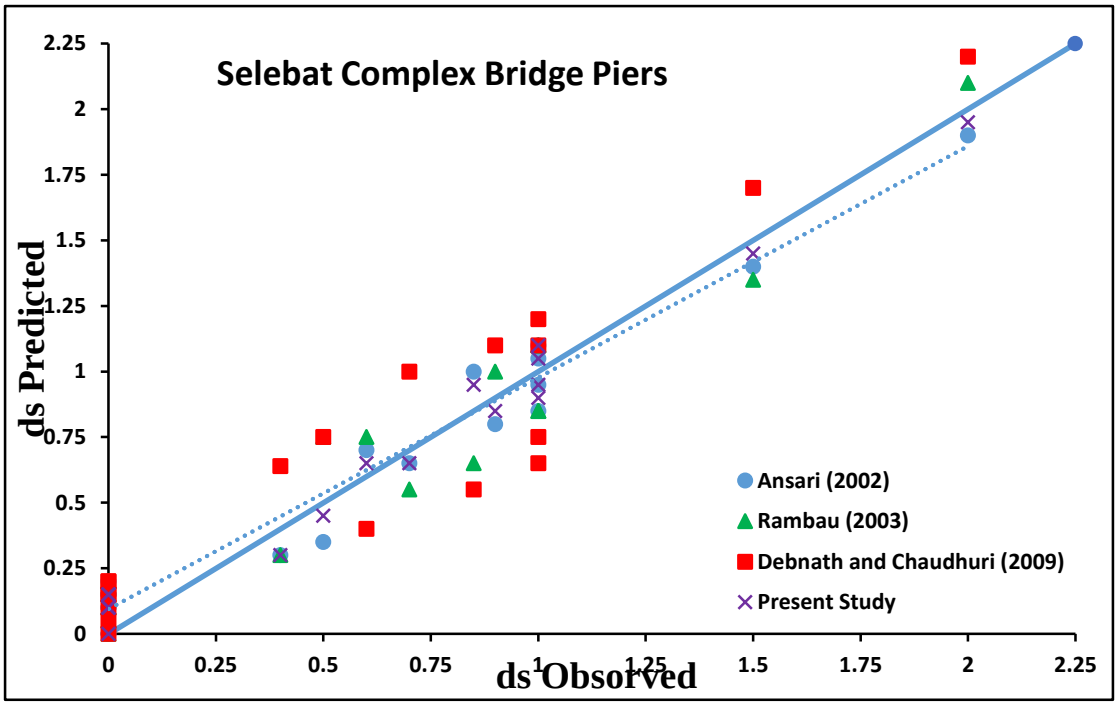

Figure 5.2: Comparison of observed and predicted equilibrium scour depths, for the Selebat bridge.

Table 5.4: The statistical analysis results for three methods above for cohesive bed materials.

Complex bridge	Method	R^2	RMSE cm	MSE	MAE	Equation
Selebat	Ansari	0.9663	0.12	0.02	0.11	Y=0.8717X+0.1066
	Rambau	0.9418	0.14	0.02	0.13	Y=0.8992X+0.1030
	Debnath	0.8884	0.21	0.04	0.19	Y=0.9514X+0.1109

The results of the statistical test show that the Ansari et al. and Rambabu et al. equations were successful in predicting scour depth in cohesive soils. These equations are proposed for the saturated soil condition. It seems that the high value in the R^2 coeffcients is due to the effects of soil properties in the empirical equations. Ansari et al. proposed an equation based on moisture content, clay percent, plasticity index, angle of repose of the sediment, and bed sediment shear strength, whereas the Rambabu et al. equation was presented under conditions of initial moisture, saturated soil, and clay percent constant. Based on R^2 coeffcients, Debnath and Chaudhuri equation was less successful in the prediction of scour depths because they are only valid for saturated soils.

The results of the comparisons show that Ansari et al. and Rambabu et al. empirical equations have better agreement with observed scour depth gained from experiments than from other equations. It can be concluded from comparisons of empirical equations in cohesive soils that saturated conditions are significant factors in predicting scour depth.

5.2.4 Non-Uniform Gravel Bed Materials

demonstrates the percentage errors between the calculated and observed experimental/field scour depths for **(Melville and Coleman, 2000), (Guo, 2012), and (Kim et al., 2015)** approaches, respectively. By analyzing in Figure 5.3 below, it was recognized that the coarser laboratory data affected the accuracy of the considered literature approaches, which means that some data sets showed some error. These errors were particularly appear in Kim et al.'s compared to the other two models. Meanwhile, the equation given by Melville and Coleman showed better agreements, as skown in table 5.5 below:

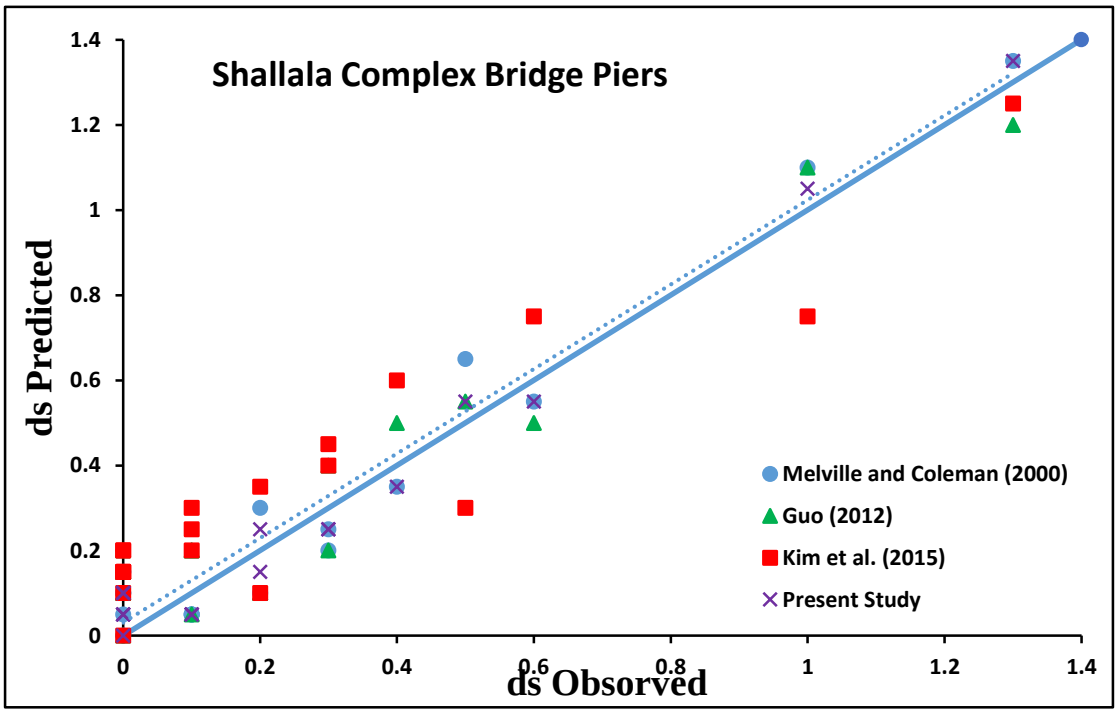

Figure 5.3: Comparison of observed and predicted equilibrium scour depths, for the Shalalla bridge.

Table 5.5: The statistical analysis results for three methods above for non-uniform gravel bed materials.

Complex Bridge	Method	R^2	RMSE cm	MSE	MAE	Equation
Shalalla	Melville	0.9431	0.09	0.0083	0.08	Y=0.9888X+0.0337
	Guo	0.9198	0.11	0.01	0.1	Y=0.8738X+0.0830
	Kim	0.8685	0.16	0.02	0.15	Y=0.7596X+0.1542

The results shows that the Melville and Coleman and Guo's approachs performed relatively well for laboratory datasets. The approach proposed by Kim et al. showed less agreements between the observed and calculated values of scour depths. The effect of non-uniform gravel size on maximum scour depth around the pier was prominent.

CHAPTER Six

Conclusions and Suggestions for Future Works

Chapter Six

Conclusions and Suggestions for Future Works

6.1 Conclusions

From this study, it can be concluded that:

1. The temporal evolution of scour depth at complex piers is generally influenced by the relative column position (H_c/h), by the relative column width (D_c/D_{pc}), and by the pile-group configuration. The different stages in the scour depth time evolution are associated with the number of structural elements of the complex pier that are exposed to the flow inside the scour hole developed along the scouring process;
2. The pile cap overhang from the column face plays the role of an obstruction to the down-flow adjacent to the column, reducing the vortex system and hence the scour depth. This reduction is most evident in the cases when the top of the pile cap is close to the initial bed level, for which the flow behavior is similar to collars in single piers;
3. For complex pier is aligned with flow, maximum scour depth occurs when pile cap above original bed level with increase (80%, 81%, 100%, 35%, and 100%) compared with the pile-cap fully buried to the bed level for (Beta, Ali AL- Gharbi, Selebat, Suspension, and Shallala) Bridges;
4. Maximum scour depth for skewed complex piers increases significantly compared to aligned piers. The increase in depth of scouring is proportional to skew angle α, it is largest in Selebat Bridge (29.4%, 33%, and 80%) for (60°, 45°, 30 and 0°) sequentially; Smallest in Ali Al-Gharbi Bridge (26%, 12%, and

25%). Sensitivity of scour development to pier skew angle increases as pile-cap elevation increases, particularly when it is completely above original bed compared with the pile-cap fully buried to the bed level;

5. The scouring depth is maximum at the front pier and minimum at the rear pier in all tests. It was obvious that the frontal pier impacts the rear pier by a "sheltering effect" which reduces the flow velocity and thus scouring. While the frontal pier experienced a "reinforcement effect" in the flow structures around the pier due to pile group;
6. The skew-angle caused more scouring than the vertical piers. The scour hole depth and extend increased with the increase in the skew-angle of the skewed piers;
7. For the bed sediment of clay content, it was observed that the rate of scouring is highly affected with the clay content. As comparing the scour in sand alone soils to that in sand-clay, it was found that the deepest scour occurs at the sides of the pier at skew-angle founded in sand-clay soil in contrast to the sand alone where the deepest scour is observed at the pier nose;
8. The influence of gravel size on equilibrium scour depth at piers is prominent. The equilibrium scours depth increases with decrease in gravel size;
9. A new formulation to predict d_s at complex piers is suggested, i.e., equations (2.15) to (2.36). for the sand bed materials, the comparison was of the HEC-18, the Auckland, and the FDOT and methods with the new predictor, it can be concluded that HEC-18 method gives estimations of d_s, which represents an acceptable compromise between safety and economy and give (R^2 = 96.94, 95.54, 98.11)%

for (Beta, Ali Al-Gharbi, and Suspension) Bridges. For the cohesive bed materials, the comparison was of the (Ansari, Debnath and Chaudhuri, and Rambau), the method of Ansari gives (R^2 = 96.63%) for (Selebat Bridge). For non-uniform gravel bed material (Melville and Coleman, Guo, and Kim), the method of Melville gives (R^2 = 94.31%) for (Shallala Bridge).

6.2 Suggestions for Future Works

1. The influence of different shapes of the three components of the complex pier on the equilibrium scour depth since enormous combinations of column, pile cap and pile group geometries are possible;
2. It is recommended to investigate the scour characteristics under live-bed conditions;
3. Evaluating the effect of meandering channels on local scour depth around different shapes and skew-angles of bridge piers;
4. Choosing a soil that contains high proportions of gravel and clay;
5. Choosing the optimal position for the complex bridge pier.

REFERENCES

References

1. Ahmed, N. Melville, B. Mohammad, T. Ali, F. and Yusuf, B. (2016). *Clear-Water Scour at Long Skewed Bridge Piers*. Journal of the Chinese Institute of Engineers. 1-9. https://doi.org/10.1080/02533839.2016.1259021
2. Al-Quraishi, Z. A. and AlShukur, A.K. (2016). *Effect of Bridge Pier Shape on the Depth and Configuration of Local Scour*. a thesis submitted to the college of engineering. University of Babylon. in partial fulfillment of the requirements for Degree of master in science in water resources.
3. Amini, A. Melville, B.W. Ali, T.M. and Ghazali, A.H. (2012). *Clear-water local scour around pile groups in shallow-water flow*. Journal of Hydraulic Engineering. 138 (2). 177 – 185. https://doi.org/10.1061/(ASCE)HY.1943-7900.0000488
4. Amini, A. Melville, B.W. and Ali, T.M. (2014). *Local scour at piled bridge piers including an examination of the superposition method*. Canadian Journal of Civil Engineering. 41 (5). 461 – 471. https://doi.org/10.1139/cjce-2011-0389
5. Amini, S. A. Mohammad, Th. A. Abdul Aziz, A. Ghazali, A. H. and Huat, B. K. (2010). *A local scour prediction method for pile caps in complex piers*. Proceedings of the Institution of Civil Engineers. Water Management. 164. Issue WM2. Pages 73–80. https://doi.org/10.1680/wama.900064
6. Amini, S.A. Mohammad, T.A. Aziz, A.A. Ghazali, A.H. and Huat, B.B.K. (2011). *A local scour prediction method for pile caps in complex piers*. Water Management, 164 (2). 73 – 80. https://doi.org/10.1680/wama.900064

7. Ansari, S.A. Kothyari, U.C. and Ranga, R.K. (2002). *Influence of cohesion on scour around bridge piers*. Journal of Hydraulic Research. 40(6). 717-729. https://doi.org/10.1080/00221680209499918
8. Arneson, L.A. Zevenbergen, L.W. Lagasse, P.F. and Clopper, P.E. (2012). *Evaluating scour at bridges (HEC-18)*. Technical Rep. No. FHWA (Federal Highway Administration) HIF-12-003. Washington. DC.
9. Ataie-Ashtiani, B. and Aslani-Kordkandi, A. (2012). Flow field around side-by-side piers with and without scour hole. European Journal of Mechanics-B/Fluids36:152-166. https://doi.org/10.1016/j.euromechflu.2012.03.007
10. Ataie-Ashtiani, B. and Beheshti, A.A. (2006). *Experimental investigation of clear-water local scour at pile groups*. Journal of Hydraulic Engineering, 132 (10). 1100 - 1104. https://doi.org/10.1061/(ASCE) 0733-9429(2006) 132:10 (1100)
11. Ataie-Ashtiani, B. Baratian-Ghorghi, Z. and Beheshti, A. A. (2010). *Experimental investigation of clear-water local scour of compound piers*. Journal of Hydraulic Engineering. 136 (6). 343 – 351. https://doi.org/10.1061/(ASCE)0733-9429(2010)136:6(343)
12. Başak, V. Başlaşlı, Y. and Ergün, Ö. (1977). *Local Scour Depths Around Linear and Circular Piles Group*. D.S.I. Head of T.A.K.K. Publication No. HI-641.
13. Başak, V. Şentürk, F. Kason, Ş. Başlaşlı, Y. and Ergün, Ö. (1975). *Local Carvings Around the Pile Group on a Line*. T.R. Energy and Natural Resources Ministry. DSI General Directorate. Head of the Research Department. Ankara. Publication No. HI-583.

14. Bozkuş Z. Çeşme M. (2010). *Reduction of Scouring Depth by Using Inclined Piers*. Can. J. Civ. Eng. 37: 1621–1630. https://doi.org/10.1139/L10-099
15. Bozkuş Z. and Yıldız O. (2004). *Effects of Inclination of Bridge Piers on Scouring Depth*. ASCE Journal of Hydraulic Engineering. Vol.130. No. 8, 827-832. August 2004. https://doi.org/10.1061/(ASCE)0733-9429(2004)130:8(827)
16. Breusers, H. N. C. Nicollet, G. and Shen, H. W. (1977). *Local Scour around Cylindrical Piers*. Journal of Hydraulic Research. 15(3). 252. https://doi.org/10.1080/00221687709499645
17. Breusers, H.N.C. and Raudkivi, A.J. (1991). *Scouring*. IAHR Hydraulic Structures Design Manual. A. A. Balkema. Rotterdam. Netherlands.
18. Briaud, J.L. Ting, F.C. Chen, F.C. Gudavalli, R. Perugu, S. and Wei, G. (1999). *SRICOS: Prediction of scour rate in cohesive soils at bridge piers*. Journal of geotechnical and geoenvironmental engineering. 125(4). 237-246. https://doi.org/10.1061/(ASCE)1090-0241(1999)125:4(237)
19. Castiblanco, M. (2016). Experimental Study of Local Scour around Complex Bridge Piers. Thesis submitted for the fulfilment of the requirements for the degree of Doctoral Program in Civil Engineering.
20. Chang, W-Y. Constantinescu, G. Lien, H-C. Tsai, W-F. Lai, J-S. and Loh, C-H. (2013). *Flow structure around bridge piers of varying geometrical complexity*. Journal of Hydraulic Engineering. 139 (8). 812 – 826. https://doi.org/10.1061/(ASCE)HY.1943-7900.0000742

21. Chiew, Y. M. and Melville, B. M. (1987). *Local scour around bridge piers.* J. Hydraul. Res. 25(1). 15-26. https://doi.org/10.1080/00221688709499285

22. Coleman, S.E. (2005). Clearwater local scour at complex piers, Journal of Hydraulic Engineering. 131 (4). 330 - 334. https://doi.org/ 10.1061/(ASCE)0733-9429(2005)131:4(330)

23. Dargahi, B. (1989). *Turbulent flow field around a circular cylinder*. Experiments in Fluids. 8(1-2). 1-12. https://doi.org/10.1007/BF00203058

24. Debnath, K. and Chaudhuri, S. (2009). *Laboratory experiments on local scour around cylinder for clay and clay-sand mixed beds*. Eng. Geol., 111(12). pp. 51- 61. https://doi.org/10.1016/j.enggeo.2009.12.003

25. Debnath, K. and Chaudhuri, S. (2010-a). *Bridge pier scour in clay-sand mixed sediments at near threshold velocity for sand*. Journal of Hydraulic Engineering. 136(9). 597-609. https://doi.org/10.1061/(ASCEHY).1943-7900.0000221

26. Debnath, K. and Chaudhuri, S. (2010-b). *Laboratory experiments on local scour around cylinder for clay and clay-sand mixed beds*. Engineering Geology. 111(1-4). 51-61. https://doi.org/10.1016/j.enggeo.2009.12.003

27. Devi, Y. S. and Barbhuiya, A. K. (2017). *Bridge Pier Scour in Cohesive Soil: a review*. Sādhanā. 42(10). 1803-1819. https://doi.org/10.1007/s12046-017-0698-5

28. Dey, S. (1996). *Sediment pick-up for evolving scour near circular cylinders*. Applied Mathematical Modelling. 20(7). 534-539. https://doi.org/10.1016/0307-904X(95)00172-G

29. Dey, S. Helkjaer, A. Molto, S.B. and Fredsoe, J. (2011). *Scour at vertical piles in sand-clay mixtures under waves*. Journal of waterway. Port. Coastal. and ocean engineering. 137(6). 324-331. https://doi.org/10.1061/(ASCE)WW.1943-5460.0000095

30. Dey, S. Raikar, R.V. and Roy, A. (2008). *Scour at submerged cylindrical obstacles under steady flow*. Journal of Hydraulic Engineering, 134 (1). 105 – 109. https://doi.org/10.1061/(ASCE)0733-9429(2008)134:1(105)

31. Eldeeb, H. M. and Fahmy, M. R. (2015*). Effect of Fully and Partial Submerged Pile Cap on Local Scour Depth around Piles*. International Journal of Engineering Research & Technology (IJERT). Vol. 4 Issue 04. April-2015.

32. Elliott, K.R. and Baker, C.J. (1985). *Effect of pier spacing on scour around bridge piers*. Journal of Hydraulic Engineering. 111 (7). 1105 -1109. https://doi.org/10.1061/(ASCE)0733-9429(1985)111:7(1105)

33. Ettema, R. Constantinescu, G. and Melville, B. (2011). *Evaluation of bridge scour research: pier scour process and predictions*. National Cooperative Highway Research Program 24-27(01). Transportation Research Board. Washington. DC.

34. Ferraro, D. Tafarojnoruz, A. Gaudio, R. and Cardoso, A.H. (2013). *Effects of pile cap thickness on the maximum scour depth at a complex pier*. Journal of Hydraulic Engineering. 139 (5). 482 – 491. https://doi.org/10.1061/(ASCE)HY.1943-7900.0000704

35. Grimaldi, C. and Cardoso, A.H. (2010). *Methods for local scour depth estimation at complex bridge piers*. Proceedings of 1st IAHR European Division Congress. Edinburgh. UK.

36. Guo, J. (2012). *Pier scour in clear water for sediment mixtures*. J. Hydraul. Res. 50. 18–27. https://doi.org/10.1080/00221686.2011.644418
37. Hamil, L. (2000). *Bridge Hydraulics*. 2nd Edition. Taylor & Francis Taylor e-Library.
38. Hannah, C.R. (1978). *Scour at pile groups*, Report Nº 78-3. Department of Civil Engineering. University of Canterbury. Christchurch. New Zealand.
39. Hussein, N.S. and Al Shukur, A.K. (2020). *Effect of Pier Shape and Skew - Angle on Clear Water Scour at Bridge Piers Alignments*. a thesis submitted to the college of engineering. University of Babylon. in partial fulfillment of the requirements for Degree of master in science in water resources.
40. International Business Machines (IBM). (2015). *IBM* SPSS Statistical V26 Commend Syntax Reference.
41. Jones, J.S. and Sheppard, D.M. (2000a). *Local scour at complex pier geometries*. Proceedings of World Environmental and Water Resources Congress 2000. USA, May. https://doi.org/10.1061/40517(2000)409
42. Jones, J.S. and Sheppard, D.M. (2000a). *Local scour at complex pier geometries*. Proceedings of World Environmental and Water Resources Congress 2000. USA, May. https://doi.org/10.1061/40517(2000)409
43. Kim, I.; Fard, M.Y. Chattopadhyay, A. (2015). *Investigation of a bridge pier scour prediction model for safe design and inspection*. J. Bridge Eng. 20. 04014088. https://doi.org/10.1061/(ASCE)BE.1943-5592.0000677

44. Kobus, H. (1974). *Applying the dimensional analysis in the experimental research of construction engineering.* The Bautechnik. Vol. 51. No. 88–94.

45. Kothyari, U.C. Kumar, A. and Jain, R.K. (2014). *Influence of cohesion on river bed scour in wake region of piers*. Journal of Hydraulic Engineering. 14(1): 1-13. https://doi.org/10.1061/(ASCE)HY.1943-7900.0000793

46. Kumar, A. Kothyari, U.C. and Ranga Raju, K.G. (2012). *Flow structure and scour around circular compound bridge piers e A review*. Journal of Hydro-environment Research. 6 (4). 251 – 265. https://doi.org/10.1016/j.jher.2012.05.006

47. Lança, R. Fael, C. Maia, R. Pêgo, J. and Cardoso, A. (2013a). *Clear-water scour at pile groups*. Journal of Hydraulic Engineering. 139 (10). 1089 – 1098. https://doi.org/10.1061/(ASCE)HY.1943-7900.0000770

48. Lanca, R. Fael, C. Maia, R. Pego, J. and Cardoso, A.H. (2012). *Effect of Spacing and Skew-Angle on Clear-Water Scour at pier Alignments*. Taylor & Francis Group. London.

49. Lança, R.C. Fael, R. Maia, J.P. Pego, and Cardoso, A.H. (2013b). *Clearwater scour at pile groups*. J. Hydraul. Eng. 139 (10): 1089–1098. https://doi.org/10.1061/(ASCE)HY.1943-7900.0000770

50. Lee, S. O. (2006). *Physical Modeling of Local Scour around Complex Bridge piers*. A Dissertation Presented to The Academic Faculty of the Civil and environmental Engineering in the Georgia Institute of Technology in Partial Fulfillment of the Requirements for the Degree Doctor of Philosophy.

51. Li, Y. (2002). *Bridge pier scour and contraction scour in cohesive soils on the basis of flume tests*. ph. D. Dissertation. Taxas A&M University. College Station. TX.

52. Manish, P. Giuseppe, O. Jaan, H.Pu. Sharma, P.K. and Ojha, C.S. (2020). *Pier Scour Prediction in Non-Uniform Gravel Beds*. Water.12, 1696. http://doi:10.3390/w12061696

53 Martín-Vide, J.P. Hidalgo, C. and Bateman, A. (1998). *Local scour at piled bridge foundations*. Journal of Hydraulic Engineering. 124 (4). 439 - 444. https://doi.org/10.1061/(ASCE)0733-9429(1998)124:4(439)

54. Melville B. W. Sutherland A.J. (1988). *Design Method for Local Scour at Bridge Piers*, Journal of Hydraulic Engineering, Vol. 114, No. 10, October 1988. ASCE, Paper No. 22830. https://doi.org/10.1061/(ASCE)0733-9429(1988)114:10(1210)

55. Melville B.W. (1997). *Pier and Abutment Scour: Integrated Approach*. Journal of Hydraulic Engineering. Vol. 123. No. 2. February 1997. ASCE. Paper No. 10923. https://doi.org/10.1061/(ASCE)0733-9429(1997)123:2(125)

56. Melville, B. Coleman, S. and Priestley, S. (2006). *Local scour at complex piers*. Proceedings of World Environmental and Water Resources Congress. USA. May. https://doi.org/10.1061/40856(200)176

57. Melville, B. W. and Raudkivi, A. J. (1977). *Flow characteristics in Local Scour at Bridge Piers*. Journal of Hydraulic Research, 15(4). 373-380. https://doi.org/10.1080/00221687709499641

58. Melville, B.W. and Chiew, Y.M. (1999). *Time scale for local scour at bridge piers*. Journal of Hydraulic Engineering. 125 (1). 59 - 65.

59. Melville, B.W. and Coleman, S.E. (2000). *Bridge scour*. Water Resources Publications. LLC. Colorado. U.S.A.

60. Melville, B.W. and Raudkivi, A.J. (1996). Effect of foundation geometry on bridge pier scour. Journal of Hydraulic Engineering. 122 (4). 203 - 209. https://doi.org/10.1061/(ASCE)0733-9429(1996)122:4(203)

61. Mia, M. Nago, H. (2003). *Design Method of Time-Dependent Local Scour at Circular Bridge Pier*. Journal of Hydraulic Engineering. 129 (6). 420-427. https://doi.org/10.1061/(ASCE)0733-9429(2003)129:6(420)

62. Moreno, M. Maia, R. and Couto, L. (2015). *Effects of Relative Column Width and Pile-Cap Elevation on Local Scour Depth around Complex Piers*. Journal of Hydraulic Engineering. September. 16. https://doi.org/10.1061/(ASCE)HY.1943-7900.0001080

63. Moreno, M. Maia, R. Couto, L. and Cardoso, A. (2014-a). *Contribution of Complex Pier Components on Local Scour Depth.* 3rd IAHR Europe Congress. Book of Proceedings. Porto - Portugal.

64. Moreno, M. Maia, R. Couto, L. and Cardoso, A. (2014-b*). Evaluation of local scour depth around complex bridge piers*. 3rd IAHR Europe Congress. Book of Proceedings. Porto - Portugal.

65. Movahedi, N. Dehghani, A. A. Aarabi, M.J. and Zahiri, A.R. (2013). *Temporal evolution of local scour depth around side-by-side piers*. Journal of Civil Engineering and Urbanism. 3 (3). 82 – 86.

66. Muto, Y. (2008). *Local scour around a submerged cylindrical pier*. Proceedings of International Conference on Scour and Erosion 2008. 180 - 185.

67. Novák, P. (2010). Hydraulic modeling - an introduction: Principles, methods, and applications. Spon. London. of streambed scour at bridges. Federal Highway Administration. https://doi.org/10.1201/9781315272498

68. Raikar, R.V. and Dey, S. (2005). *Scour of gravel beds at bridge piers and abutments*. Proceedings of the Institution of Civil Engineers. Water Management. Volume 158. Issue 4. Pages 157–162. https://doi.org/10.1680/wama.2005.158.4.157

69. Rajkumar, V.R. and Subhasish, D. (2005). *Clear-water scour at bridge piers in fine and medium gravel beds*. Can. J. Civ. Eng. 32: 775–781. http://doi: 10.1139/L05-022

70. Rambabu, M. Narasimha, R.S. and Sundar, V. (2003). *Current-induced scour around a vertical pile in cohesive soil*. Ocean Eng. 30(4). pp. 893-920. https://doi.org/10.1016/S0029-8018(02)00063-X

71. Raudkivi A.J. Ettema R. (1977). *Effect of sediment gradation on clear-water scour*. Proc. ASCE 103(HY10); 1209-1213. https://doi.org/10.1061/JYCEAJ.0004853

72. Raudkivi A.J. Ettema R. (1983). *Clear water scour at cylindrical piers*. Journal of Hydraulic Engineering. ASCE. 109(HY3). 338-350.

73. Raudkivi, A.J. (1986). *Functional Trends of Scour at Bridge Piers*. Journal of Hydraulic Engineering. Vol. 112. No.6. 1-13. https://doi.org/10.1061/(ASCE)0733-9429(1986)112:1(1)

74. Reza. M. GH. (2012). *Effect of Foundation Geometry on Short Abutment Scour*. Thesis for the degree of doctor of pholophy.

75. Richardson, E. V. and Davis, S. R. (2001). *Hydraulic Engineering Circular*. No. 18. evaluating Scour at bridges. FHWA. https://doi.org/10.1061/(ASCE)0733-9429(2001)127:7(531)

76. Saghravani, S.F. and Azhari, A. (2012). *Simulation of clear water local scour around a group of bridge piers using a Eulerian 3D.* two-phase model. Progress in Computational Fluid Dynamics. An International Journal 12. no.5:333. https://doi.org/10.1504/PCFD.2012.049097

77. Salim, M. and Jones, J.S. (1996) *Scour around exposed pile foundations*. Proceedings of the American Society of Civil Engineers North American Water and Environment Congress 96. Anaheim (U.S.).

78. Salim, M. and Jones, J.S. (1999). *Scour Around Exposed Pile Foundations*. ASCE Compendium. Stream Stability and Scour at Highway Bridges. Richardson and Lagasse (eds.). Reston, VA.

79. Sheppard, D.M. and Glasser, T. (2004). *Sediment scour at piers with complex geometries*. Proc. 2nd International conference on Scour and Erosion. World Scientific. Singapore. https://hdl.handle.net/20.500.11970/99977

80. Sheppard, D.M. and Jones, J.S. (1998). *Scour at complex pier geometries*. Complication of Conference Scour papers (1991-1998). ASCE. Reston. Va.

81. Sheppard, D.M. and Renna, R. (2010). *Florida bridge scour manual*. Florida Department of Transportation. Tallahassee.

82. Shrestha, C. K. (2015). *Bridge Pier Flow Interaction and Its Effect on the Process of Scouring*. a thesis submitted in fulfillment of the

requirement for the degree of Doctor of Philosophy. Faculty of Engineering and Information Technology. University of Technology Sydney (UTS).

83. Simarro, G. Fael, C. and Cardoso, A. (2011). *Estimating equilibrium scour depth at cylindrical piers in experimental studies*. Journal of Hydraulic Engineering. 137 (9). 1089–1093. https://doi.org/10.1061/ (ASCE)HY.1943-7900.0000410
84. Simpson, R. L. (2001). *Junction flows*. Annual Review of Fluid Mechanics. 33. 415-443.
85. Smith, W.L. (1999). *Local structure-induced sediment scours at pile groups*. M.Sc. Thesis. Florida University. Gainesville. FL.
86. Sousa, A. M. and Ribeiro, T. P. (2019). *Local scour at complex bridge piers – experimental validation of current prediction methods*. ISH Journal of Hydraulic Engineering. https://doi.org/10.1080/09715010.2019.1639223
87. Sousa, A.M. (2007). *Localized erosion along complex cylindrical pillars (in Portuguese)*. M.Sc. Thesis. Higher Technical Institute. Lisbon. Portugal.
88. Sumer, B. M. and Fredsøe, J. (2002). *The Mechanics of Scour in the Marine Environment*. Advanced Series on Ocean Engineering. World Scientific Publishing Co. Pte. Ltd. Singapore.
89. Ting, F.C. Briaud, J.L. Chen, H.C. Gudavalli, R. Perugu, S. and Wei, G. (2001). *Flume tests for scour in clay at circular piers*. Journal of hydraulic engineering. 127(11). 969-978. https://doi.org/10.1061/(ASCE)0733-9429(2001)127:11(969)
90. U.S. Dept. Of the Interior. B. O. R. USBR. (2001). revised. *Water Measurement Manual.*

91. Umeda, S. Yamazaki, T. and Yuhi, M. (2010). *An experimental study of scour process and sediment transport around a bridge pier with foundation*. Proceedings of International Conference on Scour and Erosion. 66 - 75.

92. US Federal Highway Administration. (1990). *Highways in the River Environment*. (www.fhwa.gov).

93. Veerappadevaru, G. Gangadharaiah, T. and Jagadeesh, T.R. (2011). *Vortex scouring process around bridge pier with a caisson*. Journal of Hydraulic Research. 49 (3). 378 – 383. https://doi.org/10.1080/00221686.2011.568195

94. Veerappadevaru, G. Gangadharaiah, T. and Jagadeesh, T.R. (2012). *Temporal variation of vortex scour process around caisson piers*. Journal of Hydraulic Research. 50 (2). 200 – 207. https://doi.org/10.1080/00221686.2012.666832

95. Vittal, N. Kothyari, U. C. and Haghighat, M. (1994). *Clear- Water Scour around Bridge Pier Group*. J. Hydraul. Eng. 120:1309-1318. https://doi.org/10.1061/(ASCE)0733-9429(1994)120:11(1309)

96. Yang, Y. Melville, B. W. Macky, G. H. and Shamseldin, A. Y. (2019). *Local Scour at Complex Bridge Piers in Close Proximity under Clear-Water and Live-Bed Flow Regime*. Water. 11. 1530. https://doi.org/10.3390/w11081530

97. Yang, Y. Melville, B. W. Macky, G. H. and Shamseldin, A. Y. (2020-a). *Temporal Evolution of Clear-Water Local Scour at Aligned and Skewed Complex Bridge Piers*. Journal of Hydraulic Engineering. (146) 4. https://doi.org/10.1061/(ASCE)HY.1943-7900.0001732

98. Yang, Y. Melville, B. W. Macky, G. H. and Shamseldin, A. Y. (2020-b). *Experimental study on local scour at complex bridge pier*

under combined waves and current. Journal Pre-proof. Coastal Engineering. https://doi.org/10.1016/j.coastaleng.2020.103730

99. Yang, Y. Melville, B. W. Shamseldin, A. Y. and Friedrich, H. (2017). *Effect of Skewness on Clear-Water Scour at Complex Bridge Piers*. Proceedings of the 37th IAHR World Congress. August 13 – 18. Kuala Lumpur. Malaysia.
100. Yang, Y. Melville, B. W. Sheppard, D. M. and Shamseldin, A. Y. (2018). *Clear-1 water local scour at skewed complex bridge piers.* Journal of Hydraulic Engineering.
101. Yanmaz, A. M. (2002). *Bridge Hydraulics. METU Development Foundation Publishing and Communication A.S.* Publications. METU Press. ISBN 975-7064- 55-6.
102. Zahraa, F.H. AlShukur, A.K. and AlJaf, I. (2020). *Experimental Modeling to Investigate Local Scour at Bridge Piers in a Cohesive Soil*. A Thesis submitted to the Civil Engineering Department in the University of Technology in partial fulfillment of the requirements for the degree of doctor of philosophy in Water Resources Engineering.
103. Zarrati, A. R. (2010). *Application of Collar to Control Scouring around Rectangular Bridge Piers*. Journal of Hydraulic Research. Department of Civil and Environmental Engineering. Amir Kabir University of Technology No.424. Tehran, Iran. 97-103. https://doi.org/10.1080/00221686.2004.9641188
104. Zhao, G. and Sheppard, D.M. (1999). *The effect of flow skew angle on sediment scour near pile groups*. Stream Stability and Scour at Highway Bridges. 377 - 391.

APPENDIX

Appendix-A

A.1 Beta Bridge / Babylon Province – Hilla

Below sediment size distribution analysis for Batah Bridge in Babylon province, Hilla, at depth 4-5 m, the weight of dray sand sample is 500 gm.

Table (A-1): Sediment size distribution analysis.

Sieve No.	Sieve opening (mm)	Retained weight (gm)	Retained percentage %	Cumulative percentage %	Pass percentage %
4	**4.75**	0	0	0	100
10	**2**	0	0	0	100
16	**1.19**	0	0	0	100
25	**0.707**	0	0	0	100
30	**0.595**	45	9	9	91
50	**0.297**	410	82	91	9
100	**0.15**	35	7	98	2
200	**0.074**	5	1	99	1
pan		5	1	100	0
Total		**500**	**100**		

A.2 Ali Al-Gharbi Bridge / Missan Province

Below sediment size distribution analysis for Ali Al-Gharbi Bridge in Missan province, at depth 5m, the weight of dray sand sample is 500 gm.

Table (A-2): Sediment size distribution analysis.

Sieve No.	Sieve opening (mm)	Retained weight (gm)	Retained percentage %	Cumulative percentage %	Pass percentage %
4	**4.75**	0	0	0	100
10	**2**	0	0	0	100
16	**1.19**	0	0	0	100
25	**0.707**	0	0	0	100
30	**0.595**	25	5	5	95
50	**0.297**	300	60	65	35
100	**0.15**	160	32	97	3
200	**0.074**	5	1	98	2
pan		10	2	100	0
Total		**500**	**100**		

A.3 Selebat Bridge/ Al-Muthana Province

Below sediment size distribution analysis for Selebat Bridge in Al-Muthana province, at depth 5-6 m, the weight of dray sand sample is 500 gm.

Table (A-3): Sediment size distribution analysis.

Sieve No.	Sieve opening (mm)	Retained weight (gm)	Retained percentage %	Cumulative percentage %	Pass percentage %
4	**4.75**	0	0	0	100
10	**2**	0	0	0	100
16	**1.19**	0	0	0	100
25	**0.707**	5	1	1	99
30	**0.595**	15	3	4	96
50	**0.297**	25	5	9	91
100	**0.15**	185	37	46	54
200	**0.074**	20	4	50	50
pan		250	50	100	0
Total		**500**	**100**		

A.4 Suspension Bridge/ Al-Basra Province

Below sediment size distribution analysis for Suspension Bridge in Al-Basra Province, at depth 5.5-6 m, the weight of dray sand sample is 500 gm.

Table (A-4): Sediment size distribution analysis.

Sieve No.	Sieve opening (mm)	Retained weight (gm)	Retained percentage %	Cumulative percentage %	Pass percentage %
4	**4.75**	0	0	0	100
10	**2**	0	0	0	100
16	**1.19**	0	0	0	100
25	**0.707**	41	8.2	8.2	91.8
30	**0.595**	414	82.8	91	9
50	**0.297**	43	8.6	99.6	0.4
100	**0.15**	1	0.2	99.8	0.2
200	**0.074**	0.5	0.1	99.9	0.1
pan		0.5	0.1	100	0
Total		**500**	**100**		

A.5 Al -Shallala Bridge/ Kirkuk Province

Below sediment size distribution analysis for Al -Shallala Bridge in Kirkuk Province, at depth 5-6 m, the weight of dray sand sample is 500 gm.

Table (A-5): Sediment size distribution analysis.

Sieve No.	Sieve opening (mm)	Retained weight (gm)	Retained percentage %	Cumulative percentage %	Pass percentage %
4	**4.75**	0	0	0	100
10	**2**	0	0	0	100
16	**1.19**	235	47	47	53
25	**0.707**	120	24	71	29
30	**0.595**	30	6	77	23
50	**0.297**	25	5	82	18
100	**0.15**	15	3	85	15
200	**0.074**	10	2	87	13
pan		65	13	100	0
Total		**500**	**100**		

المستخلص

بسبب الاعتبارات الفيزيائية والجيوتقنية والاقتصادية، تُبنى الجسور بشكل متكرر بأسس هندسية معقدة. في هذه الدراسة، ينطبق مصطلح "دعامات معقدة" على الأشكال الهندسية للدعامات الذي يتميز بعمود مؤسس على قبعة مدعومة بمصفوفة من الركائز. الانجراف الموقعي هو ظاهرة معقدة تنطوي على هياكل تدفق ثلاثية الأبعاد، يتم تطويرها عادةً حول الدعامات وأكتاف الجسور التي تأسست في قاع أنهار متحركة. يمكن أن يؤدي الانجراف الموقعي إلى فشل جزئي أو انهيار دعامات الجسر.

تم إجراء ما مجموع تسعين اختبارًا مع خمسة نماذج من الدعامات المعقدة لتحديد تأثير موضع القبعة، الأبعاد، الزوايا المحاذية والمنحرفة لتدفق الجريان (0°، 30°، 45°، 60°) للتربة العراقية المختلفة على تطور وقت عمق الانجراف. تم تصنيف النتائج التجريبية وفقًا لثلاث حالات للقبعة: (1) الحالة 1، التي تتميز بكون قاع القبعة أعلى من مستوى التربة الأولي؛ (2) الحالة 2، التي تتميز بكون قاع القبعة على مستوى التربة الأولي؛ و (3) الحالة 3، التي تتميز بدفن القبعة بالكامل في التربة.

بالنسبة للدعامة المعقدة المحاذية للجريان، يحدث أقصى عمق انجراف عندما تكون القبعة أعلى من مستوى التربة الأصلي مع زيادة (80٪، 81٪، 100٪، 35٪، 100٪) مقارنة بالقبعة المدفونة بالكامل للجسور: (بته، علي الغربي، صليبات، المعلق، شلالا) بالتتابع، وهذا مشابه لنتائج التحقيقات السابقة. يقلل التأثير الوقائي للقبعة من عمق الانجراف بشكل كبير بعد حدوث قيمة الذروة عند زيادة موضع القبعة عن طريق تعطيل التدفق السفلي أمام الدعامة. يزيد عمق الانجراف المتوازن للدعامات المعقدة المنحرفة بشكل كبير مقارنة بالدعامات المحاذية. تتناسب الزيادة في عمق الانجراف مع زاوية الانحراف α، وهي الأكبر في جسر الصليبات (29.4٪، 33٪، 80٪) لـ (60°، 45°، 30°) بالتتابع؛ والأقل في جسر علي الغربي (26٪، 12٪، 25٪).

تم اقتراح صياغة جديدة للتنبؤ ds عند الدعامات المعقدة، أما بالنسبة لمواد طبقة الرمل، كانت المقارنة من HEC-18، وAuckland، وFDOT، ويمكن استنتاج أن طريقة HEC-18 تعطي تقديرات ds والتي تمثل تسوية مقبولة بين الأمان والاقتصاد وتعطي (R^2 = 96.94%, 95.54%, 98.11%) لجسور (بيته، علي الغربي، المعلق). بالنسبة لمواد التربة المتماسكة كانت المقارنة بين (Ansari, Debnath and Chaudhuri, and Rambau) وطريقة الأنصاري تعطي (R^2 = 96.63٪) لجسر الصليبات، وبالنسبة لمادة الحصى غير الموحدة (Melville and Coleman, Guo, and Kim)، فإن طريقة Melville تعطي (R^2 = 94.31)٪ لجسر الشلالا.

جمهورية العراق
وزارة التعليم العالي والبحث العلمي
جامعة بابل
كلية الهندسة
قسم الهندسة المدنية

نمذجة عملية الإنجراف الموقعي لأسس الجسور المعقدة لأنواع ترب مختلفة في العراق

إطروحة
مقدمة الى كلية الهندسة / جامعة بابل
كجزء من متطلبات نيل درجة الدكتوراه فلسفة في الهندسة / الهندسة المدنية / موارد مائية

من قبل
نور سعدي حسين صالح

بإشراف
أ. د. عبد الحسن خضير الشكر
أ. م. د. زيد حميد مجيد

1444 هـ

2023 م